UNIVERSITÁ DEGLI STUDI DI MILANO
FACOLTÁ DI MEDICINA E CHIRURGIA

DOTTORATO DI RICERCA IN FISIOLOGIA
SETTORE SCIENTIFICO DISCIPLINARE BIO-09
CICLO XXIII°
Tesi di Dottorato di Ricerca

THE IMPORTANT ROLE OF AKT IN THE MODULATION OF HEART INOTROPISM THROUGH L-TYPE CALCIUM CHANNELS FUNCTION

Dottorando: Dott.ssa **Francesca Rusconi**
Matricola: R07664

Tutor: Prof. **Dario DiFrancesco**
Coordinatore: Prof. **Paolo Cavallari**
Supervisors: Prof. **Gianluigi Condorelli**
Dott. **Daniele Catalucci**

Anni Accademici 2007-2010

TABLE OF CONTENTS

DEFINITIONS

Calcium transient	A brief change in fluorescence intensity induced by calcium entering the cell through a Voltage-Gated Calcium Channel
Cardiac Hypertrophy	An adaptive response of the heart to preserve Left Ventricular function in physiological or pathological states
Congestive Heart Failure	Insufficient cardiac pumping capacity
EC coupling	Exitation-contraction coupling
Genotype	The genetic constitution of a cell, an organism or an individual
Heart failure	A complex clinical syndrome that can results from any structural of functional disorder that impairs the ability of the ventricle to fill or eject blood
Knock-out	The genotype of an organism when one or more genes have been turned off through a targeted mutation.
Inotropism	The force of cardiac contraction
Transgenic organism	Genetically modified organism
Wildtype	The phenotype of the typical form of a species as it occurs in nature

ABBREVIATIONS

AA	Amino acid
AbA	Aureobasidin A
Ad	Adenovirus vector
AID	α interaction domain (L-Type Calcium Channels)
AF	Atrial Fibrillation
AM	Acetoxymethyl
ATP	Adenosine trisphosphate
β-ARs	β-Adrenergic Receptors
BDM	2,3-butanedione monoxime
BID	β interaction domain (L-Type Calcium Channels)
Bp	Base pair
BSA	Bovine Albumine Serum
CA	Constitutive active
Ca^{2+}	Calcium ion
$[Ca^{2+}]_i$	Intracellular calcium concentration
$CaCl_2$	Calcium Chloride
cDNA	Cyclic DeoxyriboNucleic Acid
Cs	Cesium
cAMP	cyclic Adenosine-Mono-Phosphate
CHF	Congestive Heart Failure
CMC	Cardiomyocytes
CO-IP	Co-immunoprecipitation
DCM	Diabetic Cardiomyopathy
DHPR	Dihydropyridine receptors

DMEM	Dulbecco's Modified Eagle's Medium
DMSO	Dymetil sulfoxide
DN	Dominant Negative
DNA	Deoxyribonucleic acid
dNTPs	Deoxyribonucleoside triphosphate
DTT	Dithiothreitol
EC coupling	Exitation-contraction coupling
EDTA	Ethylene Diamine Tetraacetic Acid
EGTA	Ethylene Glycol-bis(beta-aminoethyl-ether)-N,N,N',N'-TetraAcetate
ER	Endoplasmatic reticulum
FBS	Fetal Bovine Serum
Fw	Forward
GAPDH	Glyceraldehyde 3-phospate dehydrogenase
GFP	Green Fluorescent Protein
Gln (Q)	Glutamine
Glu (E)	Glutamic acid
GST	Glutathione S-transferase
H	Hours
HA	Hemagglutinin
H_2O	Water
HBSS	Hank's Balanced Salt Solution
HEK	Human Embryonic Kidney
HEPES	4-(2-hydroxyethyl)-piperazineethanesulfonicacid
HF	Heart Failure
HI-FBS	Heat Inactivated Fetal Bovine Serum

His (H)	Hystidine
HRP	Horse Radish Peroxidase
$I_{Ca,L}$	L-type Calcium Current
IGF-1	Insulin growth factor-1
IGF1R	Insulin growth factor-1 receptor
IR	Insulin receptor
IRS	Insulin receptor substrates
Kb	Kilo base
KDa	Kilo Dalton
KO	Knock Out
Leu (L)	Leucine
LiAc	Lithium Acetate
Lys (K)	Lysine
LTCC	L-Type Calcium Channel
Mg^{2+}	Magnesium ion
$MgCl_2$	Magnesium Chloride
MHC	Myosin Heavy Chain
Min	Minutes
mOsM	Milli Osmolar
mRNA	Messenger RiboNucleid Acid
Na^+	Sodium ion
NaF	Sodium fluoride
Na_3VO_4	Sodium orthovanadate
NP-40	Nonidet P-40
O.D.	Optic density
OptiMEM	Opti Modified Eagle's Medium

PBS	Phosphate buffered saline
PCR	Polymerase Chain Reaction
PI3K	Phosphatidyl-inositol 3-kinase
PIP	Phosphatidylinositol (3,4,5)-trisphosphate
PLN	Phospholamban
PTEN	Phosphatase and TENsin homolog deleted on chromosome 10
PVDF	Polyvinylidene Fluoride
Rw	Reverse
RT	Room Temperature
Sec	Seconds
SD medium	synthetic dropout medium
SDS	Sodium Dodecyl Sulfhate
SDS-PAGE	Sodium Dodecyl Sulfhate-Poly Acrylamide Gel Electrophoresis
Ser (S)	Serine
SH2	Src homology 2 domain
SH3	Src homology 3 domain
SR	Sarcoplasmatic Reticulum
Thr (T)	Threonine
TEA	TetraEthylAmmonium
Trp (W)	Tryptophan
VGCC	Voltage Gated Calcium Channel
YFP	Yellow Fluorescent Protein
Y2H	Yeast Two-Hybrid
WT	Wild Type

SUMMARY

The insulin IGF1/Akt signaling pathway has recently been shown to be critical for the regulation of heart function and physiology. Indeed, compelling evidence shows activation of this pathway as one of the most important determinants for the enhancement of cardiac function and physiological growth in athletes, whereas its impairment is considered critical for the development of heart failure (HF). In this doctoral thesis, our aim was to determine the functional role of known and novel key-factors of this pathway to study whether their modulation might be envisaged as therapeutic tool for curing pathological cardiac hypertrophy (CH) and HF.

Physiological CH is an adaptive response of the heart to stimuli, such as developmental growth and training and differs markedly from pathological hypertrophy occurring in patients with HF. In this thesis, we demonstrated the involvement of Akt kinase in regulating heart inotropism by modulating L-Type Ca^{2+} Channel (LTCC) density and function. In a mouse model with inducible and cardiac specific deletion of PDK1, the upstream activator of Akt, we found that the protein stability of the LTCC pore subunit ($Ca_v\alpha_1$) can be modulated by the kinase. In particular, phosphorylation of the C-terminal coiled coil of the $Ca_v\beta_2$ chaperone subunit enhances LTCC protein stability by prevention of PEST-mediated $Ca_v\alpha_1$ degradation. Subsequently, to determine whether the modulation of this mechanism may be used for the treatment of HF, we studied the fine-regulation of LTCC density and activity by investigating the functional role of Akt-phosphomimetics $Ca_v\beta_2$ constructs. Three Akt-phosphomimetic sequences corresponding to the $Ca_v\beta_2$ C-terminal coiled coil were identified and shown to

protect $Ca_v\alpha_1$ from protein degradation, through an increase in the number of functional LTCC. Moreover, to establish whether the Akt-dependent phosphorylation of $Ca_V\beta_2$ might be a trigger for the recruitment of other protein interacting partners, yeast two-hybrid screenings of human and mouse heart cDNA expression libraries revealed a fold-back interaction of the Akt-phosphorylated-$Ca_v\beta_2$ tail with a region of the $Ca_v\beta_2$ globular domain. Co-immunoprecipitation experiments confirmed this interaction, while negative results were obtained when $Ca_v\beta_2$-WT was used as bait. This provided the proof of concept for a mechanism of action that relies on Akt-dependent phosphorylation. Site-specific mutagenesis in the identified interacting domain confirmed this mechanism. All togheter, we found that the Akt-dependent protective effect on $Ca_v\alpha_1$ stability might relay on $Ca_v\beta_2$ structural rearrangements, which follow the phosphorylated C-terminal coiled coil fold back on its globular domain.

In conclusion, results from this doctoral thesis provide further insights into the role of the insulin IGF1/Akt signaling pathway and its role in the modulation of myocardial physiology and HF. These findings may lead to the development of new therapeutical tools that will be useful for the modulation of impaired cardiac contractility in HF.

AIMS

Compensatory mechanism that lead to myocardial hypertrophy include alterations in the regulation of signal transduction pathways involved in the control of cell size, protein synthesis, Ca^{2+} handling and energy metabolism. The re-establishment of cardiac function in HF could be envisaged by finding a new equilibrium favoring physiological rather than pathological CH. This can be reached by acting on downstream targets modulated by Akt kinase, a main mediator of the insulin IGF1 pathway by positively affecting cardiac inotropism by directly modulating cardiomyocyte Ca^{2+} handling.

Accordingly, the main aims of the present Ph.D. thesis were:

- to gain insight into the mechanism of action by which Akt intervenes in the fine-regulation of heart inotropism by regulating Ca^{2+} current ($I_{Ca,L}$) and Ca^{2+} handling;
- to further demonstrate the pivotal role of Akt in the modulation of heart inotropism by unraveling the molecular mechanisms by which Akt regulates L-Type Calcium Channels density;
- to further study the Akt-dependent fine-tuning regulation of LTCC density by searching for Akt-phosphomimetics $Ca_V\beta_2$ sequences, which may increase orreestablish correct cardiac inotropism in HF by increasing the number of functional LTCC;
- to further unravel the mechanism by which Akt intervenes in the modulation of $Ca_v\alpha_1$ protein stability by identification and characterization of possible Akt-dependent protein interacting partners involved in LTCC complex structural and functional modulation.

1. INTRODUCTION

1.1. Heart failure

Heart failure (HF), with an estimated prevalence of 1-2% in the Western world and an annual incidence of 5-10 per 1000, is a syndrome resulting from impaired ability of the heart to pump sufficient blood to the body, and thus matching the oxygen needs of peripheral tissues. Importantly, in people older than 50 years, the prevalence of HF increases progressively with age, making HF the leading cause of hospitalization in the elderly [sandoval1]. Despite the fact that HF management has been improved over the last decades, HF still results with a poor quality of life and reduced longevity [2] with a prognosis that has been described as being more malignant than cancer [3]. In fact, survival after the onset of HF is grim, with a 5-year survival rate as low as 25% and sudden death in up to 50% of HF patients.

HF may have several etiologies either primary, starting from the myocardial tissue, or secondary and may be present under different clinical setting. Among the causes that lead to HF are coronary artery disease, hypertension, cardiomyopathies, valvular diseases, congenital defects, infectious diseases, diabetes and cardiotoxic substances (such as alcohol). Though no single causative mechanism or sequence of events has been found for HF, this syndrome is in general preceded by an initial insult (e.g., cardiomyocyte loss, persistently increased workload) responsible for impairing ventricular function in some way (Figure 1).

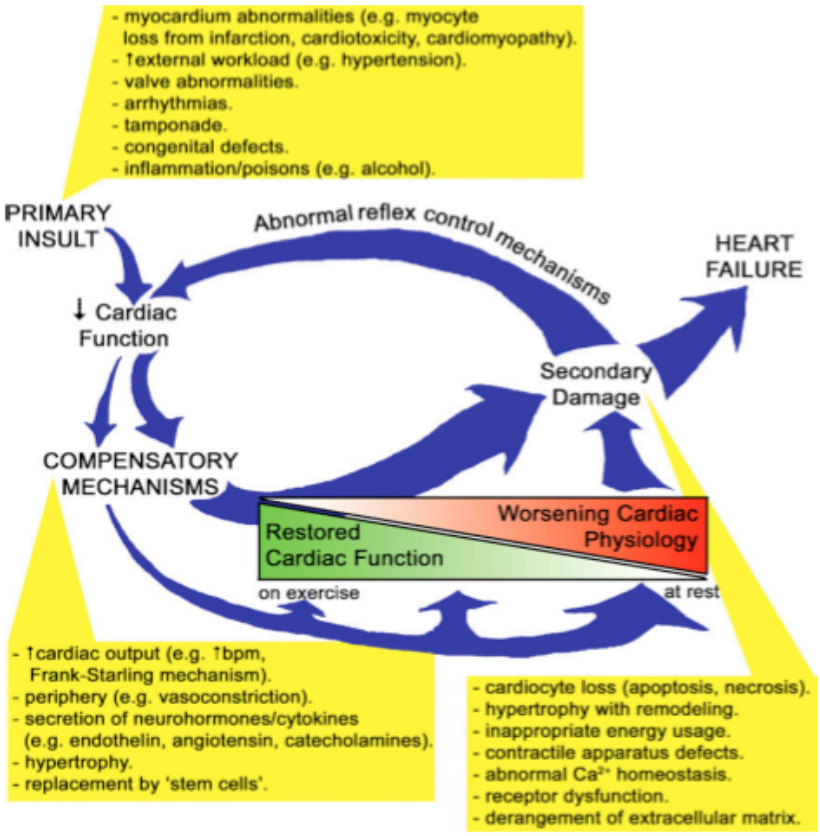

Figure 1. Schematic of principal events of heart failure onset. The compensatory mechanism summoned into action are often responsible for a paradoxical spiraling deterioration in cardiac structure and function, culminating in heart failure (from [4]).

As a result, several mechanism, initially compensatory, such as activation of the rennin-angiotensin-aldosterone system, of the sympathetic adrenergic nervous system and increase of cytokine production may take place. The consequential increase in circulating neurohormonal factors and stimulation of stretch receptors result in increased heart size (cardiomegaly) via the enlargement of individual cardiomyocytes (hypertrophy). As largely recognized, the establishment of this pathological cardiac hypertrophy (CH) plays an important role in the onset of many forms of HF [5].

Physiological CH is defined by augmentation of ventricular mass as a result of increased cardiomyocyte size and is the adaptive response of the heart to enhanced hemodynamic loads due to physiological stimuli such as postnatal developmental growth, training and pregnancy. In these cases, hypertrophy is characterized by enhanced cardiac function, normal sarcomere organization and a normal pattern of cardiac gene expression [6] without interstitial fibrosis or increased cell death. Importantly, physical training protects against cardiovascular disease and the resultant CH is usually beneficial [7]. Indeed, exercise training in HF after myocardial infarction enhances cardiac performance and aerobic exercise capacity and reverses pathological hypertrophy and remodeling both in experimental models and in patients [8]. On the other hand, CH is also observed in patients with pathological conditions such as hypertension, myocardial infarction, and valvular heart diseases. This type of cardiac growth is called pathological hypertrophy and is frequently associated with contractile dysfunction, interstitial fibrosis and re-expression of fetal-type cardiac genes such as atrial natriuretic peptide and α-myosin heavy chain [9, 10]. Therefore, in the short term, the adaptive response of the heart to enhanced hemodynamic loads apparently restores cardiovascular function (*i.e.*, hypertrophy is adaptive). However, in the long run, the sustained activation of compensatory mechanism can lead to secondary heart damage, evidenced by worsening left ventricle (LV) remodeling (*i.e.*, deleterious alterations in ventricular mass, chamber size and shape) and the hypertrophy becomes maladaptive, i.e., incapable of sustaining the hemodynamic burden. Indeed, patients undergo a transition from asymptomatic to symptomatic HF [11]. Clinically, this maladaptive hypertrophy has become recognized as a harmful reaction when generated by pathological stresses and is considered a major predictor for progressive HF and an adverse prognosis [12]. In fact, inhibition of

the development of pathological hypertrophy has been shown to have beneficial effects in animal models of pressure overload and is the target of some current therapies. Actual treatment of HF is based on the fact that neuroendocrine activation is important in the progression of the syndrome. In fact, therapeutic strategies that stem from the neurohormonal model (*i.e.*, ACE inhibitors and beta-blockers) prevent disease progression and reduce LV remodeling. Drugs derived from cardiorenal and cardiocirculatory models (diuretic and inotropes/vasodilators, respectively) provide symptom relief, but are less effective in reducing LV mass and improving prognosis [13]. Great advances have been made in the last decades in cardiac pathophysiology, but despite the knock-on effect this has had on the clinical management of HF, the syndrome is still a major killer and heart transplantation remains the ultimate treatment. Thus, new approaches are needed alongside conventional therapies to completely arrest LV pathological remodeling and progression to HF. Undoubtedly, further unraveling of the molecular mechanism governing cell size, protein synthesis and cardiac inotropism during HF is needed. This understanding will provide important information for the design of new therapeutic approaches to conquer this condition outright in the future. In particular, novel therapeutic interventions could be directed to take advantage of beneficial mechanism inherent to physiological stress-based hypertrophy that is via enhancement of important aspects controlled by the insulin IGF1/Akt pathway.

1.2. The IGF1/PI3K/Akt pathway

The insulin growth factor-1 (IGF1)/phosphatidyl-inositol 3-kinase (PI3K)/Akt pathway plays a crucial role in a broad range of biological processes involved in the modulation of local responses as well as processes implicated in cell proliferation, transcription, translation, apoptosis and growth. The insulin pathway is also a critical regulator of glucose metabolism, promoting its uptake in the heart, glycolysis and glycogen synthesis as well as inhibiting fatty acid utilization [14]. Its important role in the regulation of cardiac growth, calcium handling and contractile function has been demonstrated. Indeed, impairment of this signaling pathway is now considered an important determinant of HF [15].

1.2.1. Mediators of the signal transduction pathway

1.2.1.1. IGF1

IGF1 is a polypeptide growth factor that is characterized by insulin like short-term metabolic effects and growth factor-like long-term effects on both cell proliferation and differentiation. IGF1 is produced in numerous tissues and particularly by the liver in response to growth hormone stimulation. Interaction of IGF1 (or insulin) with its receptor (IGF1R) activates the receptor's cytoplasmatic tyrosine kinase activity, which in turn triggers phosphorylation of insulin receptor specific substrates (IRS). Phosphorylated IRSs then interact with cytoplasmic proteins containing src homology 2 (SH2) domains, such as PI3K. Within the target cells, activated PI3K then transduces the functional effects of IGF1, such as enhanced glucose transport, enhanced cardiomyocyte contractility and the inhibition of programmed cell death (apoptosis) [16].

IGF1 is an important factor in the regulation of postnatal growth and development. In fact, knock out (KO) models of IGF1 or its receptor shows reduced body growth [14]. Both IGF1R and insulin receptor (IR) are present in the adult heart and have been shown to be essential for myocardial performance through the action of PI3K/Akt pathway [17]. In athletes, increased cardiac IGF1 production is associated with physiological cardiac hypertrophy [18] and in transgenic (TG) mice with cardiac overexpression of IGF1R, physiological cardiac hypertrophy developed with increased myofiber size and enhanced contractile function [19, 20]. Cardiac-specific IR KO mice showed a decrease in heart size and impaired contractile function [21]. Intriguingly, when challenged by pathological hypertrophic stimuli, heart size was increased to a similar extent in both IR KO and wild type (WT) mice, even though IR KO heart size at baseline is smaller when compared to WT [22]. Thus, while the insulin/IGF1 pathway is involved in physiological hypertrophic growth, it does not appear to be necessary for pathological hypertrophy development. Indeed, cardiac-specific IGF1 overexpression resulted in less cardiomyocyte death and fibrosis with chronic coronary artery narrowing [23] as well as reduced injury in an *ex vivo* model of ischemia/reperfusion [24]. However, although the short-term administration of IGF1 in animal studies has been reported to be beneficial by improving cardiac contractility and counteracting apoptosis, conflicting results has been shown from clinical trials in which IGF1 was administered chronically [25-27].

1.2.1.2. Phosphoinositide 3-kinase (PI3K)

PI3K is a member of the lipid kinase family involved in the phosphorylation of membrane phosphoinositides (PIP) [28]. The PI3K family comprises eight members divided into three classes according to their sequence homology and substrate preference (Table 1).

Class	Catalitic subunit	Regulatory subunit	Activation	Products
Ia	p110α p110β p110δ	p85	RTK, RAS	PtdIns-3,4,5-P_3 PtdIns-3,4-P_2 PtdIns-3-P
Ib	P110γ	p101	Heterotrimeric G proteins	PtdIns-3,4,5-P_3 PtdIns-3,4-P_2 PtdIns-3-P
II	PI3KC2α PI3KC2β PI3KC2γ		RTK, integrins	PtdIns-3,4,-P_2 PtdIns-3-P
III	VSP34p			PtdIns-3-P

Table 1. The PI3K family members (from [29]).

Class Ia enzymes (p110α, p110β and p110δ) associate with a p85 regulatory subunit to form a heterodimeric complex. There are 8 isoforms of p85 encoded by three genes, each containing two SH2 domains that interact with phosphotyrosines on activated tyrosine kinase receptors (RTKs, e.g. growth factor receptors), antigen receptors and cytokine receptors.

Class Ib enzymes are made up of only the p110γ catalytic and the p101 regulatory subunit, which is activated by G-protein coupled receptors (GPCRs).

Class II comprises three members (PI3KC2α, β and γ) characterized by a carboxyl-terminal phospholipid-binding domain. While no regulatory subunit has

been identified, class II enzyme are predominantly membrane bound and activated by membrane receptors including RTKs, GPCRs, chemokines, and integrins.
Class III kinase (VPS34p) is responsible for producing the majority of the cellular PtdIns-3-P and is involved in protein trafficking through the lysosome.

Physiological hypertrophy involves activation of the PI3K (p110α) pathway, stimulated by RTKs, whereas pathological hypertrophy utilizes the GPCR-induced PI3K (p110γ) pathway [20]. Overexpression of a constitutively active (ca) PI3K (p110α) mutant resulted in cardiac hypertrophy *in vivo* to a similar extent to that seen in IGF1R TG mice [30]. In contrast, the physiological cardiac hypertrophy obtained by physically exercising mice, as well as in mice overexpressing IGF1R, was completely abolished by co-expression of a dominant negative (dn) PI3K (p110α) mutant [20].

PTEN (Phosphatase and TENsin homologue deleted on chromosome 10) antagonizes the activity of PI3K by catalizing conversion of active inositol lipids into inactive ones. In PTEN KO mice, increased PI3K (p110α) and PI3K (p110γ) activity occurred in combination with increased cardiomyocyte size, while cardiac function was depressed [31].

1.2.1.3. Akt

Akt (also known as protein kinase B, PKB) is at the crossroad of the IGF1/PI3K/Akt physiological hypertrophy pathway and belongs to the family of the serine-threonine protein kinase. There are three closely related enzymatic isoforms Akt1 (PKBα), Akt2 (PKBβ) and Akt3 (PKBγ) (Figure 2), that play an important role in the regulation of cardiac growth, differentiation, survival, angiogenesis and contractile function, regulating a range of downstream targets [31, 32].

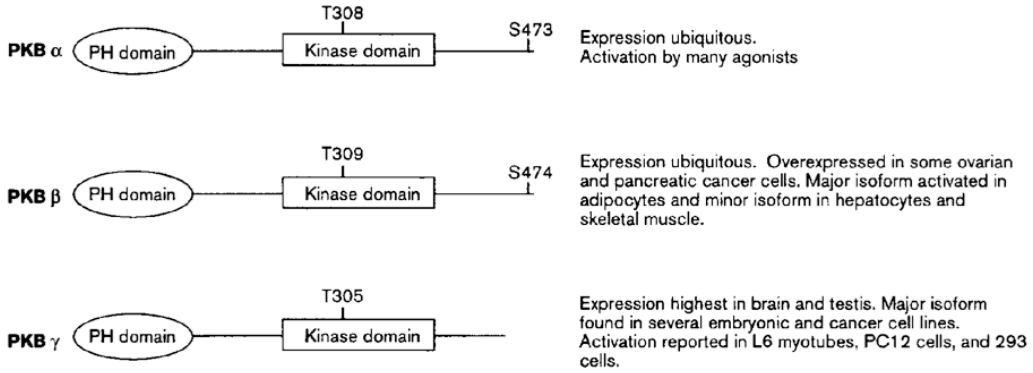

Figure 2. Akt structure domains: an N-terminal pleckstrin homology (PH) domain, a central catalytic domain and a C-terminal regulatory region with the two phosphorylation sites pT308 and pS473. (From [33])

While Akt1 and Akt2 isoforms are widely expressed, Akt3 tissue distribution is primarily expressed in brain and testis [34]. The three Akt proteins (henceforth referred to as Akt) contain an N-terminal pleckstrin homology (PH) domain, a central catalytic domain and a C-terminal regulatory region (Figure 2). They are

similar both in structure and size and are thought to be activated by a common mechanism [35] .

Akt is activated by IGF1 and insulin through PI3K. The resultant phosphorylated PIP products bind to the pleckstrin (PH) domain of Akt and induce its translocation from the cytosol to the plasma membrane where Akt becomes accessible for phosphorylation at Thr308 by phosphoinositide-dependent kinase-1 (PDK1), which results in its activation [32] (Figure 3).

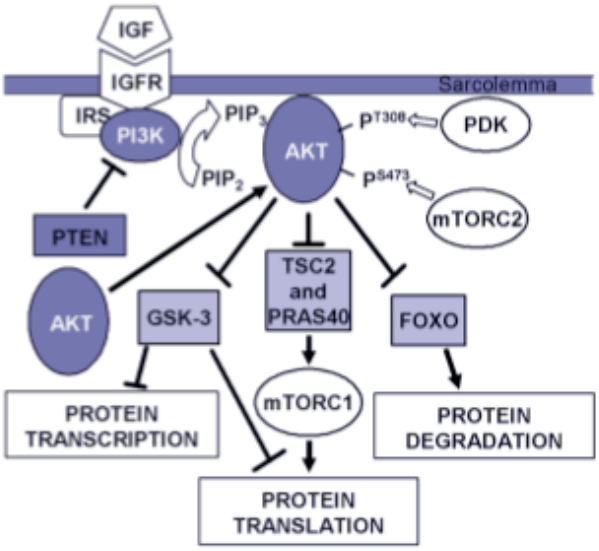

Figure 3. Schematic diagram of the upstream molecules involved in the activation of Akt and the major signaling pathways involved in protein synthesis (From [16]).

Akt can also be phosphorylated at another regulatory phosphorylation site (Ser473) from the rapamycin-insensitive complex of the mammalian target of rapamycin (mTORC2)-comprised of mTOR, rictor and G-beta-L/mMTST8 [36].

Akt is activated in response to physical exercise [20] and in caPI3K TG mice, but is repressed in dnPI3K TG mice [30]. Once fully activated, Akt migrates throughout the cell to several subcellular organelles and subdomains and

phosphorylates specific effector targets (Figure 3). Akt is eventually deactivated by dephosphorylation at T308 and S473 by protein phosphatase 2A (PPA2) and leucine-rich repeat protein phosphatase (PHLPP), respectively [37, 38].

1.2.1.3.1. Mouse models for studying the role of Akt

Several cardiac-specific mouse models have been used for studying the physiological role of Akt and its upstream molecules *in vivo*. Most models include cardiac hypertrophy and maintenance or improvement of cardiac function. In fact, the Akt E40K mutant, which overexpresses a constitutively active form of Akt, induces a physiological type of hypertrophy together with an improvement in cardiac function [15]. The activated T308D/S473D mutant, which mimics the activated phosphorylation status, is also associated with heart enlargement due to an increase in myocyte size [39]. On the other hand, overexpression of myristilated Akt, that permanently confines Akt to the plasmamembrane in proximity to its activator PDK1, was found to be detrimental for cardiac function [40].

Akt activation is increased 1.5-to 2-fold under physiological conditions in response to exercise training [20] and 6-fold in IGF1 TG mice [24]. It has been shown that short-term Akt activation or "physiological" activated Akt induces physiological hypertrophy, whereas prolonged Akt activation results in pathological hypertrophy with a drastic increase in heart size [40, 41]. These observation support the notion that the activation of the IGF1/Akt pathway may sustain either physiological or pathological hypertrophy, depending on the extent

and timing of stimulation.

In KO mouse model studies, deletion of a single or a combination of the various Akt isoforms resulted in a number of different phenotypes. Global Akt1 KO mice had a reduction in growth [42], while Akt2 KO resulted in insulin resistance and a mild growth delay [43]. On the other hand, Akt3 KO did not result in any growth problems but rather in a reduction in the size of brain cells [44].

1.2.1.3.2. Effects of Akt on Ca^{2+} -handling and contractility

It has been reported that increased inotropism and calcium transient are typical features of isolated cardiomyocytes from exercised mice [45], HF patients subjected to acute IGF1 administration [46] and mice in which the IGF1/PI3K/Akt pathway has been activated [14]. As discussed in more detail in the paragraph 1.3. (Cardiac excitation-contraction coupling), contractility in cardiomyocytes is determined by the entrance of Ca^{2+} through the L-type Ca^{2+} channel (LTCC) and release of Ca^{2+} from the sarcoplasmatic reticulum (SR) through the ryanondine receptor (RyR). Relaxation is mediated by Ca^{2+} reuptake into the SR through the SR Ca^{2+} ATPase pump (SERCA2A). As shown in Figure 4, Akt seems to be involved in this process by the fine-tuning modulation of Ca^{2+} -handling.

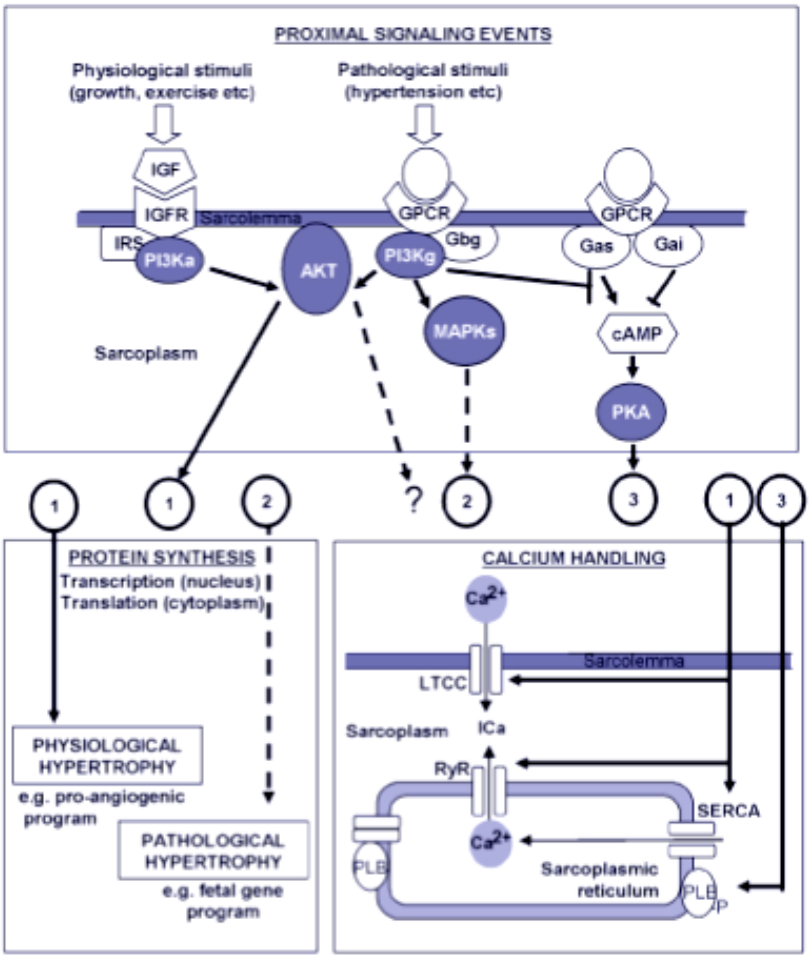

Figure 4. Schematic diagram of some different signaling events involved in physiological and pathological hypertrophy. The PI3Ka dependent pathway is responsible for transcription of genes and increasing calcium-handling in the development of physiological hypertrophy triggered by IGF1. Activation of PI3Kg, through GPCR, is antagonistic and triggers various mitogen-activated protein kinase (MAPKs) pathways, which results in protein synthesis of fetal genes and differential activation of Akt. Moreover, it can be responsible for decreasing contractility through the inhibition cAMP production. Gas: G-alpha s proteins, Gai: G-alpha i proteins, Gbg: G-beta/gamma protein. From [16].

Overexpression of an active form of Akt1 results in improved cardiac inotropism both *in vivo* [15] and *in vitro* [47], augmenting Ca^{2+} current ($I_{Ca,L}$). Similar results were recently obtained in a mouse model with cardiac specific Akt1 nuclear-overexpression [48] and in mice deficient for PTEN, an antagonizer of PI3K

activity [49]. In addition, activation or inhibition of Akt in cardiomyocytes as well as in neuronal cells has been shown to increase[32] {Viard, 2004 #1151;Blair, 1999 #676;Catalucci, 2006 #28;Sun, 2006 #61} or reduce {Viard, 2004 #1151;Blair, 1999 #676;Catalucci, 2006 #28;Sun, 2006 #61} $I_{Ca,L}$, respectively, suggesting a pivotal role of Akt in regulating LTCC function (Figure 5).

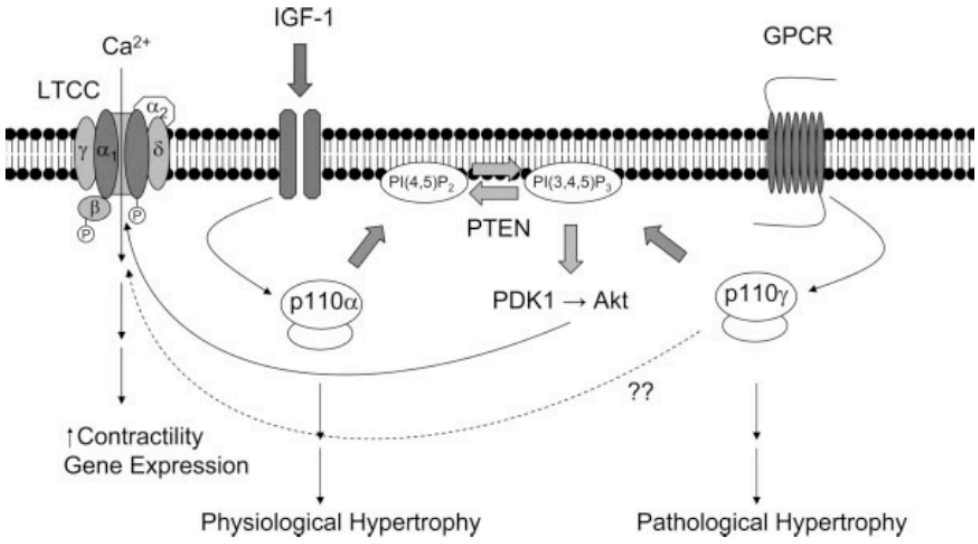

Figure 5. Diagram illustrating that the pathway IGF1/PI3K/Akt is involved in the modulation of the LTCC (from [50]).

1.3. Cardiac excitation-contraction coupling

The ubiquitous second messenger Ca^{2+} is essential in cardiac electrical activity and is the direct activator of the myofilaments, which cause contraction. Myocyte mishandling of Ca^{2+} is a central cause of both contractile dysfunction and arrhythmias in pathophysiological conditions. In healthy cardiomyocytes, electrical excitation starting during the upstroke of action potential leads to

cytosolic Ca^{2+} influx through opening of the LTCC [51, 52]. This triggers the calcium-induced calcium release (CICR) of intracellular Ca^{2+} from the SR through activation of the ryanodine receptor (RyR), eventually leading to cardiomyocyte contraction. The combination of Ca^{2+} influx and release raises the free intracellular Ca^{2+} concentration ($[Ca^{2+}]_i$), allowing Ca^{2+} to bind to the myofilament protein troponin C, which then switches on the contractile machinery. For relaxation to occur, $[Ca^{2+}]_i$ must decline, allowing Ca^{2+} to dissociate from troponine. This requires Ca^{2+} transport out of the cytosol by different pathways involving, sarcolemmal Na^+/ Ca^{2+} exchange (NCX), sarcolemmal SR Ca^{2+} -ATPase (SERCA2) or mithocondrial Ca^{2+} uniport [53](Figure 6).

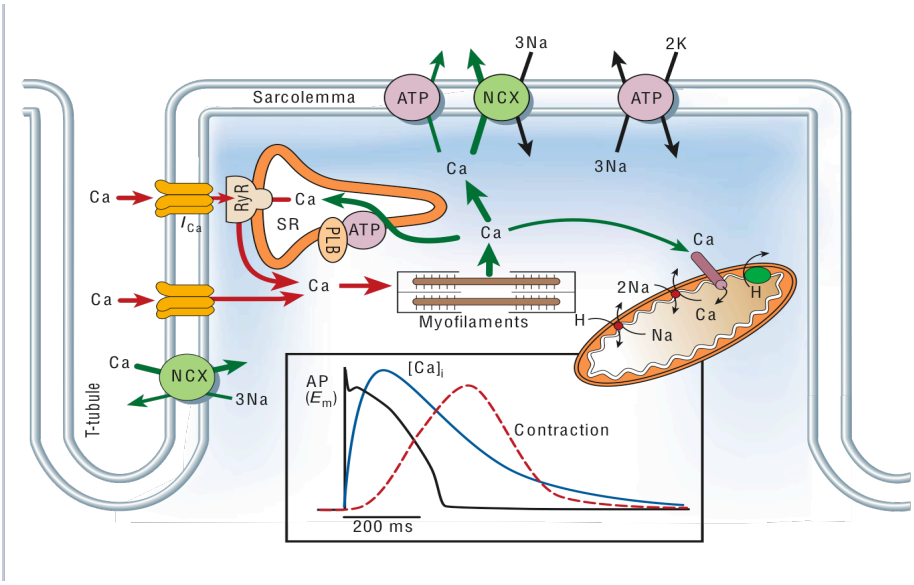

Figure 6. Ca^{2+} transport in ventricular myocytes and the time course of an action potential, Ca^{2+} transient and contraction (from [53]).

1.4. Voltage-gated dependent Ca^{2+} channels

LTCC belongs to the family of Voltage-gated dependent Ca^{2+} channels (VGCCs), that are activated in response to membrane depolarization and are essential in cytoplasmic Ca^{2+} signaling processes in a variety of cells. VGCCs regulate a number of cellular processes including muscle contraction, secretion, neurotransmitter, gene regulation and neuronal migration. Two classes of VGCCs have been described and summarized in Table 2.

Ca^{2+}-current type	Voltage	α1 Subunit (gene name)	Specific blockers	Primary locations
L	HVA	$Ca_v1.1$ (CACNA1S)	Dihydropyridines	Skeletal muscle
L	HVA	$Ca_v1.2$ (CACNA1C)	Dihydropyridines	Cardiac muscle, smooth muscle, endocrine cells, neurons
L	HVA	$Ca_v1.3$ (CACNA1D)	Dihydropyridines	Endocrine cells, neurons
L	HVA	$Ca_v1.4$ (CACNA1F)	Dihydropyridines	Retina
P/Q	HVA	$Ca_v2.1$ (CACNA1A)	ω-Agatoxin	Nerve terminals, dendrites
N	HVA	$Ca_v2.2$ (CACNA1B)	ω-Conotoxin	Nerve terminals, dendrites
R	Intermediate-voltage activated	$Ca_v2.3$ (CACNA1E)	None	Nerve terminals, dendrites
T	LVA	$Ca_v3.1$ (CACNA1G)	None	Cardiac muscle, smooth muscle, neurons
T	LVA	$Ca_v3.2$ (CACNA1H)	None	Cardiac muscle, neurons
T	LVA	$Ca_v3.3$ (CACNA1I)	None	Neurons

Table 2. Ca^{2+}channel types based on their electrophysiological and pharmacological properties. HVA is High-voltage activated and LVA Low-voltage activated, respectively (from [54]).

The first class includes High Voltage Activated (HVA) channels, which are activated by strong depolarization. These are further classified according to their electrophysiological properties (activation threshold, conductance, time and voltage dependence of inactivation, selectivity to divalent cations, channel gating, open-and close-time duration) into the P/Q, N, R, and L-type [55, 56].

The second class of channels is Low-Voltage Activated (LVA) and consists of only T-type Ca^{2+} channels that open at low membrane potentials and inactivate very rapidly.

1.4.1. Cardiac L-Type Calcium Channels structure

L-type Ca^{2+} channels ("L"ong lasting) (LTCC) are often called dihydropyridine receptors (DHPR), because they are sensitive to various 1,4-dihydropyridines, some of them with either blocking (nifedipine, nicardipine) or increasing (Bay K8644) Ca^{2+} current regulatory effect. LTCC are distributed in various tissues such as skeletal muscle, heart, brain, neurons, endocrine [55].

Cardiac LTCC are composed of four polypeptide subunits comprising the $Ca_v\alpha_1$, $Ca_v\alpha_2/\delta$, $Ca_v\beta$ and form hetero-tetrameric complex with molecular mass of about 400 kDa, which is considered the functional minimum core for Ca^{2+} channel assembly. In brain and skeletal muscle, Ca^{2+} channels have the fifth subunit ($Ca_v\gamma$), but it's not expressed in the heart [56-58]. The hydrophobic $Ca_v\alpha_1$ polypeptide is entrenched in cell membrane, while $Ca_v\beta$ subunit locates in cytoplasm. The $Ca_v\delta$ subunit is anchored to cell membrane and has a single transmembrane segment with a short intracellular part and a long glycosylated extracellular part, while the $Ca_v\alpha_2$ peptide is extracellular subunit of the Ca^{2+} channel. The $Ca_v\alpha_2$ and $Ca_v\delta$ subunits of the LTCC are tightly bound together through a disulfide bridge. The accessory subunits ($Ca_v\beta$, $Ca_v\alpha_2/\delta$) are tightly, but not covalently bound to the $Ca_v\alpha_1$ subunit and modulate the biophysical properties and trafficking of the $Ca_v\alpha_1$ subunit to the membrane (Figure 7).

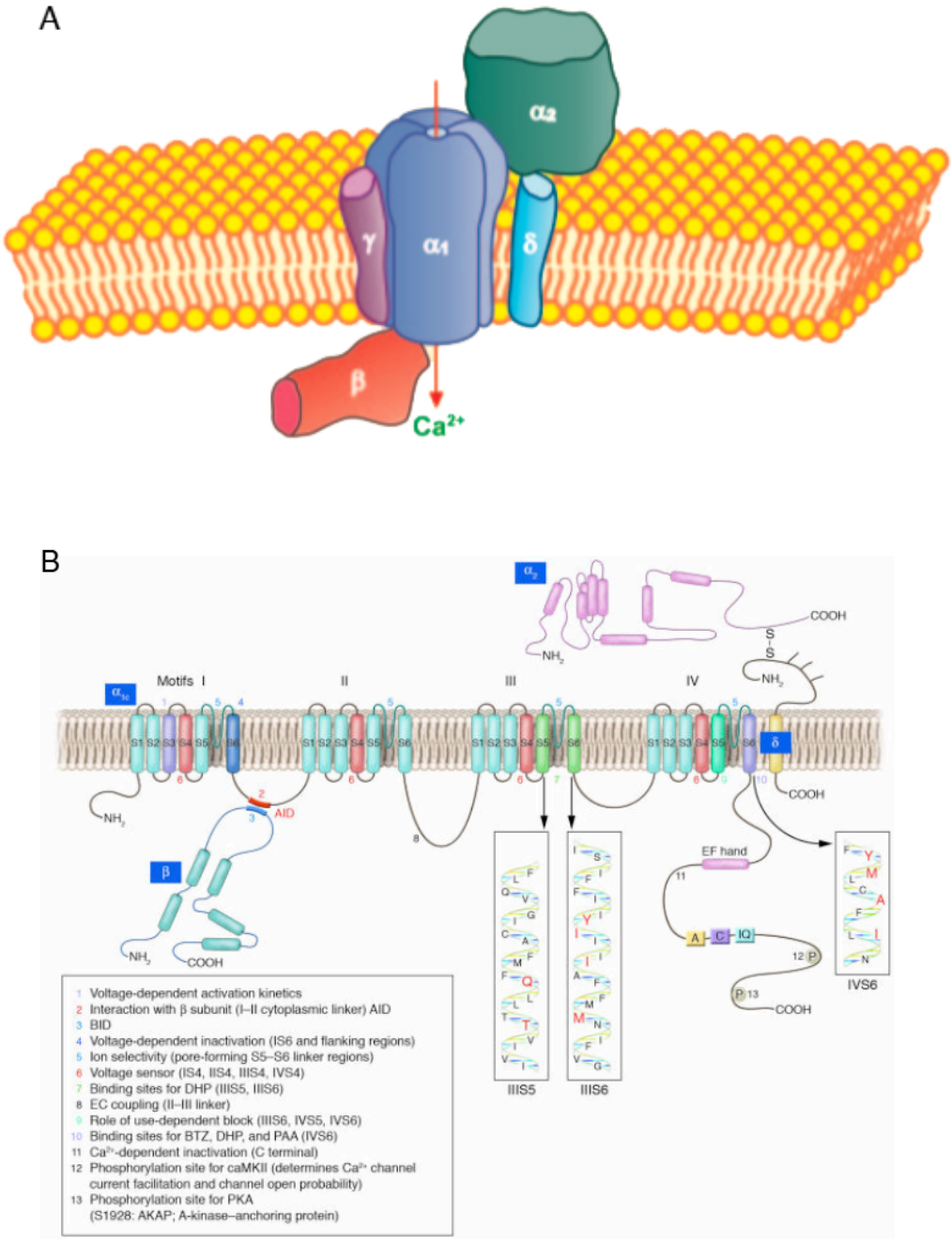

Figure 7. Structural organization of the LTCCs. A) A Ca_v channel subunit assembly in the plasma membrane. Pore-forming subunits $Ca_v\alpha_1$ complex with auxiliary subunits $Ca_v\beta$, $Ca_v\gamma$ and $Ca_v\alpha_2/\delta$ to form functional Ca_v channels in the plasma membrane (from [59]. B) The predicted membrane organization of the core subunits, their interactions, the structural domains of the auxiliary subunits presented here are described in detail in the text. (from [58])

1.4.1.1. $Ca_v\alpha_1$ subunits

The $Ca_v\alpha_1$ subunit (170−240 kDa) consists of four homologous motifs (I−IV), each composed of six membrane-spanning α-helices (S1-S6) linked by variable cytoplasmic loops (linkers) and a membrane-associated pore loop (P-loop) between the S5 and S6 segments (Figure 7B). This four homologous repeat structure endows the $Ca_v\alpha_1$ subunit with a Ca^{2+} -conducting pore (ion-selective pore) controlled by voltage sensors and gating machinery (activation and inactivation gates). The S5 and S6 segments along with the P-loops form the pore lining of Ca_v channels [60-62]. There are four glutamic acid (EEEE) residues situated in the four P-loops, that are responsible for selective filtration of Ca^{2+} and form a Ca^{2+} selectivity filter [63]. 10 $Ca_v\alpha_1$ subunit genes have been identified and separated into 4 classes (Figure 8): Cav1.1 (α_{1S}), 1.2 (α_{1C}), 1.3 (α_{1D}), and 1.4 (α_{1F}). Only the $Ca_v\alpha_{1C}$ (dihydropyridine-sensitive [DHP-sensitive]) subunit is expressed in high levels in cardiac muscle. In brain, Cav2.1 (α_{1A}), 2.2 (α_{1B}), and 2.3 (α_{1E}) form P/Q-, N- and possibly R-type channels, respectively. These are primarily responsible for initiation of synaptic transmission at fast synapses in the nervous system.

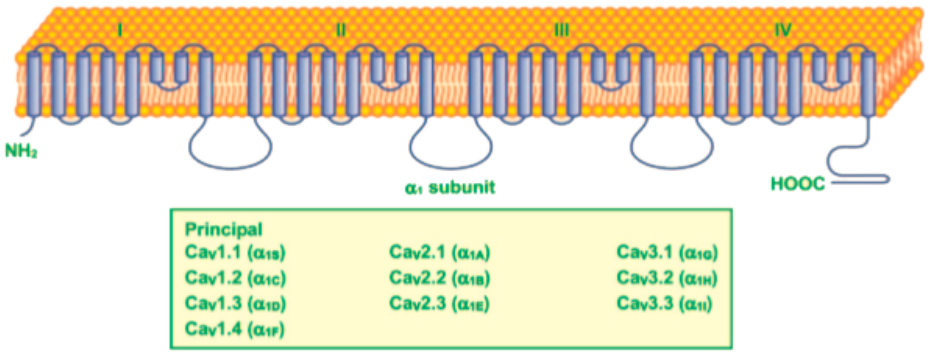

Figure 8. Predicted topology and nomenclature of $Ca_v\alpha$ channel subunits (from [59]).

Cav3.1 (α_{1G}), 3.2 (α_{1H}), and 3.3 (α_{1I}) form T-type channels that are localized into the brain, kidney, and heart and were originally called Low-Voltage–Activated channels. Unlike L-type channels, they are relatively insensitive to DHPs. Cav3 channels conduct T-type Ca^{2+} currents, which are important in a wide variety of physiological functions, including neuronal firing, hormone secretion, smooth muscle contraction, cell proliferation and myoblast fusion. In the heart, T-type channels are abundant in sinoatrial pacemaker cells and Purkinje fibers of many species and are important for maintenance of pacemaker activity by setting the frequency of action potential (AP) firing [58].

Different KO mice lacking Cav1.2 or Cav1.3 were generated to study the pathophysiological roles of LTCC *in vivo*. As showed in Figure 9, some of the LTCC roles as mediators of signaling between cell membrane and intracellular processes like blood pressure regulation, smooth muscle contractility, insulin secretion, cardiac development has been elucidated. In particular, conditional Cav1.2 ko mice show several cardiovascular and visceral phenotypes, while Cav1.3 null mice are viable but completely deaf and with sinoatrial node dysfunction, such as arrythmia and bradicardia [64].

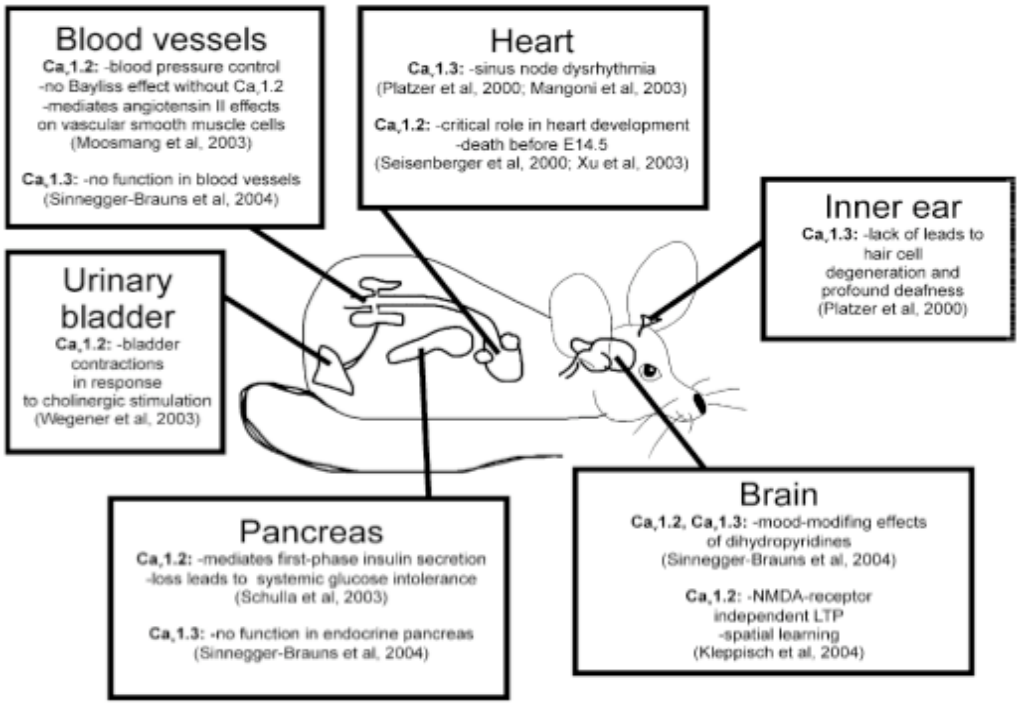

Figure 9. Distribution and function of LTCC subtypes Cav1.2 and 1.3 revealed by transgenic mouse models. (from [64]).

1.4.1.2. Accessory subunits

1.4.1.2.1. $Ca_v\alpha_2/\delta$ subunits

Four genetically distinct $Ca_v\alpha_2/\delta$ subunits ($Ca_v\alpha_2/\delta_{1,\ 2,\ 3,\ 4}$) have been described, each one of these is differentially expressed in various tissues, including skeletal muscle, heart and brain [65-67].

The $Ca_v\alpha_2\delta$ subunits are closely associated with the $Ca_v\alpha_1$ subunit by surface interaction and are intracellularly linked through a disulfide bridge to a small protein, the $Ca_v\delta$ subunit (Figure 7). The $Ca_v\alpha_2$ subunit is entirely extracellular,

while the $Ca_v\delta$ subunit has a single transmembrane region with a very short intracellular part. The $Ca_v\alpha_2$ and $Ca_v\delta$ subunits are encoded by the same gene, which is separated by proteolytic cleavage [65]. In heterologous expression systems, coexpression of the $Ca_v\alpha_2/\delta$ subunit affects $Ca_v\alpha_1$ function by increasing channel density, charge movement, and maximal binding capacity (Bmax) of drug binding (*e.g.*, the DHP isradipine) with smaller effects on dissociation constant (KD) and variable minor effects on channel kinetics [68, 69]. The $Ca_v\alpha_2/\delta$ subunit allows an enhancement in the membrane trafficking of the $Ca_v\alpha_1$, associated with an increase in the number of ligand binding sites. In addition, coexpression of the $Ca_v\alpha_2/\delta$ subunit causes an increase in current amplitude, faster activation and inactivation kinetics [70].

1.4.1.2.2. $Ca_v\beta$ subunit

1.4.1.2.2.1. $Ca_v\beta$ subunit structure

Four distinct genes encode the $Ca_v\beta$ subunit isoforms ($Ca_v\beta_1$-β_4) and numerous splice variants for each gene are known [71](Table 3).

Subunit isoform	HUGO/GDB gene nomenclature	Tissue distribution
$\beta1$	CACNB1	$\beta1$a: skeletal muscle, $\beta1$b: brain
$\beta2$	CACNB2	Heart, lung, trachea, aorta, brain
$\beta3$	CACNB3	Smooth muscle, trachea, aorta, lung, brain
$\beta4$	CACNB4	Brain

Table 3. The Ca^{2+} channel β subunits-classification and tissue distribution (from [54]).

$Ca_v\beta_1$-β_4 (54 kD) is the only subunit of the channel that is entirely cytosolic and has a common structure consisting of five different domains, with the two central

domains sharing significant homology amongst the $Ca_v\beta$ subunits [72] (Figure 7-10B). The amino and carboxy termini are relatively less well conserved. $Ca_v\beta$ subunits associate with the $Ca_v\alpha_1$ subunit predominantly through a highly affinity interaction that is mediated by the Alpha interaction domain (AID) in the $Ca_v\alpha_1$ subunit [73] and a corresponding Beta interaction domain (BID) in the $Ca_v\beta$ subunit [74] (Figure 7B-10A).

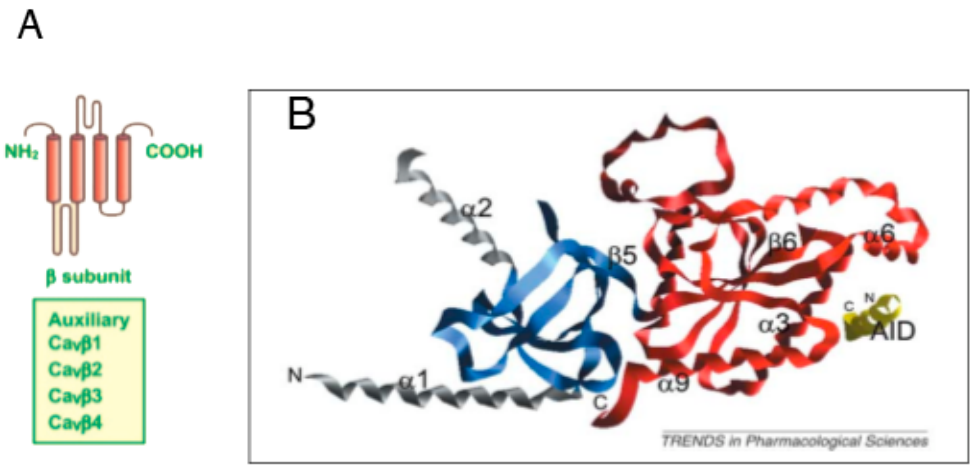

Figure 10. A) Predicted topology and nomenclature of the $Ca_v\beta$ channel accessory subunits (from [59]). B) Structure of a complex between the $Ca_v\beta$ subunit and the AID of the $Ca_v\alpha_1$. AID complex is shown as a ribbon representative, $Ca_v\beta$ consists of an SH3 domain (blue) and a guanylate kinase (GK) domain (red). Two long helices (α1 and α2; grey) are appended onto the SH3 domains of $Ca_v\beta$ subunits. The AID (yellow) binds into its pocket on the opposite side of the GK domain from the SH3. The central variable region would fall in the gap that is visible between α2 and β5 (from [75].

Despite the ability of $Ca_v\beta$ subunits to form heterogeneous complexes, it is clear that each type of channel has a predominant $Ca_v\beta$ subunit associated with it. $Ca_v\beta_4$ is the predominant subunit associated with the P/Q-type channels, the N-type channels predominantly contain $Ca_v\beta_3$, whereas L-type channels contain $Ca_v\beta_2$.

In the heart, $Ca_v\beta_2$ is encoded by Cacnb2 gene and evaluation of the 3D structure showed that is structured in a globular portion (aa 1-460) and in a coiled coil

region (aa 461-655, in blue), which contains the predicted Akt consensus site (RPDRS) (Figure 11) [75, 76].

The amino acidic sequence of 655 aa is:

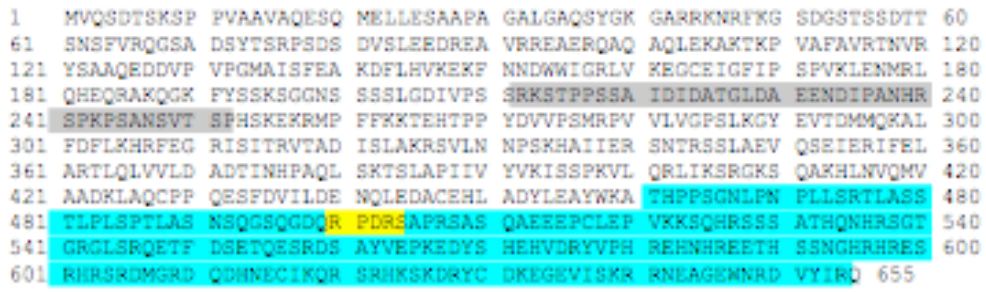

Figure 11. Cacnb2 amino acidic sequence (655 aa). The globular portion is not highlighted (1-460 aa), the BID sequence (212-252 aa) is highlighted in grey, the coiled-coil region is highlighted in light blue (461-655), the Akt consensus site is in yellow (500-504).

1.4.1.2.2. The roles of the $Ca_v\beta$ auxiliary subunits

The $Ca_v\beta$ subunits have marked effect on LTCC channel expression and modulation of the pore-forming $Ca_v\alpha_1$ subunit. It has been shown that overexpression of the $Ca_v\beta$s subunit increased the density of endogenous calcium currents, indicating an increase in the functional expression of $Ca_v\alpha_1$ subunits [77, 78]. The $Ca_v\beta$ subunits aid in the trafficking of $Ca_v\alpha_1$ to the plasma membrane, partly by its ability to mask an endoplasmic reticulum retention signal in the $Ca_v\alpha_1$ subunit [79]. In addition to its role in membrane trafficking, the $Ca_v\beta$ subunits modulate a host of biophysical properties of the channel with characteristics to the $Ca_v\alpha_1$-β combination. The $Ca_v\beta$ subunits can accomplish these dual functions independently, as illustrated by their ability to modulate the

biophysical properties of channels in the presence of a mutation in the AID region, which disrupts its ability to enhance membrane trafficking of $Ca_v\alpha_1$ [80]. It has been suggested that this is due to the ability of some $Ca_v\beta$ subunits to associate with other intracellular loops of the channel through weaker interactions. This supports a model in which the conserved high-affinity binding of the $Ca_v\beta$ subunit to the AID anchors it to the $Ca_v\alpha_1$ subunit and facilitates low-affinity interactions of other $Ca_v\beta$ subunit domains/regions with different parts of the $Ca_v\alpha_1$ subunit, which in turn are responsible for the modulation of gating [81].

All four $Ca_v\beta$ subunit isoforms hyperpolarize the voltage-dependent activation of all HVA. In contrast, steady-state inactivation properties reveal differences, both with regard to different $Ca_v\alpha_1$ and different $Ca_v\beta$ subunits. In general, the $Ca_v\beta_{1,3,4}$ subunits expressed with $Ca_v\alpha_1$ result in hyperpolarization of voltage-dependent inactivation, so that channels inactivate at more negative potentials and speed up the inactivation kinetics. On the other hand, partly due to palmitoylation of two cysteines in its N-terminus, the rat and human $Ca_v\beta_{2a}$ subunit depolarizes the voltage dependance inactivation, making the channels inactivate at more positive potentials, and dramatically slowing down the kinetics of inactivation [82].

Regulation of calcium channel activity also occurs through modification of the $Ca_v\beta$ subunits. $Ca_v\beta_{2a}$ is a substrate for protein kinase A (PKA) and phosphorylation of $Ca_v\beta_{2a}$ is important for the ability of PKA to stimulate the currents generated by the $Ca_v\alpha_1$ 2.1 channels in mammalian expression systems and in cardiac myocytes [83]. The $Ca_v\beta$ subunit also plays a role in the modulation of the $Ca_v\alpha_1$ 2.2 channels through the mitogen-activated protein kinase (MAPK) pathway [84]. It is clear that the functional effects of the $Ca_v\beta$ subunits, and hence the calcium channels, can be modulated in response to a variety of cellular stimuli. Stimulus induced modification of the auxiliary subunits may

provide an additional level of modulation of intracellular communication mediated by the LTCC.

1.4.1.2.3. Role of accessory subunits in disease

Mutations or deletions of $Ca_v\beta$ subunit result in a discernible phenotype and a loss of normal function in mouse models. KO mouse model of the $Ca_v\beta_1$ isoform resulted in a lethal phenotype with reduced skeletal muscle mass and structural abnormalities. On the other hand, heterozygotes mice were asymptomatic, indicating that residual amount of $Ca_v\beta_1$ subunit, is sufficient for normal physiological activity [85].

Deletion of $Ca_v\beta_2$ gene gave rise to an embryonic lethal phenotype, presumably because of cardiac defects, thus underlining the essential role of $Ca_v\beta_2$ in cardiac contraction. In contrast, KO of the $Ca_v\beta_3$ isoform appear to be normal in appearance with no obvious phenotype in the heart, lung, kidney, spleen, pancreas, liver, ovary or testis, indicating that other $Ca_v\beta$ subunits are able to substitute for its function [86]. As described in Table 4, deletions or mutations of the auxiliary subunits in many mouse models result in a phenotype with a loss of normal functions and severe physiological consequences, further emphasizing their role in maintaing normal neuronal and muscular function.

Subunit	Spontaneous mutation/ targeted deletion	Phenotype
$\alpha_2\delta$-1	None known	?
$\alpha_2\delta$-2	Spontaneous — ducky *(du/du)*, allele of ducky - du^{2J}	Ataxia, paroxysmal dyskinesia, synchronous spike wave discharges, accompanied by behavioral arrest and response to ethosuximide.
$\alpha_2\delta$-3	None known	?
$\alpha_2\delta$-4	None known	?
β_1	Targeted deletion	Die at birth, fetuses are unable to move, reduced muscle mass with structural abnormalities, lack of skeletal excitation contraction coupling, transgenic mice that express β_1 in the skeletal muscle appear normal.
β_2	Targeted deletion	Embryonic lethal, retinal abnormalities in transgenic mice that express β_2 in the cardiac tissue.
β_3	Targeted deletion	Normal in appearance with no obvious phenotype, no gross morphological changes in brain or other tissues, elevated blood pressure on a high salt diet.
β_4	Spontaneous – lethargic *(lh/lh)*	Ataxia, lethargic behavior, spontaneous focal motor seizures, brief episodes of behavioral immobility, accompanied by generalized cortical spike wave discharges.
γ_1	Targeted deletion	Viable, normal in appearance, no phenotypic abnormalities.
γ_2	Spontaneous — stargazer *(stg/stg)*, waggler	Head tossing, ataxia, spike wave seizures and behavioral arrest, impaired motor coordination
γ_3–γ_8	None known	N/A

Table 4. Spontaneous mutations and targeted deletions of the auxiliary subunits in mice (from [87]).

1.5. Regulation of intracellular Ca^{2+}: cardiac dysfunction

The importance and ubiquity of Ca^{2+} as an intracellular signaling molecule suggests that altered channel function could give rise to widespread cellular and organ defects. Indeed, a variety of cardiovascular diseases, including atrial fibrillation, heart failure, ischemic heart disease, Timothy syndrome, and diabetic cardiomyopathy have been related to alterations in the density or function of the LTCC [58, 88-90]. However, the molecular basis for dysregulation of LTCC function and the possible involvement of Akt in $I_{Ca,L}$ regulation remains unresolved.

1.5.1. LTCC in Heart Failure, Diabetic Cardiomyopathy and Atrial Fibrillation

It is evident that EC coupling in the heart depends on the function of the LTCC, but the consequence of increased/decreased Ca^{2+} channel density in hypertrophy and cardiac failure remains speculative. Most investigators report no change in the LTCC or downregulation in end-stage HF, but there is an agreement that alteration of intracellular Ca^{2+} handling in the myocardium is relevant to both human and animal models of heart disease [91]. A significant increase in the number of $Ca_v\alpha_1$ subunits was found in hypertrophied hearts compared to normal hearts [92]. Impaired Ca^{2+}-induced Ca^{2+} release in obesity-linked type 2 diabetes underlies depressed cardiac function, showing that the contractile dysfunction linked with the cardiomyopathy can be explained by disturbed Ca^{2+} cycling, reduced Ca^{2+} influx via LTCC, lowered Ca^{2+} reuptake and increased Ca^{2+} efflux [88]. During the early phase of electrical remodeling in a rabbit model of rapid atrial pacing, a reduction in $Ca_v\beta_2$ subunit expression paralleled a reduction in I_{caL} prior to changes in the $Ca_v\alpha_{1c}$ subunit mRNA levels. These data supports the evidence that reduced expression of $Ca_v\beta$ subunits is responsible for the reduction of functional LTCCs [93]. Moreover, mutations of the G406R as well as G402S in the $Ca_v\alpha_{1c}$ subunit were found in patients identified with Timothy Syndrome, a disease characterized by syncope and sudden death from cardiac arrythmias [94]. Based on these evidences, it appears clear that LTCCs play a key role in HF, Diabetic CardioMyopathy (DCM), Atrial Fibrillation (AF) and Timothy Syndrome.

1.5.2. L-type Calcium Channel abundance and function

Cardiac LTCCs are the main entrance for Ca^{2+} influx into cardiac cell and determine the activity of the whole heart. Therefore, changes in channel expression and regulation may alter the heart activity and badly influence functions of whole body. Despite some reports where LTCC density were shown increased in hypertrophied and failing hearts, many researchers demonstrated that HF is associated with reduction or no change of LTCC density and I_{caL}.

In failing heart not only cardiac remodeling happens, but also alteration of several regulatory systems. In ischemic and failing heart, the sympathetic system is activated and the level of catecholamines is raised. Consequently, the β-adrenergic receptors (β-AR) are activated and the LTCC stimulation occurs through cAMP. In patients with HF, this pronounced activation of the sympathetic system is inversely correlated with survival. Indeed, the level of cardiac β-ARs in failing heart is reduced and the β-AR-Gs coupling of remaining receptors is altered. β-AR blockade is a widely used treatment in HF, when cardiac activity is regulated by cAMP-dependent cascade suppression [89].

Alterations in the peak of I_{caL} have been documented in hypertrophic states induced in various animal models [95]. To a large degree, the development of severe hypertrophy and CHF in animal models is associated with abnormalities in LTCC abundance and/or function. However, abnormalities in LTCC function are not consistently manifest in milder forms of cardiac pathologies. Alterations in LTCC function with end-stage human CHF remain equivocal. With mild/moderate (compensated) hypertrophy, basal $I_{Ca,L}$ may be unchanged, or even increased, from control values. Nevertheless, a reduction in the β-AR mediated augmentation of $I_{Ca,L}$ is an early event in the transition from hypertrophy to CHF. With the

development of severe hypertrophy and/or CHF, basal $I_{Ca,L}$ is, in general, reduced from the control values. One possible explanation for these findings is that abnormalities in the β-AR signal transduction pathway occur early in the transition from hypertrophy to failure. Specifically, the number of β-ARs may be reduced and may be associated with a reduced capacity for cAMP production. In addition, the phosphorylation capacity of the LTCCs can be reduced with the progression of this disease process. The reduction of $I_{Ca,L}$ with severe hypertrophy and/or failure may be associated with a reduction in the abundance of LTCCs (Figure 12 from [89]).

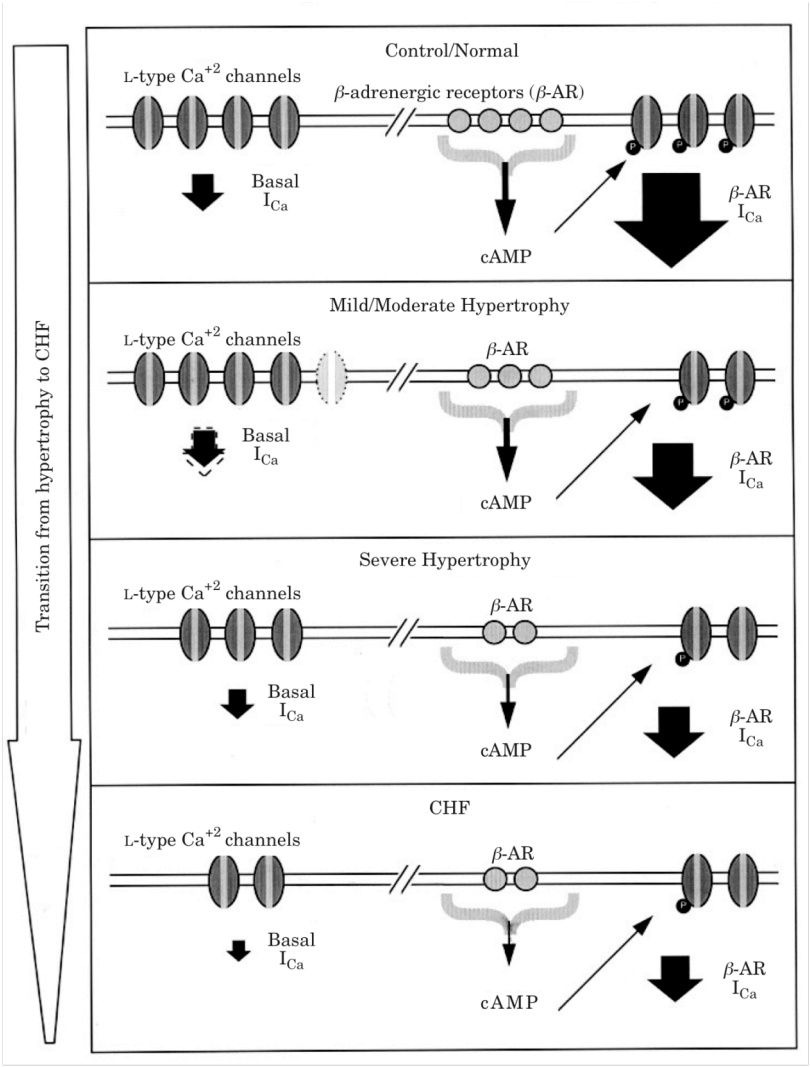

Figure 12. Schematic representation of changes in LTCC abundance and function during the progression of a cardiac pathologic process. Changes in basal LTCC abundance and function with the progression of the disease process are shown on the left and changes in β-AR mediated augmentation of LTCC function are shown on the right (from [89]).

While the development of cardiac hypertrophy and CHF have been associated with abnormalities in specific components of the β-AR transduction pathway and may lead to diminished β-adrenergic-mediated augmentation of the L-type Ca^{2+} current, inherent defects in the phosphorylation potential of the LTCC

themselves cannot be ruled out. Specifically, a differential expression of the LTCC subunit isoforms with the development of cardiac hypertrophy and/or failure may lead to altered subunit isoform assembly of the LTCC [89].

2. METHODS

2.1. Generation of Genetically Modified Mice.

Cardiac-specific PDK1 inducible (MerCreMer-α-MHC PDK1) knockout mice (kindly given by Dr.Dario Alessi) were generated by breeding $PDK1^{floxed/floxed}$ transgenic mice where exon 3 and 4 of the pdk1 gene were flanked by loxP excision sequences [96], with mice expressing the cardiac-specific MerCreMer-α-MHC promoter-driven Cre recombinase gene (kindly given by Dr.Jeffrey D.Molkentin) [97]. The resulting background strain of the MerCreMer mice was C57BL/6-SV129 and was unchanged throughout all experiments. Control animals used in this study were $PDK1^{floxed/floxed}$ littermates not expressing the cre recombinase gene and were treated with the same tamoxifen regiment. Tamoxifen dissolved in corn oil was injected intraperitoneally once a day for 6 days at a dose of 75 μg/g body weight. Male animals 7-8 weeks old were used.

All animal procedures were performed in accordance with the Guide for the Care and Use of Laboratory Animals and approved by the Institutional Animal Care and Use Committee.

2.2. Cell culture, transfection and treatment of cells

2.2.1. Isolation of adult ventricular myocyte

Cardiomyocytes were dissociated from the ventricles of 4 month-old-mice, by methods previously described [98]. Briefly, the heart was rapidly excised and placed in Tyrode solution containing (in mM): 120 NaCl, 5.4 KCl, 1.2 NaH_2PO_4,

5.6 glucose, 20 $NaHCO_3$, 1.6 $MgCl_2$, 10 2,3-butanedione monoxime (BDM) and taurine 5 (buffer A). The heart was retrogradely perfused with buffer A for 4-5 min, then with buffer A containing 1 mg/ml trypsin and 4 mg/ml liberase 4 blendzyme (Roche) by the Langerdorff method at 37°C. After 2 min of enzyme perfusion, 50 μM Ca^{2+} was added to the enzyme solution. After ~5 min of digestion that the heart became ”swollen and soft”, the enzyme was ricirculated and the heart was perfused for an additional 8-12 min or until flow rate surpassed pre-enzyme flow rate. Only Ca^{2+} tolerant cells with clear cross striations and without spontaneous contractions or significant granulation were selected for the experiments of Ca^{2+}current measurement and fluorescent measurement of $[Ca^{2+}]_i$. Isolated cells were plated in dishes precoated with 20 μg/mL laminin (Collaborative Biomedical Products) in DMEM (Sigma) supplemented with 1 mM $CaCl_2$, 15 mM BDM, 25 mM HEPES and 100 U/ml penicillin and 0.1 mg/ml streptomycin (Euroclone). Cells were infected with an adenovector expressing either no transgene (mock), HA-E40K-Akt (AdAkt) or Akt-K179M (AdAktDN) at MOI 100 and harvested 48 h post infection. The viral vector was amplified and purified in 3% Sucrose/PBS by ViraQuest, Inc.

2.2.2. Cell lines and transfection

293T cells (Human Embryonic Kidney) were used for western blot analysis, calcium assay and electrophysiological experiments. This cell line was grown in DMEM (Sigma) with 10% HI-FBS (Invitrogen) and 100 U/ml penicillin and 0.1 mg/ml streptomycin (Euroclone). Transfection of 293T cells was performed in serum-starved medium (Opti-MEM I reduced-serum medium, Invitrogen) by using LipoFectamine2000 (Invitrogen) according to the manufacture’s

instructions.

293T cells were plated at 70% confluence in a 60 mm Petri dish in OptiMEM (Invitrogen) and co-transfected with a DNA mix containing 1 μg of a plasmid encoding GFP-$Ca_v\alpha_1$, 2 μg of a plasmid encoding $Ca_v\beta_2$ subunit (either $Ca_v\beta_2$–WT or $Ca_v\beta_2$–SE), 2μg of a plasmid encoding $Ca_v\beta_2$-XB, -XX, -Akt or $Ca_v\beta_2$–SE-XB,-XX, -Akt or 1 μg of a plasmid encoding GFP-$Ca_v\alpha_1$ together with 2 μg of a plasmid encoding $Ca_v\beta_2$-K141Q, -K149Q, -K161Q, -K149-161Q or $Ca_v\beta_2$-SE-K141Q, -K149Q, -K161Q, -K149-161Q. After 48 h, cells maintained in serum-free condition were used for western blot or calcium assay experiments.

For electrophysiological recordings of recombinant $Ca_v\alpha_1$ currents, experiments were performed as followed: 293T cells were plated at 50-70% confluence in a 35 mm Petri dish in OptiMEM (Invitrogen) and transfected with a DNA mix containing 1 μg of a plasmid encoding YFP-$Ca_v\alpha_1$, 2 μg of a plasmid encoding $Ca_v\beta_2$ subunit (either $Ca_v\beta_2$–WT or $Ca_v\beta_2$–SE or $Ca_v\beta_2$–SE-XB,-XX, -Akt), 0.5μg of a plasmid encoding $Ca_v\alpha_2\delta_1$ subunit and 0.1 μg of a plasmid encoding CD8. After 24 h, cells were plated at low density ~$35x10^3$ cells per 35 mm Petri dish in DMEM with or without 10% FBS for 36 h and electrophysiological recordings were performed on cells expressing both YFP-$Ca_v\alpha_1$ and CD8, which is identified using anti-CD8 coated beads (Dynabeads, Dynal).

2.3. Ca^{2+} analysis

2.3.1. Ca^{2+} current measurement.

Macroscopic $I_{Ca,L}$ was recorded at room temperature (~22 °C) using the whole-cell patch clamp technique with an Axopatch 200B amplifier (Axon Instruments, CA, USA) as previously described in native cells {Maier, 2003 #1204;Aimond, 2005 #1575}. External recording solution contained (in mM): 136 TEA-Cl, 2 $CaCl_2$, 1.8 $MgCl_2$, 10 HEPES, 5 4-aminopyridine and 10 glucose (pH 7.4 with TEA-OH). Pipette solution contained (in mM): 125 CsCl, 20 TEA-Cl, 10 EGTA, 10 HEPES, 5 phosphocreatine, 5 Mg_2ATP, and 0.3 GTP (pH 7.2 with CsOH). Myocytes were held at -80 mV and 10 mV depolarizing steps from -50 mV to +50 mV for 300 ms were applied. Analysis was performed using a microscope (Diaphot 200, Nikon) equipped with 10x NA 20 objective lenses (CFWN, Nikon) and pCLAMP9 (MDS Analytical Technologies) was used as acquisition software. Recording solutions allowed for the specific measurement of the Ca^{2+} current in the absence of contaminating Na, K, or Na-Ca^{2+} exchange currents.

For electrophysiological recordings of recombinant $Ca_v\alpha_1$ currents in cotransfected cells, the extracellular solution contained (in mM): 135 NaCl, 20 TEACl, 5 $CaCl_2$, 1 $MgCl_2$ and 10 HEPES (pH adjusted to 7.4 with KOH, ~330 mOsM). Borosilicate glass pipettes have a typical resistance of 1.5-3 MΩ when filled with an internal solution containing (in mM): 140 CsCl, 10 EGTA, 10 HEPES, 3 Mg-ATP, 0.6 GTP-Na and 2 $CaCl_2$ (pH adjusted to 7.2 with KOH, ~315 mOsM). Analysis was performed using a microscope (x71, Olympus). Data acquisition was performed with pCLAMP9 software.

2.3.2. Fluorescent measurement of $[Ca^{2+}]_i$

Isolated myocytes were loaded with 5 μM Fura-PE3 acetoxymethyl (AM) ester (TefLabs) which was dissolved in DMSO (Sigma) containing 0.02% pluronic acid for 30-35 min in buffer A (in mM: 120 NaCl, 5.4 KCl, 1.2 NaH_2PO_4, 5.6 glucose, 20 $NaHCO_3$, 1.6 $MgCl_2$, 1 Ca^{2+} and 5 taurine) and analyzed as previously described {DeSantiago, 2002 #1201;Bassani, 1994 #1202}. The Fura-PE3 fluorescence ratio was determined at RT using a Diaphot 2000 microscope, operating at an emission wavelength of 510 nm with excitation wavelength of 340 and 380 nm. The stimulating frequency for Ca^{2+} transient measurements was 0.5 Hz. Baseline amplitude (estimated by 340 nm/380 nm ratio) of the Ca^{2+} signal was acquired and data were analyzed using software from IonWizard (IonOptix).

2.3.3. Calcium Assay

2.3.3.1. Principle

The FLIPR Calcium 5 Assay kit (Molecular Devices) was used for this assay and it provides a reliable fluorescent-based assay for detecting changes in intracellular calcium. During incubation, the indicator passes through the cell membrane and esterases in the cytoplasm cleave the AM portion of the molecule. After incubation, the cells are ready to be assayed. The masking dye does not enter the cell, but significantly reduces background originating from residual extracellular fluorescence of calcium indicator, media and other components. Once the target is

activated, direct measurement of intracellular fluorescence change due to increased calcium concentration is enabled (Figure 13).

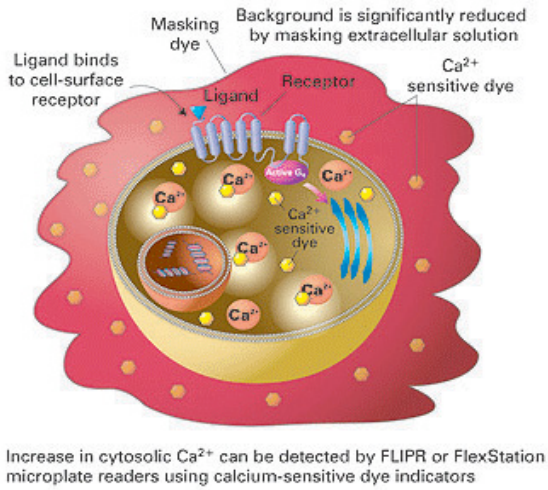

Figure 13. The FLIPR Calcium Assay kit principle for detecting changes in the intracellular calcium.

2.3.3.2. Procedure

Transfected 293T cells were seeded overnight in a 96 well plate at density ~50x10^3. Cells were incubated with 100 µl of Loading Buffer (Calcium 5 Assay Reagent Component A + 1X HBSS Buffer with 20 mM HEPES pH 7.4) for 1h at 37°C, 5% CO_2, without removing the supernatant. A final concentration of 1 µM Bay K8644 (Sigma Aldrich) as LTCC agonist was added per well with the dispenser during detection on the Synergy 2 with the following fluorescence parameters:

- Excitation wavelength: 485/20 nm
- Emission wavelength: 528/20 nm
- Automatic emission cut-off: 510 nm

The calcium kinetic collecting data last 1,30 min per well and the acquisition time was every 5 seconds. Results are expressed as relative fluorescence units (RFU) and were analyzed using Prism Software (GraphPad Software). Each experiment (n=8) is representative of a total of four independent FLIPR experiments.

2.4. Molecular cloning

2.4.1. Preparation of plasmids

Cacnb2 cDNA (complete coding sequence, cDNA clone MGC: 129335, IMAGE: 40047531; ATCC #10959168) was cloned in pcDNA3 vector. Site-directed mutagenesis was performed using the QuikChange Site-Directed Mutagenesis Kit (Stratagene). $Ca_v\alpha 1$ PEST deletion mutants and GFP fusion proteins were generated by PCR. YFP-$Ca_v\alpha 1$ expression plasmids were provided by N.Soldatov (National Institute on Aging, National Institutes of Health, Baltimore, MD, USA). A lentivirus vector was generated and used as an expression vector for siRNA-mediated silencing of the akt gene (siAkt). The sequence used (5'-tgcccttctacaaccaggatt-3') was chosen in a conserved region between rat, mouse, human and has been validated for targeting Akt-1 and -2. All constructs were confirmed by DNA sequencing.

2.4.2. DNA transformation (Heat Shock method)

The ligated DNA (5 µl), pure plasmid DNA (100 ng) or mutagenesis PCR product (2 µl) was added to 50 µl of competent cells (DH5α, Invitrogen or XL10Gold, Stratagene), which were pre-thawed on ice. The mixture was incubated on ice for 50

30 min, heat-shocked for 2 min at 37°C water and immediately put back on ice for 1 min. 250 µl pre-warmed LB was added to the mixture, followed by shaking at 37°C for 1h. Everything was spread on LB agar plates containing the appropriate antibiotic.

2.4.3. DNA ligation

50 ng of vector DNA and 3-fold molar excess of insert was combined, followed by addition of T4 ligase (1U/µl) and 10X Ligation Buffer (New England Biolabs). The total volume was adjusted with H_2O to 10 µl and the mixture was incubated ON at 16°C. 5 µl of the ligation producted was used for transformation.

2.4.4. DNA preparation

2.4.4.1. Small-scale preparation

The Wizard Plus SV Minipreps DNA Purification System (Promega) provides a simple and reliable method for rapid isolation of small-scale plasmid DNA. 5 ml overnight bacteria culture was harvested by centrifugation for 5 min at 5000 x g and the supernatant was discarded. Pellet was completely resuspended in Cell Resuspension Solution [50 mM Tris-HCl (pH 7.5), 10 mM EDTA and 100 µg/ml RNase A] by vortexing, followed by the addition of Cell Lysis Solution (0.2 M NaOH and 1% SDS). After incubation of the mixture for 5 min at RT, Alkaline Protease Solution was added, followed by another 5 min incubation. The bacterial lysate was centrifuged at 14000 x g for 10 min, immediately after the addition of Neutralization Solution (4.09 M guanidine hydrochloride, 0.759 M potassium

acetate and 2.12 M glacial acetic acid, pH 4.2). The cleared lysate was transferred to the Spin column and centrifuged for 1 min at 14000 x g at RT. Column Wash Solution [162.8 mM potassium acetate, 22.6 mM Tris-HCl (pH 7.5) and 0.109 mM EDTA (pH 8.0) previously diluted with 95% ethanol was added to the Spin Column, followed by another centrifugation. The wash procedure was repeated one more time eluting the DNA with Nuclease-Free Water or TE buffer [10 mM Tris-HCl (pH 7.5) and 1 mM EDTA].

2.4.4.2. Large-scale preparation

Large-scale plasmid DNA isolation was carried out by using the Pure Yield Plasmid Maxiprep System (Promega), according to the manifacturer's instruction. The 200 ml overnight bacteria culture was harvested by centrifugation for 10 min at 5000 x g and the supernatant was discarded. The pellet was completely resuspended in Cell Resuspension Solution by vortexing, followed by the addition of Cell Lysis Solution. The bacterial lysate was centrifuged at 14000 x g for 20 min, immediately after the addition of Neutralization Solution. Then the supernatant was poured into PureYield Maxi Binding Column and it was applied maximum vacuum, followed by washing with Endotoxin Removal Wash (previously diluited with isopropanol) and Column Wash. The DNA was eluted in Nuclease-Free Water before centrifugation at 2000 x g for 5 min.

2.4.5. DNA purification

The Wizard SV Gel and PCR Clean-Up System (Promega) is designed to extract and purify DNA fragments of 100bp to 10kb from standard agarose gel or to purify PCR products directly from a PCR amplification.

The DNA was excided from the agarose gel with scalpel and weighted. Three volumes (100 mg ~100 µl) of Membrane Binding Solution [4.5 M guanidine isothiacyanate, 0.5 M potassium acetate (pH 5)] were added to solubilize the gel slice completely by incubating at 55°C for 5 min.

An equal volume of Membrane Binding Solution was added to PCR reactions.

The dissolved gel mixture or prepared PCR product were transferred to SV Spin Column and, after an incubation of 1 min at RT, centrifugated at 16000 x g for 1 min. The column was washed twice with Membrane Wash Solution [10 mM potassium acetate, 80% ethanol, 16.7 µM EDTA (pH 8)]. The DNA was eluted in Nuclease-Free Water before centrifugation at 14000 x g for 1 min.

2.4.6. PCR (Polymerase chain reaction)

PCR was performed by using the Platinum Pfx DNA Polymerase kit (Invitrogen) and the primers were synthetized by Primm, Milan (Italy).

Three different nucleotide sequences encoding either the whole $Ca_V\beta_2$ terminal coiled coil region or two shortest sequences encompassing the Akt consensus site (RXXRS/T) were cloned in pcDNA3 vector. Cacnb2 wt and Cacnb2-SE (Ser625 of the Akt consensus site was replaced by Glutamate to mimic Akt phosphorylation, S625E) were used as template.

Three couples of oligonucleotide containing the XbaI (tctaga) and BamHI (ggatcc) restriction sites were designed for PCR amplification:

1) β_2 -XB, β_2 -SE XB: 585 bp (1383-1965 nt Cacnb2)

Xba Fw : 5'gctctagaatgccaccctcccagcggtaacctcc

Bam Rw : 5'gggatcccgctggagccactctgttgagatggca

2) β_2 -XX, β_2 -SE XX: 273 bp (1383-1656 nt Cacnb2)

Xba Fw: 5'gctctagaatgccaccctcccagcggtaacctcc

X 1 Rw: 5'cgggatcctcaagagtcaaacgtctcttgcctagagagg

3) β_2 -Akt, β_2 -SE Akt, lenght insert: 108 bp (1458-1566 nt Cacnb2)

Akt Fw: 5'gctctagaatgcccaccctcgcctctaattcacagggttt

Akt Rw: 5'cgggatcctcatttgacgggttctaggcaaggttcttcttc

The PCR reaction was performed by a DNA pre-denaturation for 5 min at 94°C and followed by 5 cycles of DNA denaturation at 94°C for 30 sec, primer annealing at 66°C for 30 sec and DNA extension at 72°C for 1 min and by 25 cycles of DNA denaturation at 94°C for 30 sec and DNA extension at 72°C for 1 min. The reaction was maintained at 4°C after a final step of DNA extension at 72°C for 10 min.

The following PCR conditions were used:

Mix	**Volume**
10X Pfx Amplification Buffer	5 µl
10mM dNTP mixture	1.5 µl
50mM $MgSO_4$	1 µl
primer mix (10 µM each)	1.5 µl

template DNA (100ng)	x µl
Platinum Pfx DNA polymerase	0.4 µl
dH_2O	Up to volume
TOT	50 µl

Zero Blunt TOPO PCR Cloning (Invitrogen) was used for direct insertion of PCR products into a plasmid vector pCR-Blunt II-TOPO as followed:

Reagent	**Volume**
Fresh PCR product	0.5 to 4 µl
Salt solution	1 µl
Water	Add to a final volume of 5 µl
pCRII-Blunt-TOPO vector	1 µl
Final volume	6 µl

After a 5 min incubation, 2 µl of TOPO Cloning product each were transformed into competent E.coli cells. Cells were plated on agar plates containing Kanamycin resistance gene carried by the plasmid.

2.4.7. Site-directed mutagenesis

Site-directed mutagenesis was performed using the QuikChange Site-Directed Mutagenesis Kit (Stratagene):

- to replace Serine (tcc) with Glutamate (gag) to have S625E in the Cacnb2 template:

SE Fw: 5'aacatgtggacgggtatggagcacaccgcga

SE Rw: 5'tcgcggtgtgctccatacccgtccacatgtt

- to replace Lysine (aaa) with Glutamine (caa) in the amino acidic sequence found to interact with $Ca_v\beta_2$-SE .

As template Cacnb2 wt and Cacnb2-SE were used to have the following mutations: K141Q, K149Q, K161Q and K149-161Q or SE-K141Q, SE-K149Q, SE-K161Q and SE-K149-1611Q.

The mutagenic oligonucleotide primers that contained the desired mutation were:

1) Lys 141 Fw: 5'gccatctccttcgaggccCaagattttctg
   Lys 141 Rw: 5'cagaaaatcttgggcctcgaaggagatggc
2) Lys 149 Fw: 5'catgttaaagaaCaatttaataatgactggtggatgga
   Lys 149 Rw: 5'tcctatccaccagtcattattaaattgttctttaacatg
3) Lys 161 Fw: 5'tggataggacggctggttCaagaaggctgtgaa
   Lys 161 Rw: 5'ttcacagccttcttgaaccagccgtcctatcca

The following PCR conditions were used:

Mix	**Volume**
10X Reaction Buffer	5 µl
dNTP mix	1 µl
Quick solution	3 µl
125 ng primer Fw	x µl
125 ng primer Rw	x µl
template DNA (10 ng)	x µl
PfuUltra HF DNA Polymerase	1 µl
dH_2O	up to µl volume
total volume	51 µl

The PCR reaction was performed by a DNA pre-denaturation for 1 min at 95°C and followed by 18 cycles of DNA denaturation at 95°C for 50 sec, primer annealing at 60°C for 50 sec and DNA extension at 68°C for 7 min. The reaction was maintained at 4°C after a final step of DNA extension at 68°C for 7 min.
After addition of 1 µl of DpnI (10U/µl) at 37°C for 1 hour to digested the non-mutated supercoiled dsDNA, XL10-Gold Ultracompetent cells were transformed with 2 µl of the DpnI-treated DNA following the manufacturer's instruction. The mutated DNA was confirmed by DNA sequencing.

2.5. Western blot analysis and Antibodies

Proteins expression was evaluated in total lysates or cell fractions by Western blot analysis according to standard procedures. Samples were homogenized in RIPA buffer (150 mM NaCl, 10 mM Tris pH 7.2, 0.1 % SDS, 1% Triton-X100, 5 mM EDTA, 100 µM Na_3VO_4, 10 mM NaF, Protease inhibitor 1X (Thermo Fisher Scientific), loaded onto a 4-12% or 10-20% NuPAGE Tris-Glycine Gel, or 3-8% NuPAGE Tris-Acetate Gel (Invitrogen), separated by electrophoresis and trasferred to a PVDF membrane (Millipore).
Antibodies against the following proteins were used:

Primary antibodies	**Dilution**	**Company**
Mouse anti CACNA1	1:500	Abcam
Mouse anti DHPR $Ca_v\alpha_1$	1:500	Abcam
Rabbit anti CACNB2 Rabbit anti $Ca_v\beta_2$	1:500 1:500	Abcam Provided by Dr.Haase
Rabbit anti PDK1	1:1000	EMD

Rabbit anti Akt pan, pAkt-Thr308	1:1000	Cell Signaling Technology
Rb anti –phospho-(Ser/Thr) Akt substrate (PAS)	1:1000	Cell Signaling Technology
Rabbit anti HA	1:500	Abcam
Rabbit anti tubulin	1:2000	Novus Biological
Rabbit anti GAPDH	1:2500	Cell Signaling Technology

All protein levels were normalized to GAPDH or tubulin. Horseradish peroxidase-conjugated secondary antibodies (Goat anti mouse and Goat anti rabbit-HRP, 1:10000) and ECL (Thermo Fisher Scientific) were used for protein detection with GBox iChemi System (Syngene). Image J software (National Institutes of Health) was used to perform densitometry analysis.

2.6. Pulse chase and immunoprecipitation experiments

36 h post transfection, 293T cells were starved for 30 minutes in methionine- and cysteine-free DMEM medium (Sigma) and then were labeled for 30 minutes by adding 500 μCi [35S]-L-methionine and 2 mM L-cysteine. Radioactive media was eventually washed out with PBS (time 0 pulse) and replaced with normal DMEM. Time points were at 4, 10 and 25 h post pulse. Labeled cells were then lysed in RIPA buffer, lysates incubated on ice for 30 min and centrifuged at 400 x g for 15 min. The supernatants (500 μg of protein) were eventually used for immunoprecipitation experiments with anti-GFP polyclonal IgG (GTX20290). Immunoprecipitates were separated on a 3-8% SDS–PAGE gel and exposed to X-

ray film. Radioactivity was quantitated with ImageQuant 5.2 software (GE Healthcare).

2.7. GST pull-down assay

Affinity-purified GST fusion proteins were generated using pGEX system (GE Healthcare) and phosphorylated as described below. GST fusion protein bound to glutathione-Sepharose 4B beads (GE Healthcare) was incubated with 25 µl of ^{35}S-labeled Met with moderate shacking at 25 °C for 2 h in 200 µl of binding buffer containing 20 mM Hepes, pH 7.9, 1 mM EDTA, 10 % glycerol, 0.15 M KCl, 0.05 % NP-40 and 1 mM DTT. ^{35}S-labeled probes were generated from the C-terminal region of $Ca_v\alpha1$ cDNA fragments under control of the T7 promoter using the TnT Quick Coupled Reticulocyte Lysate System L1170, Promega), washed three times with washing buffer (20 mM Hepes, pH 7.9, 1 mM EDTA, 10 % glycerol, 250 mM KCl and 0.1 %NP-40) and centrifuged. Bound proteins were eluted in SDS sample buffer, subjected to SDS-PAGE and detected by autoradiography by incubation with recombinant Akt (Millipore). In brief, 5 µg GST-$Ca_v\beta2$ or GST beads were incubated at 30°C for 45 min in a 50 µl solution containing 2 µg activated kinase, 10 mM Hepes-KOH, pH 7.5, 50 mM γ–glycerophosphate, 50 mM NaCl, 1 mM dithiothreitol, 10 mM $MnCl_2$ and 1 mM ATP.

2.8. Yeast two hybrid screening

2.8.1. Principle

The yeast two-hybrid system (Y2H) can be used to identify novel protein interactions by screening cDNA libraries, to confirm suspected interactions and to define interacting domains.

In the Y2H system a bait gene is expressed as a fusion to the Gal4-binding domain (DNA-BD), while libraries of prey proteins are expressed as fusions to the Gal4 activation domain (AD; [99]). When bait and library (prey) fusion proteins interact, the DNA-BD and AD are brought into proximity to activate transcription of four independent reporter genes (AUR1-C, ADE2, HIS3 and MEL1) (Figure 14).

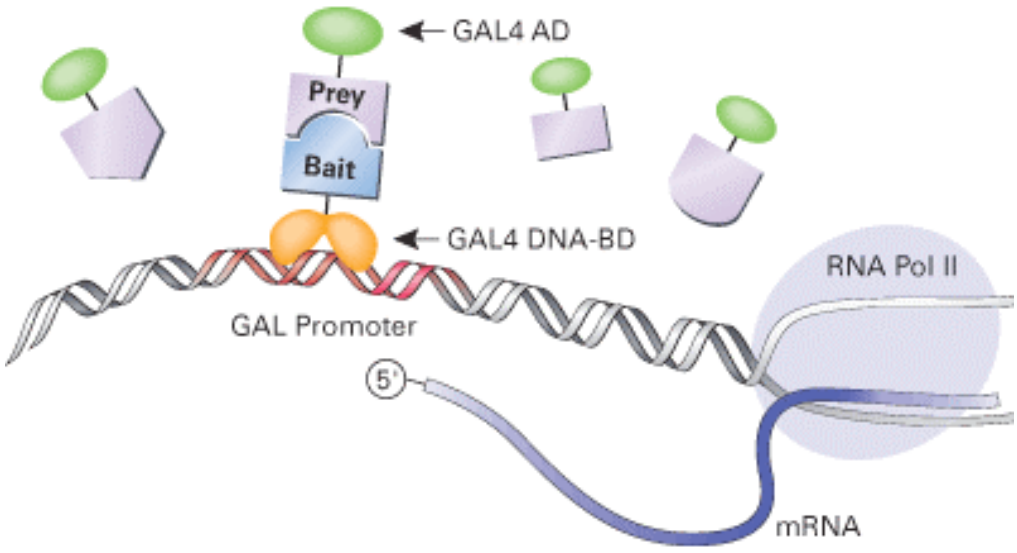

Figure 14. The Yeast Two Hybrid system principle.

There are four integrated reporter genes under the control of three distinct Gal4-responsive promoters (Figure 15):

1) AUR1-C. A dominant mutant version of the AUR1 gene that encodes the enzyme inositol phosphoryl ceramide synthase. AUR1-C is expressed in Y2HGold Yeast Strain in response to protein-protein interactions that bring the GAL4 transcriptional activation and DNA binding domains into close proximity. In *Saccharomyces cerevisiae*, its expression confers strong resistance (AbA^r) to the otherwise highly toxic drug Aureobasidin A. This drug reporter is preferable to nutritional reporters alone, due to lower background activity.

2) HIS3. Y2HGold is unable to synthetize histidine and is therefore unable to grow on media that lack this essential amino acid. When bait and prey proteins interact, Gal4-responsive His 3 expression permits the cell to biosynthetize histidine and grow on –His minimal medium.

3) ADE2. Y2HGold is also unable to grow on minimal media that does not contain adenine. However, when two proteins interact, Ade2 expression is activated, allowing these cells to grow on –Ade minimal medium.

4) MEL1. MEL1 encodes α-galactosidase, an enzyme occurring naturally in many yeast strains. As a result of two-hybrid interactions, α-galactosidase (MEL1) is expressed and secreted by the yeast cells. Yeast colonies that express Mel1 turn blue in the presence of the chromagenic substrate X-α -gal.

Three promoters controlling the four reporter genes AUR1-C, HIS3, ADE2 and MEL1 in Y2HGold are unrelated except for the short protein binding sites in the UAS region that are specifically bound by the Gal4 DNA-BD. Thus, library

proteins that interact with unrelated sequences flanking or within the UAS (i.e., false positives) are automatically screened out.

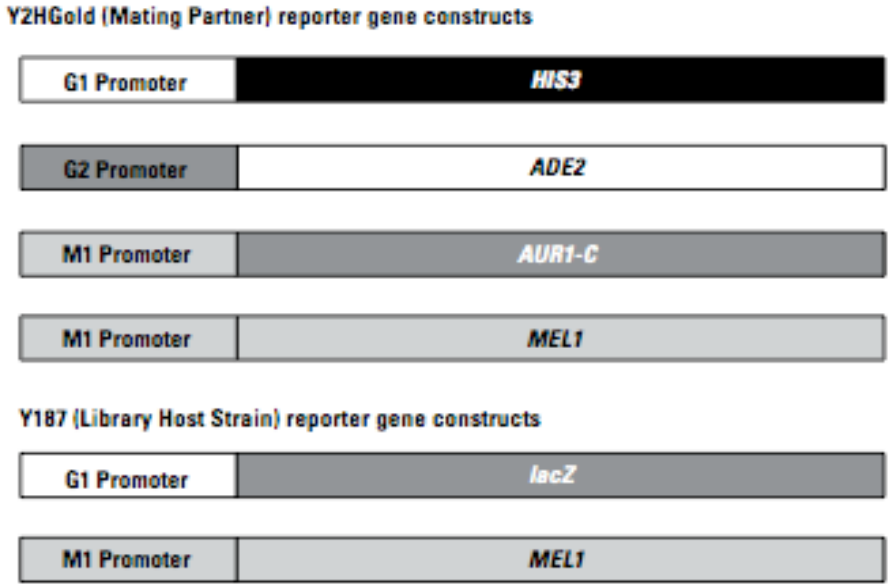

Figura 15. Reporter gene constructs in Matchmaker yeast strains. In Y2HGold, the HIS3, ADE2 and MEL1/AUR1-C reporter genes are under the control of three completely heterologous Gal4-responsive promoter elements-G1, G2 and M1, respectively. The protein-binding sites within the promoters are different, although each is related to the 17-mer consensus sequence recognized by Gal4.

After cotransformations of the bait and the prey plasmids into the yeast host strain, the transformants are plated on minimal medium lacking Leu, Trp, His and Ade to select for those clones that contain both types of plasmid (i.e, Leu^+, Trp^+,His^+, Ade^+). To further eliminate false positives, candidates prey plasmids are tested for reporter gene activation when cotransformed into yeast cells in combination with the bait vector (without insert), the bait plasmid and an unrelated bait plasmid with an unrelated noninteracting protein.

2.8.2. Procedure

2.8.2.1. Cloning and screening

Cacnb2-wt and Cacnb2-SE cDNAs were used to perform Y2H screens. Amplified PCR product were cloned in frame into the pGBKT7 vector to obtain GAL4 DNA-BD fusion. (In-Fusion Advantage PCR Cloning kit, Clontech). The following PCR conditions were used:

Mix	**Volume**
10X Pfx Amplification Buffer	5 µl
10 mM dNTP mixture	1.5 µl
50 mM $MgSO_4$	1 µl
Primer mix (10 µM)	1.5 µl
Template DNA (200 ng)	x µl
Platinum Pfx DNA Polymerase	0.4 µl
dH_20	Up to volume
TOT	50 µl

The PCR reaction was performed by a DNA pre-denaturation for 5 min at 94°C and followed by 5 cycles of DNA denaturation at 94°C for 30 sec, primer annealing at 56°C for 30 sec and DNA extension at 72°C for 1 min and by 25 cycles of DNA denaturation at 94°C for 30 sec and DNA extension at 72°C for 2 min. The reaction was maintained at 4°C after a final step of DNA extension at 72°C for 10 min.

PCR primers were designed that share 16 bp of homology with the sequence at the ends of the linearized vector pGBKT7 (in order to keep the BamHI and EcoRI sites intact) and 24 bp homology to our bait (Cacnb2-wt and -SE):

1) beta 2 Fw: 5'catggaggccgaattc gtcccaaagcgacacgtccaagtcg
2) beta 2 Rw: 5'gcaggtcgacggatcc ctcgccagcctcattccttctctt

After obtaining pure PCR product with a single specific band and no background, the PCR product was treated with DpnI per 1 h at 37°C and Spin-column purified with Wizard SV PCR clean-up system (Promega) following manifacturer's instructions.

Then purified PCR insert and vector together at a 2:1 molar ratio were mixed as follows in the In-Fusion cloning reaction:

MIX	**VOLUME**
5X In-fusion reaction buffer	2 µl
In-Fusion Enzyme	1 µl
Vector pGBKT7	x µl
Purified PCR insert (b2 wt or SE)	x µl
H_2O (as needed)	x µl
Total volume	10 µl

The reaction was incubated for 15 min at 37°C, followed by 15 min at 50°C, then placed on ice. The reaction volume was brought up to 50 µl with TE buffer, pH 8

and mixed well. Competent *E.coli* cells were transformed with 2.5 µl of the diluted In-Fusion reaction mixture, following the transformation protocol. Each transformation reaction was spread on LB plate containing the appropriate antibiotic and incubated overnight at 37°C. The next day, isolated colonies were picked and plasmid DNA was isolated with the standard method of Wizard Plus SV Miniprep (Promega), according to the manufacturer's instruction. To determine the presence of insert, DNA was checked by sequencing. For screening, bait constructs were transformed into Saccharomyces cerevisiae, strain Y2HGold (Matchmaker Gold Yeast Two-Hybrid System, Clontech). Subsequently, cells were transformed with either human or mouse heart cDNA expression libraries in the pGADT7-Rec prey vector (Mate & Plate Libraries, Clontech).

2.8.2.2. Transformation of bait plasmid

5 ml of synthetic dropout (SD) medium was inoculated with the bait yeast strain Y2HGold and grown overnight at 30°C with maximal shaking. The following morning, OD_{600} was measured and 50 ml of YPD was inoculated with $2.5x10^8$ cells ~ $5x10^6$ cells/ml (OD_{600} ~ $3x10^7$ cells/ml). After 3-4 hours of incubation with maximal shaking until the cell titer reached $2x10^7$ cells/ml, cells were harvested by centrifugation at 3000g for 5 min. Cells were washed with H_2O and 0.1 M LiAc and after completely removing the H_2O, the following components from the YeastMaker Yeast Transformation System 2 (Clontech) were added in the given order :

- 2.4 ml 50% PEG
- 360 µl 0.1 M LiAc

- 50 µl 10 mg/ml Herring testis carrier DNA

- 1.05 ml H_2O

After vigorously shaking, 400 µl of transformation mixture were added to each transformation tube containing 1 µg of each plasmid:

1) Bait plasmid (pGBKT7+ beta 2 SE) plated on -T

2) Bait plasmid (pGBKT7+ beta 2 SE) + library plasmid plated on –TL or -TL/X-α-gal

3) Bait plasmid (pGBKT7+ beta 2 SE) + library plasmid plated on –HTLA/ -HTLA/AbA^r/ X-α-gal

After incubation at 30°C for 30 min, reactions were incubated at 42°C for 30 min and subsequently cooled in ice-water. 1 ml of water was added to each tube and the cells were collected by centrifugation. Cells were resuspended in 100 µl of water and plated on SD-plates lacking the amino acids Trp$^-$, Leu$^-$ and/or His$^-$Ade$^-$. Plates were incubated at 30°C until colonies appeared (~5 days). Transformation 2) showed the transformation frequency, while transformation 3) was used to test if the bait was autoactivating, *i.e.* could activate the expression of the reporter gene in the absence of the GAL4 binding domain. Typically, no colonies should grow on this plate.

2.8.2.3. Transformation of the yeast strain containing the bait plasmid plasmid with the chosen library

50 ml of SD- Trp$^-$ medium was incubated with bait containing yeast colonies and

incubated overnight at 30°C with maximal shaking. As described above, cells were diluted at $5x10^6$ cells/ml in 150 ml of YPDA and incubated for approximately 4.5 h until the cell titer reached $2x10^7$ cells/ml. Cells were harvested and pooled , washed with water and 0.1 M LiAc and the following component from the YeastMaker Yeast Transformation System 2 were added:

- 7.2 ml 50% PEG

- 1.08 µl 0.1 M LiAc

- 150 µl 10 mg/ml Herring testis carrier DNA

- 30 µg of library plasmid DNA (pGADT7-Rec, Matchmaker, Clontech)

- 2.1 ml H_2O

After vigorously mixing, the transformation mixture was incubated for 30 min at 30°C shaking, then for 30 min at 42°C and subsequently cooled in ice. Cells were collected by centrifugation, then resuspended in 10 ml of water and plated out on 50 large 150 mm SD-TL/AbA^r/ X-α-gal. Plates were incubated at 30°C for up to 7 days until colonies appeared. Colonies were picked, restreaked onto higher stringency SD-HTLA/AbA^r/ X-α-gal plates.

To eliminate any positive colonies containing the $Ca_v\alpha_1$ constructs, yeast colony PCR was performed with oligos designed to recognize the AID domain (Ca_v α 1 interaction domain):

- AID Fw: 5' tcacggtgttccagtgcatcacc
- AID Rw: 5' atcactcaggccgaagacatcga

The PCR reaction was performed by a DNA pre-denaturation for 5 min at 94°C and followed by 30 cycles of DNA denaturation at 94°C for 30 sec, primer

annealing at 60°C for 30 sec and DNA extension at 72°C for 1 min.The reaction was maintained at 4°C after a final step of DNA extension at 72°C for 10 min.

The remaining library plasmids from yeast were rescued using the Easy Yeast Plasmid Isolation Kit (Clontech), following the manufacturer's instructions. Plasmids were transformed into E.coli, the DNA was purified and then sequenced using a standard T7 primer.

Colonies were re-transformed into yeast with either the bait or the prey vector using the transformation protocol that was used for the initial test of the bait plasmid (transformation of bait plasmid), to confirm that the positive interactions are genuine:

1) bait + candidate prey plated on SD-LT/X-α-gal and SD-HTLA/AbA^r/ X-α-gal plates (blue colonies expected)
2) empty pGBKT7 + candidate prey plated on SD-LT/ X-α-gal (white colonies expected) and SD-HTLA/AbA^r/ X-α-gal plates (no expected colonies)

Co-Immunoprecipitation assay from mammalian cell extracts (transfected 293T cells) allowed to identify and double-confirm true physical interaction between the bait cloned in plasmid pXJ40-cMyc (pXJ40-cMyc beta2-SE) and the preys cloned in the plasmid pXJ40-HA (pXJ40-HA Ms or H prey).

2.9. Statistical Analysis

Statistical comparison was performed within at least three independent experiments by paired or unpaired Student's t-test, whereas comparison between groups was analyzed by one-way repeated-measures analysis of variance (ANOVA) combined with a Newman-Keuls post-test to compare different values using Prism 4.0 software (GraphPad Software, CA). Differences with $P<0.05$ were considered statistically significant.

3. RESULTS

3.1. Characterization of mice lacking PDK1 expression

To gain insight into the mechanism of action by which Akt regulates $I_{Ca,L}$ and Ca^{2+} handling in the heart, we studied a mouse line with tamoxifen-inducible [97] and cardiac-specific deletion of PDK1, the upstream activator of all three Akt isoforms. Mice in which exons 3 and 4 of the pdk1 gene were flanked by loxP excision sequences [100] were crossed with transgenic (Tg) mice expressing an inducible and cardiac-specific MerCreMer α-MHC promoter driving the cre recombinase gene [97], resulting in MerCreMer α-MHC PDK1 mice (KO). Similar to the muscle creatine kinase-Cre PDK1 mouse model [100], PDK1 gene deletion in the adult mouse heart (KO) (Figure 16A) resulted in a lethal phenotype with a mortality that reached 100% at 10 days after tamoxifen injection (Figure 16B) [101].

Age-matched littermate control mice without cre (wildtype (WT)) were unaffected by tamoxifen treatment. Consistent with findings from the previously reported analysis of the PDK1 KO mouse model [100], cardiac function evaluated by echocardiography at 7 days after tamoxifen injection, revealed dramatically impaired systolic function with severe dilated cardiomyopathy and an abrupt drop in fractional shortening in KO, but not in WT mice (Figure 16C). Histological examination substantiated the echocardiographic findings, revealing significant dilatation of both ventricles and atria (Figure 16D) [101].

These observations indicate that PDK1/Akt activity plays a major role in maintaining adult heart function.

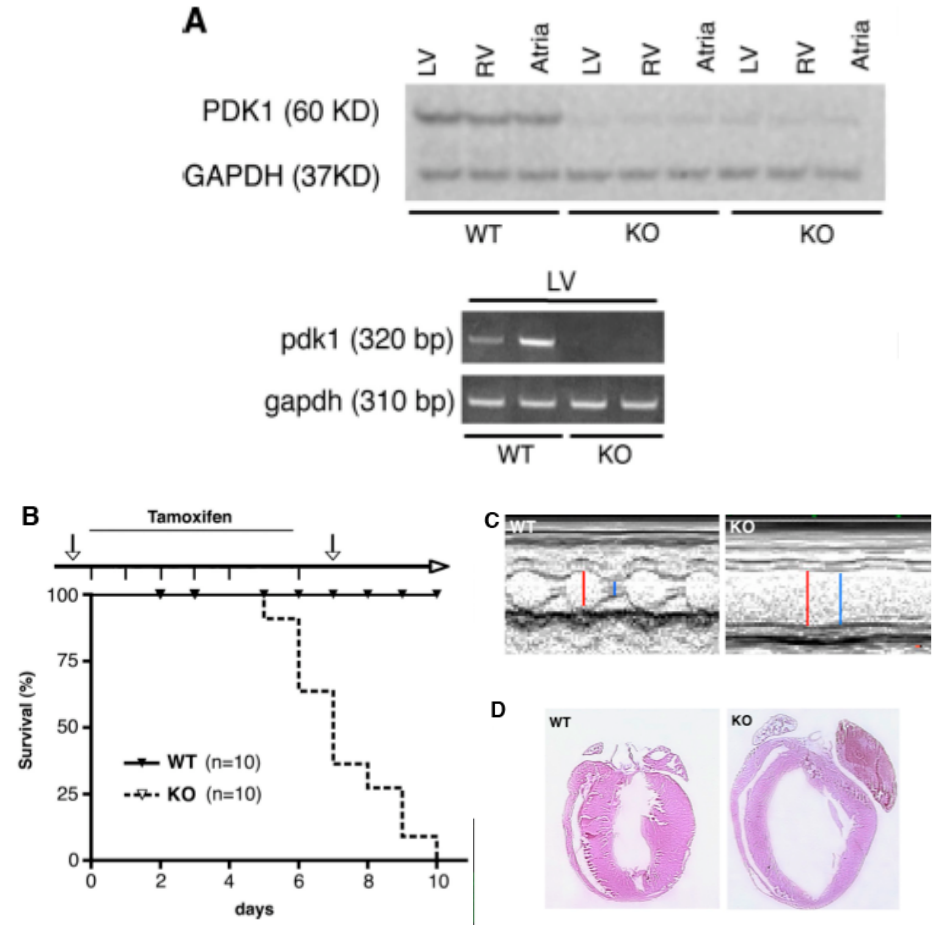

Figure 16. Characterization of mice lacking PDK1 expression. A) PDK1 protein and RNA levels assessed by western blot (top) and RT-PCR (bottom) analysis of atria and left (LV) and right (RV) ventricular CMCs from WT and KO mice. Protein and RNA loading were normalized to GAPDH levels. B) Survival curve for mice lacking PDK1 (KO) in the heart. Mortality begins 5 d after tamoxifen injection and reaches 100% by day 10 after the beginning of the treatment. Time point of tamoxifen injections (hash marks) and echocardiography analysis (arrows) are shown (n=10). C) Echocardiographic (M mode) assessment of LV size and function. Left ventricular diastolic internal dimensions (red lines) and Left ventricular systolic internal dimensions (blue lines) were increased in ko mice. Heart rates were 486 bpm and 511 bpm in the wt and the ko hearts, respectively. D) Ematoxylin- and eosin-stained paraffin sections show severe dilatation and thinning of ko hearts.

3.2. Deficiency in Akt activity leads to a reduction in the $Ca_v\alpha_1$ protein level

Using this cardiac specific PDK1 knockout mouse model, we investigated whether deficiency in Akt activity results in changes in expression or activation of signaling molecules that are implicated in Ca^{2+} handling and cardiac function. Western blot analysis of extracts from WT and KO mouse ventricle revealed striking changes in protein expression upon induction of the PDK1 knockout (Figure 17A-B). Notably, KO mice had decreased protein levels of the pore-forming Ca^{2+} channel subunit ($Ca_v\alpha_1$), which progressed as PDK1 protein expression gradually declined. No change in the protein level of the regulatory $Ca_v\beta_2$ subunit was observed. As PDK1 expression decayed, levels of Akt activation also dramatically decreased (assessed by phosphorylation of Akt at the PDK1 phosphorylation site, Thr308), despite unaltered expression of total Akt protein (Figure 17A-B). Based on this evidence, we decided to perform further experiments by day 6 after the beginning of treatment.

Although the main physiological action of PDK1 is on Akt activation, PDK1 can potentially influence other members of the cAMP-dependent, cGMP-dependent and protein kinase C (AGC) kinase protein family, such as PKC and PKA, which could also affect the cellular Ca^{2+} handling [96, 102]. However, PKC activity was unchanged, no apparent effect of PDK1 deletion on SERCA2a as well as PKA activity because the phosphorylation of specific PKA regulatory sites in two SR Ca^{2+}-regulatory proteins, ryanodine receptor (Ryr2-P2809) and phospholamban (PLN; PLN-P16) were unchanged in KO mice [101].

Taken together, these data suggest that an acute reduction in Akt activation affects expression of proteins involved in the Ca^{2+} influx through the cell.

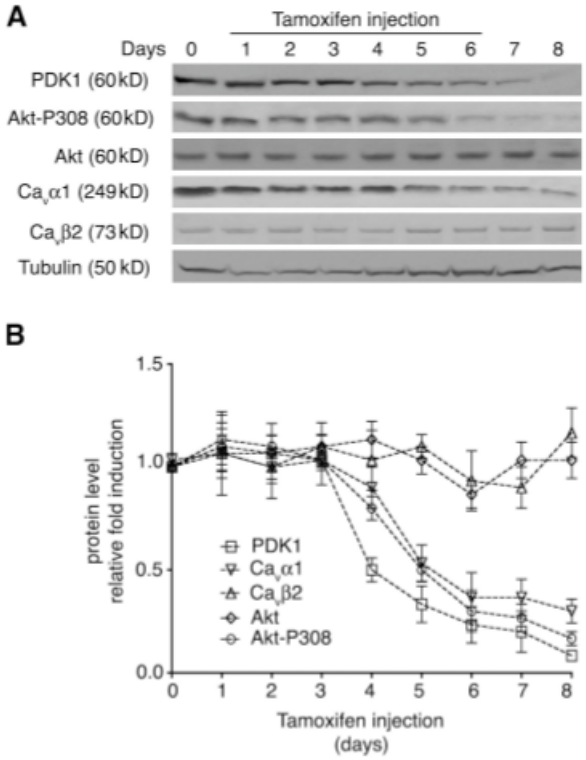

Figure 17. Alteration of Ca^{2+} handling proteins in PDK1 KO CMCs. A) Western blot and B) densitometric analysis of ventricular homogenates along a time course of tamoxifen inductions (day 1-6 treatment is indicated by the line in A) using various antibodies. A representative experiment is shown (n=3). Error bars show SD.

3.3. Deficiency in Akt activity affects $I_{Ca,L}$

Ca^{2+} handling and inotropism were examined in adult cardiomyocytes freshly isolated from WT and KO mice. Using the whole-cell voltage-clamp technique, we recorded and analyzed LTCC $I_{Ca,L}$ properties. No difference in cell size was observed between WT and KO cells as deduced from membrane capacitance (Mc) measurements. Mc was 116±6 pF in WT cells (n=18) and 115±6 pF in KO cells (n=18). However, the density of $I_{Ca,L}$ (pA/pF) was decreased in KO vs. WT (Figure 18B). At 0 mV, density of $I_{Ca,L}$ was -9.08±0.96 pA/pF in KO cells (n=12) vs. -16.26±0.96 pA/pF in WT cells (n=12; $p<0.001$). In addition, there was no significant difference in either steady-state activation or inactivation curves (data not shown). Indeed, mean half activation occurred at -12.97±0.53 mV in WT cells vs. -15.07±0.66 mV in KO cells and mean half inactivation occurred at -31.11±0.48 mV in WT cells vs. -30.77±0.42 mV in KO cells. The absence of a shift in the voltage-dependence of these properties (Figure 18B) was consistent with the absence of modification in gating properties of the LTCC, suggesting that a reduction in the number of functional LTCCs can account for the observed decrease in $I_{Ca,L}$ in KO mice. Of note, the decay kinetics of $I_{Ca,L}$ was slower in KO cells compared to WT cells with a decrease in the early fast inactivating component (Figure 18A). Consistent with previous observations by us and others regarding the role of Akt in cardiac function [15, 47, 49, 103], contraction (Figure 18C) and systolic Ca^{2+} amplitudes (Ca^{2+} transients) (Figure 18D) were significantly depressed (by ~35% and 30%, respectively, $P<0.05$) in KO cardiomyocytes compared to WT littermates.

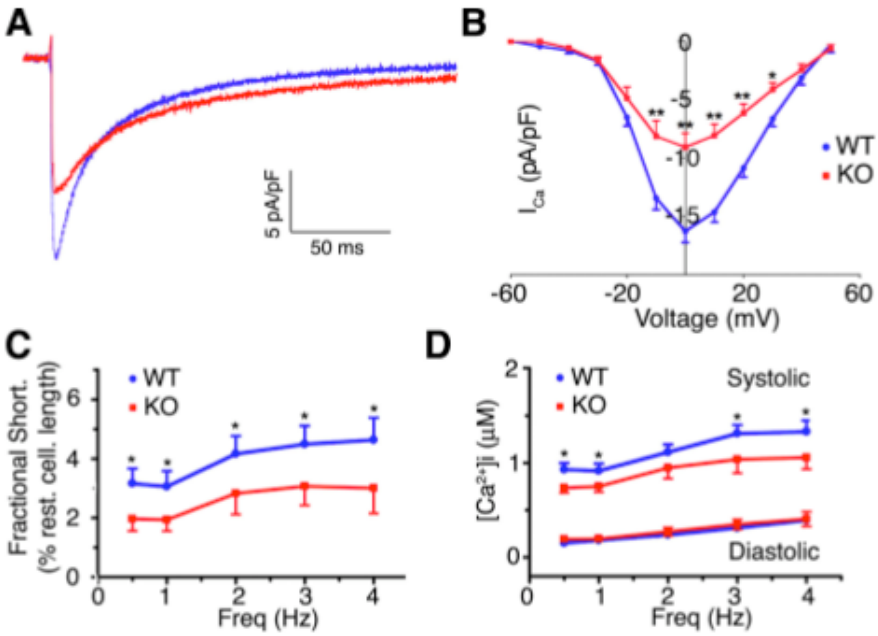

Figure 18. Impaired intracellular Ca^{2+} handling and contractility in PDK1 KO CMCs. (A and B) Smaller Ca^{2+} current in KO CMCs. A) Whole cell representative $I_{Ca,L}$ currents normalized for difference in cell size. B) $I_{Ca,L}$ I-V current/voltage relationships (n=12; *, P < 0.05; **, P<0.01). C and D) CMC contraction and Ca^{2+} shortening is decreased in KO compared with WT CMCs (*, P<0.05; ANOVA). Error bars show SEM.

The observed reduction cardiac contractility could be explained by reduced Ca^{2+} entry into cells via the LTCC, but decreased intracellular Ca^{2+} release from the sarcoplasmic reticulum (SR) may also contribute. This is consistent with the observed slowing of the early fast inactivation of $I_{Ca,L}$ (Figure 18A), which is highly dependent on CICR-triggered SR Ca^{2+} release during the action potential [52]. Therefore, we conclude that the reduced $I_{Ca,L}$ may contribute to the reduced contractility in KO hearts.

3.4. Akt regulates the $Ca_v\alpha_1$ protein level at the plasma membrane

The properties of the $Ca_v\alpha_1$ subunit are known to be markedly affected by LTCC accessory subunits [61, 104]. Among the LTCC accessory subunits expressed in the heart, $Ca_v\beta_2$ is known to act as a chaperone for the $Ca_v\alpha_1$ subunit, both as a positive modulator of channel opening probability and for its trafficking from the endoplasmic reticulum (ER) to the plasma membrane [105, 106]. Because $Ca_v\beta_2$ is the only LTCC accessory subunit containing an Akt-phosphorylation consensus site [105], we hypothesized that $Ca_v\beta_2$ might lose this chaperone activity in the absence of Akt-induced phosphorylation, resulting in $Ca_v\alpha_1$ protein degradation. In support of this hypothesis, forced expression of the active E40K-Akt mutant restored $Ca_v\alpha_1$ protein levels in isolated cardiomyocytes from KO mice (Figure 19A). Similarly, cardiomyocytes from transgenic mice expressing constitutively active HA-E40K-Akt (Tg Akt) [15] showed increased $Ca_v\alpha_1$ levels compared to WT controls (Figure 19B).

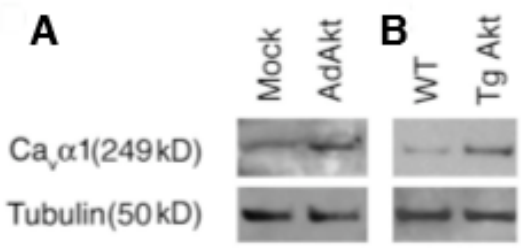

Figure 19. Akt mediates regulation of $Ca_v\alpha_1$ protein density at the plasma membrane. $Ca_v\alpha_1$ protein levels in KO CMCs infected with empty (mock) or active E40K-Akt (AdAkt) expressing adenoviral vector (A) and in whole lysates of WT and E40K-Akt (Tg Akt) hearts (B).

3.5. Akt is determinant for $Ca_v\alpha_1$ protein level regulation by direct phosphorylation of the $Ca_v\beta_2$ chaperone-subunit

To assess whether Akt is directly involved in modulation of $Ca_v\beta_2$ chaperone activity in the heart, we first confirmed the interaction between Akt and $Ca_v\beta_2$. Ventricular homogenates derived from either WT or Tg Akt mice were immunoprecipitated with anti-HA antibody and assayed for $Ca_v\beta_2$, which revealed association of the $Ca_v\beta_2$ subunit with active Akt (Figure 20A).

To determine whether $Ca_v\beta_2$ can be phosphorylated by Akt, $Ca_v\beta_2$-immunoprecipitates from cardiac homogenates were incubated with recombinant active Akt and [γ-^{32}P]ATP. A band corresponding to phosphorylated $Ca_v\beta_2$ was detected only in the presence of the kinase (Figure 20B, left).

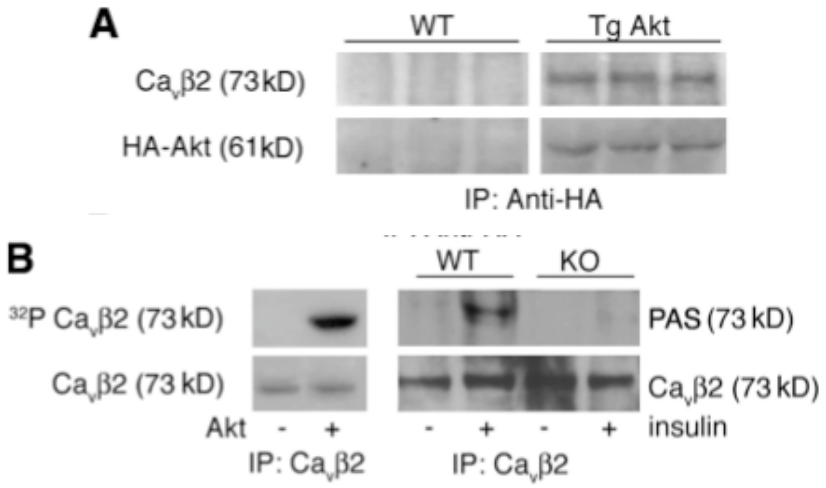

Figure 20. Akt interacts with and phosphorylates $Ca_v\beta_2$. A) Coimmunoprecipitation assay of Akt and $Ca_v\beta_2$. Ventricular homogenates from WT and HA-E40K-Akt Tg mice (Tg Akt) immunoprecipitated with antibodies against HA and immunoblotted for $Ca_v\beta_2$ as well as HA as a control. B) Examination of $Ca_v\beta_2$ phosphorylation by Akt. In vitro kinase assays were performed with immunoprecipitation $Ca_v\beta_2$ incubated with recombinant active Akt and ^{32}P-labeled ATP (left) or immunoprecipitated $Ca_v\beta_2$ from WT and KO cardiac extracts from mice treated or not treated with 1 mU/g insulin using phospho-Akt substrate (PAS) antibody (right).

To determine whether the $Ca_v\beta_2$ subunit was phosphorylated by Akt *in vivo*, we treated overnight-starved mice with 1 mU/g insulin, which causes activation of Akt [107]. 20 min post treatment, $Ca_v\beta_2$ was immunoprecipitated from ventricular homogenates, subjected to Western blot analysis and probed for phosphorylated Akt consensus sites using PAS (Phospho-Akt Substrate) antibody. This revealed insulin-stimulated phosphorylation of $Ca_v\beta_2$ in WT but not in KO hearts (Figure 20B, right). Taken together, these data demonstrate that Akt binds to and phosphorylates $Ca_v\beta_2$, the chaperone for $Ca_v\alpha_1$.

To directly assess whether Akt phosphorylation of $Ca_v\beta_2$ protects $Ca_v\alpha_1$ from protein degradation, we constructed a mutant of $Ca_v\beta_2$, in which the Serine contained in the putative Akt-consensus site (R-X-X-R-S/T) was replaced by Glutamate ($Ca_v\beta_2$-SE) to mimic phosphorylation. Cotransfection of 293T cells with $Ca_V\alpha_1$ and $Ca_v\beta_2$-SE resulted in $Ca_V\alpha_1$ protein levels that were increased compared to those found when cotransfected with $Ca_v\beta_2$-WT (Figure 21A). Similarly, $Ca_V\alpha_1$ expression was increased in insulin treated $Ca_v\beta_2$-WT cotransfected cells (Figure 20A). Notably, the active phosphomimic $Ca_v\beta_2$-SE also counteracted the downregulation of $Ca_V\alpha_1$ induced by an Akt inhibitor (Figure 21B).

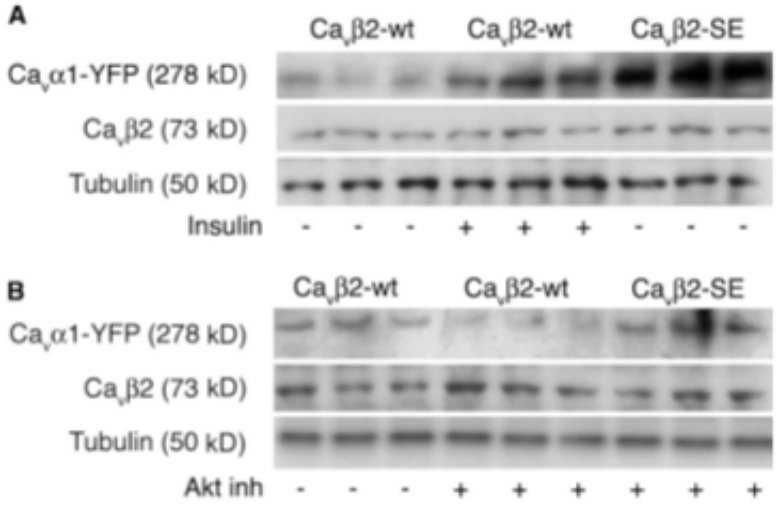

Figure 21. Akt phosphorylation of $Ca_v\beta_2$ protects $Ca_v\alpha_1$ from protein degradation. A) YFP- $Ca_v\alpha_1$- cotransfected 293T cells with the mutant variant $Ca_v\beta_2$-SE. Cells were serum starved overnight and treated with 100 µM insulin (A) or 5 µM Akt inhibitor (Akt inh (B) as indicated. The expression of YFP- $Ca_v\alpha_1$ in lysates was monitored by western blot analysis with anti-YFP antibody and normalized as assed on transfection efficiency ($Ca_v\beta_2$) and protein amount (tubulin; n=3).

To support the evidence that Akt-dependent phosphorylation of $Ca_v\beta_2$ is determinant for $Ca_v\alpha_1$ stability and functionality, we measured the effect of the $Ca_v\beta_2$-SE mutant on Ca^{2+} current. While cotransfection of cells with $Ca_v\alpha_1$ and $Ca_v\beta_2$-WT resulted in significant depressed $I_{Ca,L}$ in serum-free medium compared to serum-containing medium where Akt is phosphorylated, cotransfection of $Ca_v\alpha_1$ and $Ca_v\beta_2$-SE mutant completely counteracted this reduction (Figure 22A-B).

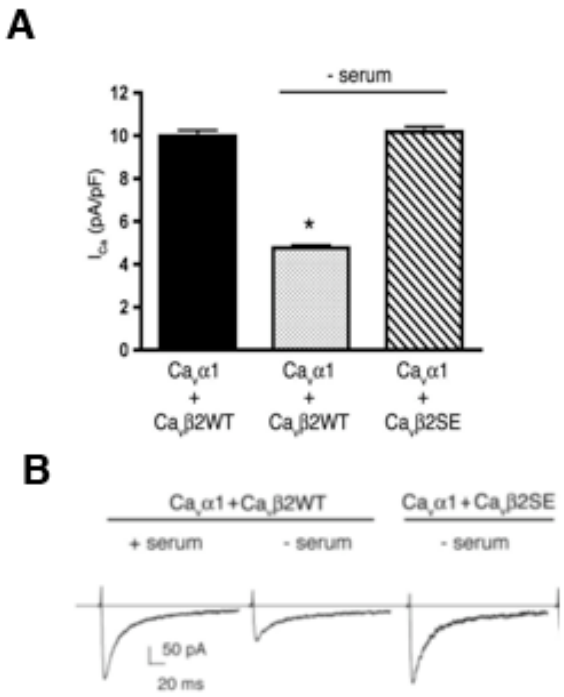

Figure 22. Akt phosphorylation of $Ca_v\beta_2$ preserves $Ca_v\alpha_1$ currents. A) Ca^{2+}currents recorded in co-transfected 293T cells with YFP- $Ca_v\alpha_1$ and $Ca_v\beta_2$-WT or $Ca_v\beta_2$-SE mutant cultivated for 36 h in the presence or absence of 10% FBS. B) Representative current traces are shown. n> 35 at each condition (*, P< 0.05 compared with YFP- $Ca_v\alpha1$; ANOVA). Error bars show SEM.

3.6. Akt regulates $Ca_v\alpha_1$ protein stability

PEST sequences have been suggested to serve as signals for rapid proteolytic degradation through the cell quality control system [108-111]. Notably, PEST-mediated protein degradation has recently been suggested to play an essential role in modulating neuronal Ca^{2+} channel function through regulation of the $Ca_v\beta_3$ accessory subunit [111]. Our findings raise the possibility that processing of the $Ca_v\alpha1$ protein may be affected in a similar way. To test this hypothesis, we used the web-based algorithm PESTFind {Rogers, 1986 #1198} in a search for

potential $Ca_v\alpha_1$ PEST sequences and found several putative motifs (aa 435-460; 807-820; 847-858; 1732-1745; 1839-1865). Intriguingly, the highest-scored potential PEST sequences obtained are highly conserved among species (Table 5), with one located in the I–II linker of the $Ca_V\alpha_1$ subunit and overlapping with the α_1-interacting domain (AID), the primary binding region for $Ca_V\beta_2$ [58].

Species	Fragment	Sequences	PESTfind score
Mouse	PEST I	435-KGYLDWITQAEDIDPENEDEGMDEDK-460	8.45
Rat	PEST I	476-KGYLDWITQAEDIDPENEDEGMDEDK-501	8.45
Human	PEST I	446-KGYLDWITQAEDIDPENEDEGMDEEK-471	8.66
Mouse	PEST II	807-KSITADGESPPTTK-820	9.45
Rat	PEST II	848-KSITADGESPPTTK-861	9.45
Mouse	PEST III	837-HSNPDTAGEEDEEEPEMPVGPR-858	19.51
Rat	PEST III	878-HSNPDTAGEEDEEEPEMPVGPR-899	19.51
Human	PEST II	845-KSPYPNPETTGEEDEEEPEMPVGPR-869	20.26
Mouse	PEST IV	1,732-KTGNNQADTESPSH-1,745	5.5
Rat	PEST IV	1,772-KTGNNQADTESPSH-1,785	5.5
Mouse	PEST V	1,839-RMSEEAEYSEPSLLSTDMFSYQEDEH-1,865	5.86
Human	PEST IV	1,937-HDTEACSEPSLLSTEMLSYQDDENR-1,961	7.54
Human	PEST V	2,214-RGAPSEEELQDSR-2,226	7.71

Table 5. PEST sequences are highly conserved in $Ca_V\alpha_1$. Occurrence of PEST sites within the amino acid sequence of $Ca_V\alpha_1$ from the mouse, rat and human. Amino acid identity is underlined.

To determine whether these PEST sequences are involved in $Ca_v\alpha_1$ degradation control, we generated two in-frame deletion mutants encompassing either the I-II ($Ca_v\alpha_1$-ΔP) or II-III ($Ca_v\alpha_1$-ΔH) cytosolic linker region (Figure 22A). A pulse-chase analysis, with a chase starting 36 h post-cell starvation, revealed that both $Ca_v\alpha_1$-ΔP and $Ca_v\alpha_1$-ΔH exhibited markedly increased protein stability compared to $Ca_v\alpha_1$-WT (Figure 22C). In particular, $Ca_v\alpha_1$-WT showed a short half-life typical of proteins containing PEST sequences [112] with a rapid and progressive degradation starting 4 h from the chase and reaching 50% of degradation 25 h after the chase. In contrast, $Ca_v\alpha_1$-ΔP and $Ca_v\alpha_1$-ΔH mutants were less sensitive to degradation and were degraded by only 23% and 15% after 25 h, respectively

(P<0.001). Notably, cotransfection of $Ca_v\beta_2$-SE with $Ca_v\alpha_1$-WT resulted in a considerable increase in the half-life of $Ca_v\alpha_1$-WT (Figure 22C).

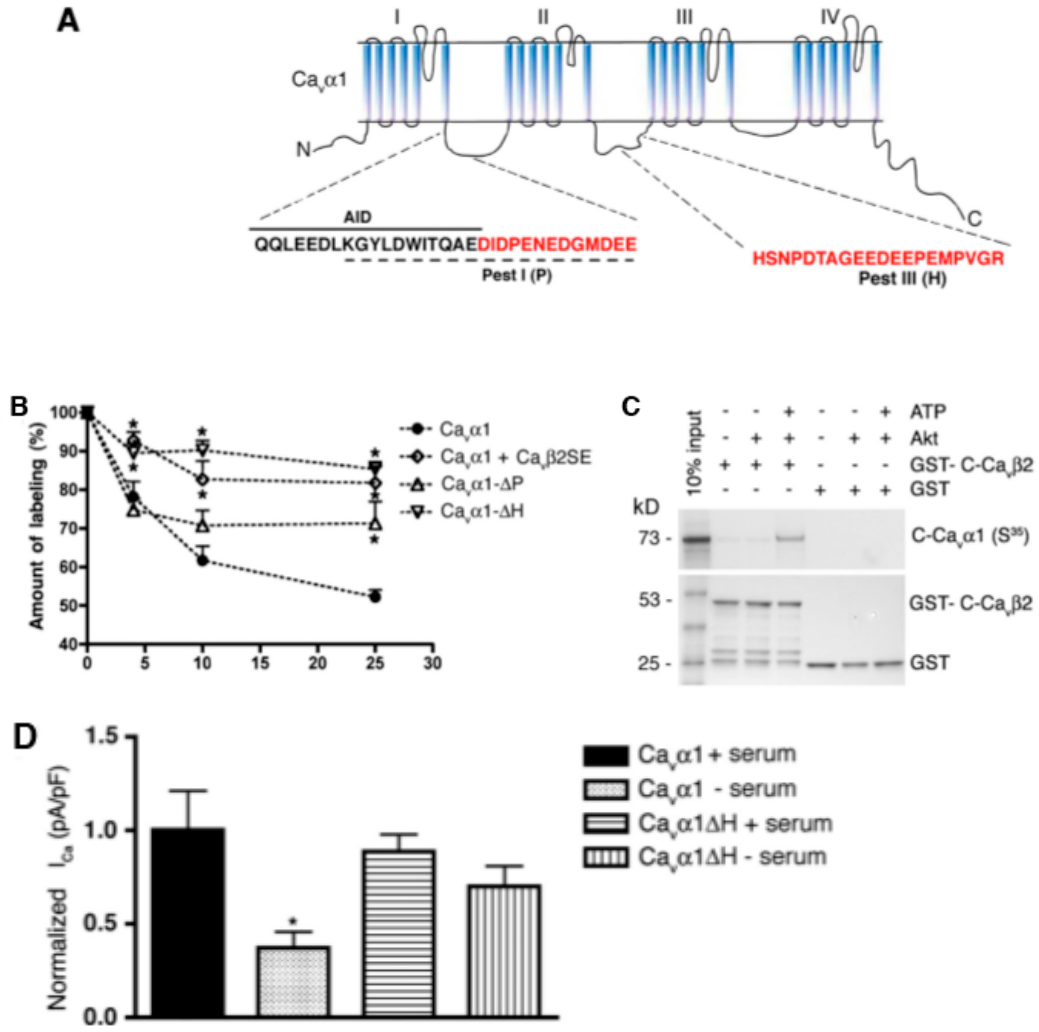

Figure 23. Rapid protein degradation PEST sequences determine $Ca_v\alpha_1$ protein instability. A) Schematic representation of $Ca_v\alpha_1$ mapping the AID and PEST sequences in the I-II and II-III cytosolic loops. Deleted PEST sequences (P and H) are highlighted in red. B) Half-lives of WT $Ca_v\alpha_1$ subunit (alone or cotransfected with $Ca_v\beta_2$-SE) and its in-frame ΔPEST mutants ($Ca_v\alpha_1$-ΔH and $Ca_v\alpha_1$-ΔP) were determined in 293T cells. After ON starvation, transfected cells were pulse chased and analyzed along a time course (*, P<0.001 compared with $Ca_v\alpha1$; ANOVA; n=3). C) The $Ca_v\alpha_1$C terminus interacts with the Akt phosphorylated GST- $Ca_v\beta_2$ coiled-coil region. D) $I_{Ca,L}$ recorded in 293T cells

cotransfected with $Ca_v\beta_2$-WT or either $Ca_v\alpha_1$-WT or $Ca_v\alpha_1$-ΔH and cultivated for 36 h in presence or absence of 10%FBS.

Notably, direct interaction took place between the Akt-phosphorylated $Ca_v\beta_2$ C-terminal coiled-coil region and the $Ca_v\alpha_1$ C-terminal domain (Figure 23C). No interaction was found with other $Ca_v\alpha_1$ cytosolic domains, although it cannot be excluded that other binding sites may exist.

To assess whether PEST-deleted $Ca_v\alpha_1$ channels are still functional, traffic appropriately to the membrane and associate with the $Ca_v\beta_2$ subunit, we measured Ca^{2+} current in $Ca_v\alpha_1$-ΔH mutant-transfected cells. No significant differences in $I_{Ca,L}$ were found in cells transfected with $Ca_v\alpha_1$-WT compared to $Ca_v\alpha_1$-ΔH. Conversely, although serum deprivation resulted in $I_{Ca,L}$ reduction in $Ca_v\alpha_1$-WT transfected cells, no significant changes were observed in $Ca_v\alpha$1-ΔH mutant-transfected cells (Figure 23D). Current densities (pA/pF) were normalized to the control condition and n >35 at each condition ($_*$, $P<0.05$ compared with $Ca_v\alpha_1$;ANOVA). This confirms that PEST-deleted $Ca_v\alpha_1$-ΔH is resistant to rapid protein degradation and maintains its integrity and physiological function.

Taken together, our results suggest that Akt-mediated phosphorylation of $Ca_v\beta_2$ C-terminal coiled coil regulates $Ca_v\alpha_1$ density through protection of $Ca_v\alpha_1$ PEST motifs from the cell protein degradation machinery. Impairment of this mechanism is expected to result in dysregulation of cardiomyocyte contractile function .

3.7. Akt-phosphomimetic $Ca_v\beta_2$ constructs mediate LTCC density

To search for potential Akt-phosphomimetic constructs active on LTCC density control, we cloned three different nucleotides sequences encoding either the whole $Ca_V\beta_2$ terminal coiled coil region ($Ca_v\beta_2$-XB, 194 aa) or two shortest sequences ($Ca_v\beta_2$-XX of 91 aa and $Ca_v\beta_2$-Akt of 36 aa) encompassing the Akt consensus site above identified (Figure 24). $Ca_V\beta_2$ wt and $Ca_v\beta_2$-SE cDNAs were used as templates.

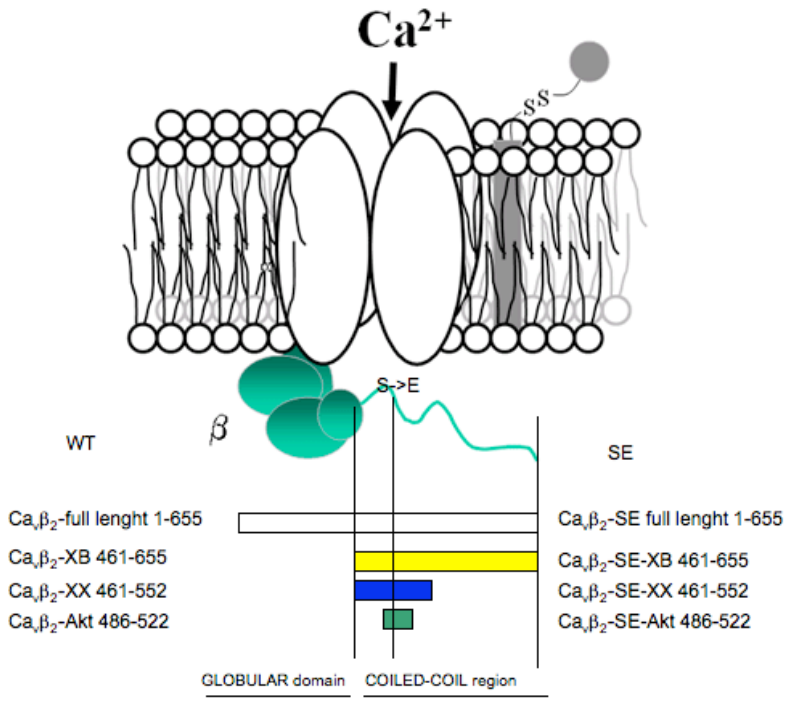

Figure 24. Identification of potential Akt-phosphomimetic constructs active on LTCC density control: the $Ca_v\beta_2$-wt control ($Ca_v\beta_2$-XB, $Ca_v\beta_2$-XX, $Ca_v\beta_2$-Akt) and the phosphomimetic $Ca_v\beta_2$-constructs ($Ca_v\beta_2$-SE-XB, $Ca_v\beta_2$-SE-XX, $Ca_v\beta_2$-SE-Akt).

First, to determine the effect of Akt-phosphomimetic constructs effect on $Ca_v\alpha_1$ protein stability, each $Ca_v\beta_2$ wt control ($Ca_v\beta_2$-XB, $Ca_v\beta_2$-XX or $Ca_v\beta_2$-Akt) or

phosphomimetic-β_2 construct ($Ca_v\beta_2$-SE-XB, $Ca_v\beta_2$-SE-XX or $Ca_v\beta_2$-SE-Akt) was cotransfected in 293T cells together with plasmids encoding $Ca_v\alpha_1$ and $Ca_V\beta_2$. Western blot analysis showed that upon serum removal, both $Ca_v\beta_2$-SE-XB and $Ca_v\beta_2$-SE-XX were able to maintain $Ca_v\alpha_1$ protein levels when compared to WT conditions. A mild effect was found with the shortest $Ca_v\beta_2$-SE Akt (Figure 25A).

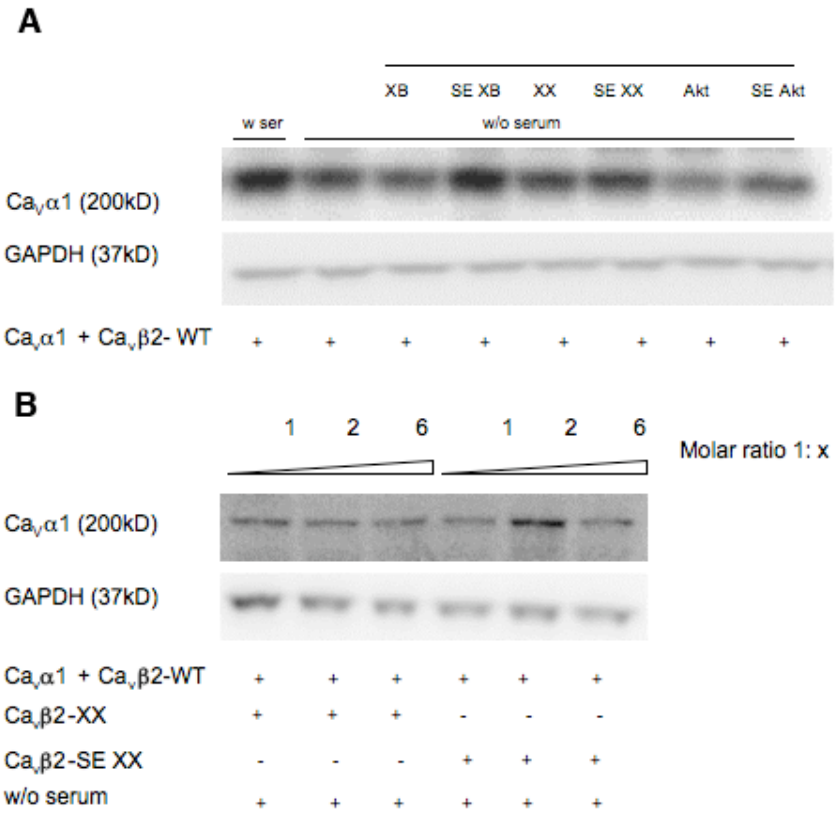

Figure 25. Akt phosphomimetic constructs effect on $Ca_v\alpha_1$ protein stability. A) Western blot analysis in 293T cells cotransfected with each $Ca_v\beta_2$-wt control ($Ca_v\beta_2$-XB, $Ca_v\beta_2$-XX or $Ca_v\beta_2$-Akt) o or Akt-phosphomimetic $Ca_v\beta_2$-constructs ($Ca_v\beta_2$-SE-XB, $Ca_v\beta_2$-SE-XX or $Ca_v\beta_2$-SE-Akt) for monitoring $Ca_v\alpha_1$ levels. Protein levels were normalized to GAPDH. B) Western blot analysis in 293T cells cotransfected with different concentrations of $Ca_v\beta_2$ -wt or $Ca_v\beta_2$ –SE constructs. Protein levels were normalized to GAPDH.

Recently, oligomerization of $Ca_v\beta_2$ subunits has recently been suggested to play an essential role in modulating Ca^{2+} channel function [113]. Therefore, to evaluate the presence of any possible effect of $Ca_v\alpha_1$:β_2-peptide stoichiometric on $Ca_v\alpha_1$ stability, an increasing molar ratio of $Ca_v\alpha_1$:β_2-peptide was used. Results showed the 1:2 ratio to be the optimal condition (Figure 25B). Based on this evidence, we decided to perform further experiments with this experimental setting.

To establish whether the effect of the phosphomimetic $Ca_v\beta_2$-SE constructs on $Ca_v\alpha_1$ protein leads to an increased stability of pore subunits that are also functional, $I_{Ca,L}$ was measured in 293T cells cotransfected with each construct. While cotransfection of cells with $Ca_v\alpha_1$ and $Ca_v\beta_2$-WT resulted in significant depressed $I_{Ca,L}$ in serum-free medium (3,06 ± 0,82 pA/pF, n=11) compared to serum-containing medium (5,08 ± 1,86 pA/pF, n=9) where Akt is phosphorylated, cotransfection of $Ca_v\alpha_1$ and each of $Ca_v\beta_2$-SE-XB, $Ca_v\beta_2$-SE-XX, or $Ca_v\beta_2$-SE-Akt constructs led to a significant counteract effect on $I_{Ca,L}$. In particular, remarkable increase of $I_{Ca,L}$ was found when cells were cotransfected with $Ca_v\beta_2$-SE-XB (4,21 ± 0,88 pA/pF, n=17). Similarly but to a lesser extent, $I_{Ca,L}$ increased in cells cotransfected with $Ca_v\beta_2$-SE-XX (3,2 ± 0,7 pA/pF, n=12), while no increase was found with $Ca_v\beta_2$-SE-Akt (1,91 ± 0,65 pA/pF, n= 9) (Figure 26A).

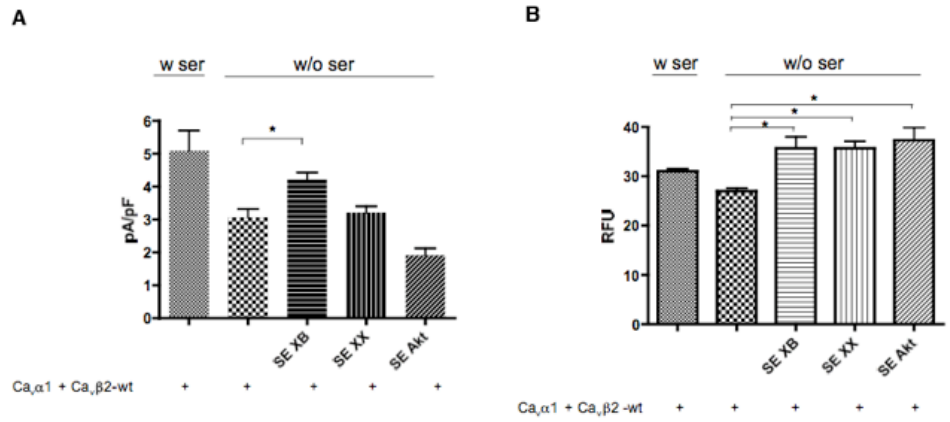

Figure 26. $Ca_v\beta_2$-SE constructs lead to stable as well as functional $Ca_v\alpha_1$ protein. A) $I_{Ca,L}$ measurement in 293T cells cotransfected with each $Ca_v\beta_2$-SE-XB, $Ca_v\beta_2$-SE-XX, or $Ca_v\beta_2$-SE-Akt together with plasmids encoding $Ca_v\alpha_1$ + $Ca_v\beta_2$ cultivated for 36 h in presence or absence of 10% FBS. B) Fluorescent-based calcium assay for analyzing changes in intracellular calcium flux in cells cotransfected with each $Ca_v\beta_2$-SE-XB, $Ca_v\beta_2$-SE-XX, or $Ca_v\beta_2$-SE-Akt together with plasmids encoding $Ca_v\alpha_1$ + $Ca_v\beta_2$ cultivated for 48 h in presence or absence of 10% FBS. (*, P< 0.05 compared with $Ca_v\beta_2$ w/o serum condition; ANOVA). BayK8644 (1 µM) was used for LTCC activation. Here a representative experiment is shown (n=4). Error bars show SEM.

Finally, to further validate the effect of these constructs on $Ca_v\alpha_1$ protein stability and function, a fluorescence-based calcium assay was used for analyzing changes in LTCC-mediated intracellular calcium flux. While cotransfection of cells with $Ca_v\alpha_1$ and $Ca_v\beta_2$-WT determined a calcium flux reduction upon serum removal, a significant increase of calcium flux (~32% ,*, $P<0.05$) was found when cells were cotransfected with $Ca_v\beta_2$-SE-XB, $Ca_v\beta_2$-SE-XX or $Ca_v\beta_2$ -SE-Akt constructs together with plasmids coding for $Ca_v\alpha_1$ with $Ca_v\beta_2$.

In conclusion, the three Akt-phosphomimetic constructs ($Ca_v\beta_2$-SE-XB, $Ca_v\beta_2$-SE-XX, or $Ca_v\beta_2$-SE-Akt) resulted with protective action toward $Ca_v\alpha_1$ protein stability and function.

3.8. Akt-phosphorylated $Ca_v\beta_2$ C-terminal tail interacts with the globular domain of the $Ca_v\beta_2$

A yeast two-hybrid system approach was employed to establish whether the Akt-dependent phosphorylation of $Ca_V\beta_2$ might be a trigger for the recruitment of other protein interacting partners involved in $Ca_v\alpha_1$ protein stability modification. $Ca_V\beta_2$-SE (bait) was screened versus both adult human and mouse heart cDNA expression libraries (preys). 11 and 91 positive clones were obtained from human and mouse libraries, respectively. To exclude any clones corresponding to $Ca_v\alpha_1$, the main interactor of $Ca_v\ \beta_2$, yeast colony PCR was performed with oligos designed to recognize the AID domain ($Ca_v\alpha_1$ interaction domain). 7 and 22 $Ca_v\ \alpha_1$ clones were obtained from the human and mouse colonies, respectively, and thus discarded. The remaining clones were subjected to DNA isolation, sequencing and classification as shown in Table 6. Surprisingly, 1 (human) and 3 (mouse) clones resulted with an aminoacid sequence (ISFEAKDFLHVKEKFNNDWWIGRLVKEGCEI) that corresponds to the globular region of the $Ca_v\ \beta_2$ bait itself.

HUMAN HEART LIBRARY	MOUSE HEART LIBRARY	
VDAC 1 (1 clone)	ZFHX4 (6 clones)	TROPONIN T (6 clones)
ADIPSIN (1 clone)	LRIT2 (7 clones)	TROPONIN I (6 clones)
NADH DEHYDROGENASE (1 clone)	TNNI3K (5 clones)	MITOCHONDRIAL PROTEINS (4 clones)
CACNB2 (1 clone)	cKAP (3 clones)	ATP SYNTHASE (6 clones)
CACNA1 (7 clones)	HSP16 (11 clones)	28s rRNA (2 clones)
	DYNEIN (7 clones)	NADH DEHYDROGENASE (2 clones)
	CACNB2 (3 clones)	CACNA1 (22 clones)
11 clones	91 clones	

Table 6. Potential interactors of the bait $Ca_V\beta_2$-SE obtained in the human and mouse heart library, respectively. They were classified as i) of potential interest and ii) false positive (mithocondrial proteins, ATP synthase, 28rRNA, NADH dehydrogenase, HSP16).

Retransformation of yeast cells with the $Ca_V\beta_2$-SE bait and $Ca_V\beta_2$ preys confirmed an interaction that was similar in intensity to a positive control consisting of a p53 bait with a large T-antigen prey. However, no interaction was found when the same preys were cotransformed with $Ca_V\beta_2$ WT bait, thus corroborating the presence of a mechanism of action that rely on Akt-dependent phosphorylation (Figure 27).

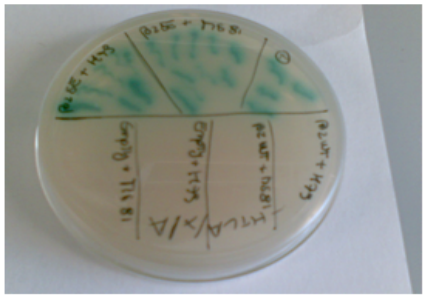

Sample	Colonies	Interaction
$Ca_V\beta_2$-SE bait + MOUSE candidate prey	+	yes
$Ca_V\beta_2$-SE bait + HUMAN candidate prey	+	yes
Empty + MOUSE candidate prey	-	-
Empty + HUMAN candidate prey	-	-
$Ca_V\beta_2$ wt bait + MOUSE candidate prey	-	no
$Ca_V\beta_2$ wt bait + HUMAN candidate prey	-	no

Figure 27. Validation in yeast of the interaction of the human (H79) and mouse (Ms81) candidate preys with $Ca_V\beta_2$-SE bait after cotransformation. No colonies were obtained when the same preys were cotransformed with $Ca_V\beta_2$ wt bait.

Subsequently, co-immunoprecipitation of either $Ca_V\beta_2$-mouse or $Ca_V\beta_2$-human from lysates of cotransfected cells with either these two proteins also pulled down $Ca_V\beta_2$-SE (data not shown).

Sequence overlapping of the 3 mouse sequences (Seq.1-3) and 1 human sequence (Seq.4) obtained, identified a minimal common region of interaction with the $Ca_V\beta_2$-SE bait (in bold in Figure 28A). We named this minimal region as Tail Interacting Domain (TID).

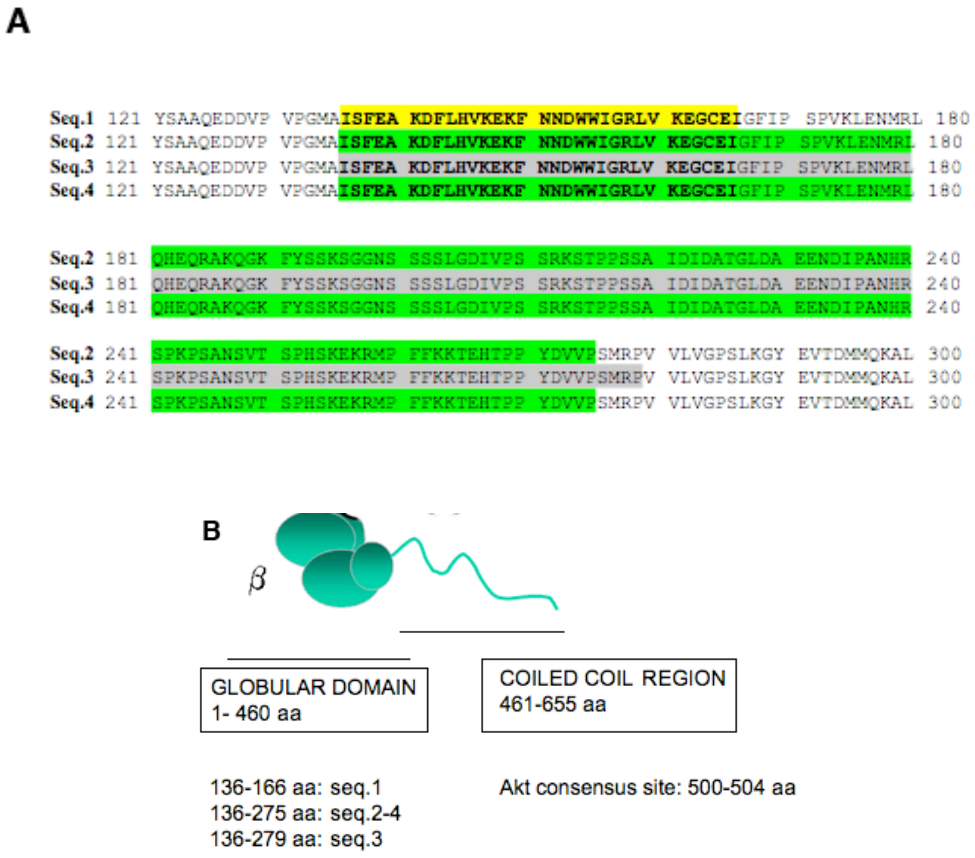

Figure 28. A) Sequence overlapping of the 3 mouse sequences (Seq.1-3) and 1 human sequence (Seq.4) identified a minimal common region of interaction with the $Ca_V\beta_2$-SE bait (in bold). Sequence 1 (136-166 aa), Sequence 2 (136-275 aa), Sequence 3 (136-279 aa), Sequence 4 (136-275 aa). B) Structure of $Ca_v\beta_2$ subunit: the globular domain, the coiled-coil region and the sequences obtained in the Y2H screening.

Evaluation of the $Ca_v\beta_2$ 3D protein structure showed that TID sequence lyes in a solvent exposed cleft of the globular domain and thus accessible to potential protein-protein interaction (Figure 29). Intriguingly, in line with this and with the hypothesis that the interaction of the Akt-phosphorylated tail (negatively charged) might relay on accessible positively charged aminoacids, 3 Lysines (K141, K149, K161) were identified in the TID sequence (ISFEAKDFLHVKEKFNNDWWIGRLVKEGCEI).

A

```
1   MVQSDTSKSP PVAAVAQESQ MELLESAAPA GALGAQSYGK GARRKNRFKG SDGSTSSDTT 60
61  SNSFVRQGSA DSYTSRPSDS DVSLEEDREA VRREAERQAQ AQLEKAKTKP VAFAVRTNVR 120
121 YSAAQEDDVP VPGMAISFEA KDFLHVKEKF NNDWWIGRLV KEGCEIGFIP SPVKLENMRL 180
181 QHEQRAKQGK FYSSKSGGNS SSSLGDIVPS SRKSTPPSSA IDIDATGLDA EENDIPANHR 240
241 SPKPSANSVT SPHSKEKRMP FFKKTEHTPP YDVVPSMRPV VLVGPSLKGY EVTDMMQKAL 300
301 FDFLKHRFEG RISITRVTAD ISLAKRSVLN NPSKHAIIER SNTRSSLAEV QSEIERIFEL 360
361 ARTLQLVVLD ADTINHPAQL SKTSLAPIIV YVKISSPKVL QRLIKSRGKS QAKHLNVQMV 420
421 AADKLAQCPP QESFDVILDE NQLEDACEHL ADYLEAYWKA THPPSGNLPN PLLSRTLASS 480
481 TLPLSPTLAS NSQGSQGDQR PDRSAPRSAS QAEEEPCLEP VKKSQHRSSS ATHQNHRSGT 540
541 GRGLSRQETF DSETQESRDS AYVEPKEDYS HEHVDRYVPH REHNHREETH SSNGHRHRES 600
601 RHRSRDMGRD QDHNECIKQR SRHKSKDRYC DKEGEVISKR RNEAGEWNRD VYIRQ 655
```

B

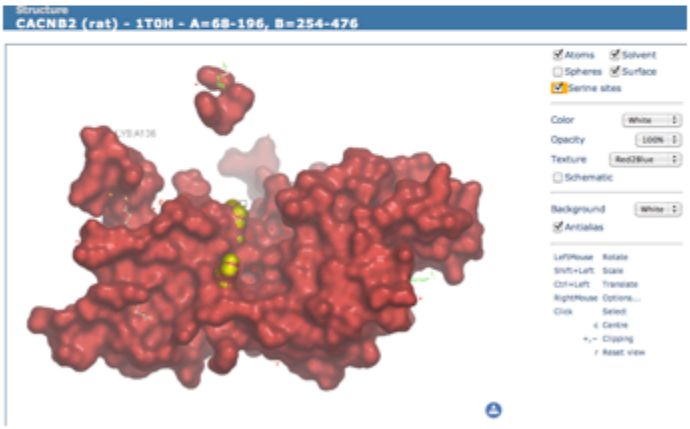

Figure 29. $Ca_v\beta_2$ (Cacnb2) amino acidic sequence (655 aa). A) The globular portion is 1-460 aa, the coiled-coil region is highlighted in light blue (461-655 aa), the Akt consensus site in yellow (500-504 aa), the minimal sequence (136-166 aa) found to interact with $Ca_v\beta_2$-SE bait in our Y2H screening in red and the other sequences (136-275 aa) in green and (136-279 aa) in orange, respectively. The Lysines (K) identified and then mutated are highlighted in grey. B) Evaluation of the $Ca_v\beta_2$ 3D structure. The globular domain is shown in red, while the 3 Lysines found to be exposed to solvent and accessible to protein-protein interaction in yellow (from www.phosphosite.org).

To investigate the role of these accessible aminoacids in the proposed interaction process, site-specific mutagenesis of each positively charged Lysine with the neutral charged glutamine (K141Q, K149Q, K161Q) was performed. Interestingly, western blotting analysis derived from cells cotransfected with $Ca_v\alpha_1$ and $Ca_v\beta_2$-SE-K161Q constructs showed an evident decrease of $Ca_v\alpha_1$ protein levels upon serum removal. Similarly but to a lesser extent, cotransfection of $Ca_v\alpha_1$ with $Ca_v\beta_2$-SE-K149Q in serum-free condition showed a lower decrease of the $Ca_v\alpha_1$ levels when compared to serum conditions (Figure 30C). These results resemble the decrease of $Ca_v\alpha_1$ protein levels seen when $Ca_v\beta_2$-WT was used (Figure 30B). No difference was found instead with $Ca_v\beta_2$-SE-K141Q mutant both in serum-free and serum-containing medium (Figure 30C), similarly to the $Ca_v\alpha_1$ levels when $Ca_v\beta_2$-SE was used (Figure 30A). To confirm that any of the point-mutation introduced wouldn't affect $Ca_v\beta_2$ protein stability, same protein samples described above were subjected to western blotting analysis for total $Ca_v\beta_2$ (Figure 31).

These data suggest that K161 is the main aminoacid responsible for $Ca_v\beta_2$ C-terminal tail binding to the TID and its mutation is sufficient for determining the loss of the protective effect that the $Ca_v\beta_2$-SE phosphomimetic-mutant has on $Ca_v\alpha_1$ protein stability.

Surprisingly, no differences in $Ca_v\alpha_1$ protein levels alteration were found when cells were cotransfected with $Ca_v\alpha_1$ together with each $Ca_v\beta_2$-WT control ($Ca_v\beta_2$-K141Q, $Ca_v\beta_2$-K149Q or $Ca_v\beta_2$-K161Q) (Figure 30D).

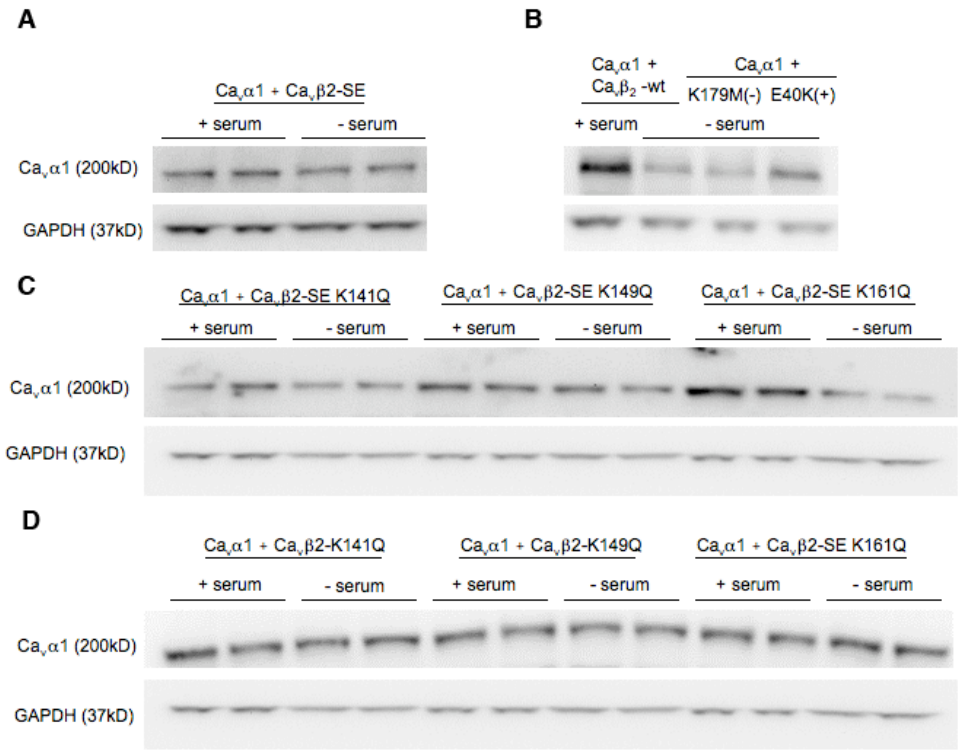

Figure 30. Investigation of the interaction of Akt-phosphorylated tail (-) with accessible neutral charged aminoacids (Q). A) and B) Control western blot analysis in 293T cells cotransfected with $Ca_v\alpha_1$ and $Ca_v\beta_2$ -SE (A) or β_2 -wt for monitoring $Ca_v\alpha_1$ protein levels (n=2 for each condition) in presence or absence of serum. C) and D) Western blot analysis in 293T cells cotransfected with either β_2 -SE (C) or β_2 -wt mutants (D) for monitoring $Ca_v\alpha_1$ protein levels (n=2 for each condition). Protein levels were normalized to GAPDH.

These data show that mutation K161Q in $Ca_v\beta_2$-WT prevent the loss of $Ca_v\alpha_1$ protein stability, suggesting an acquired protein-to-protein interaction mechanism. No additional effect was found with double mutation $Ca_v\beta_2$-K149-161Q or $Ca_v\beta_2$-SE-K149-161Q (Figure 31).

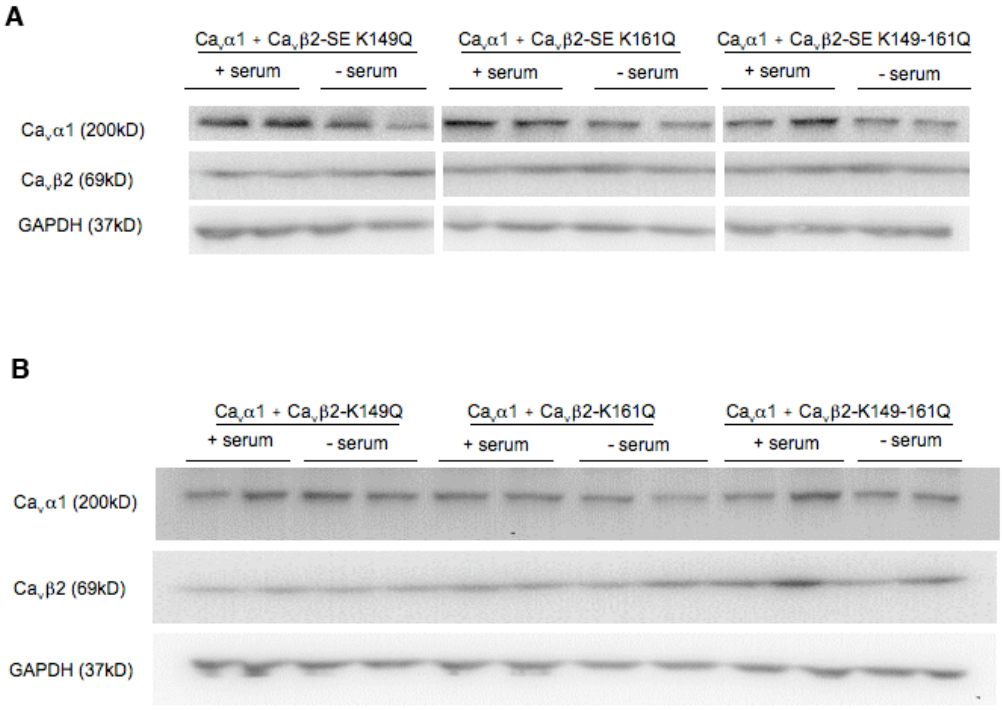

Figure 31. No alteration in $Ca_v\beta_2$ protein stability with any of the point-mutation introduced. Western blot analysis in 293T cells cotransfected with either $Ca_v\beta_2$-SE (A) or $Ca_v\beta_2$-wt mutants (B) for monitoring $Ca_v\beta_2$ protein levels (n=2 for each condition). Protein levels were normalized to GAPDH.

To further understand the importance of the interaction with Akt-phosphorylated tail, changes in cellular calcium flux were measured as previously described (Figure 32). Interestingly, similar to the control condition ($Ca_v\alpha_1$ + $Ca_v\beta_2$), cotransfection of cells with each of the phosphomimetic mutant ($Ca_v\beta_2$-SE-K149Q, $Ca_v\beta_2$-SE-K161Q, or $Ca_v\beta_2$-SE-K149-161Q) resulted with a significant calcium flux reduction upon serum removal (~30% ,***, $p<0.001$) (Figure 32A). On the other hand, a significant increase of calcium flux (~29%,***, $p<0.01$) was found when cells were cotransfected with each $Ca_v\beta_2$-WT control ($Ca_v\beta_2$-K141Q, $Ca_v\beta_2$-K149Q, $Ca_v\beta_2$-K161Q, $Ca_v\beta_2$-K149-161Q) (Figure 32B).

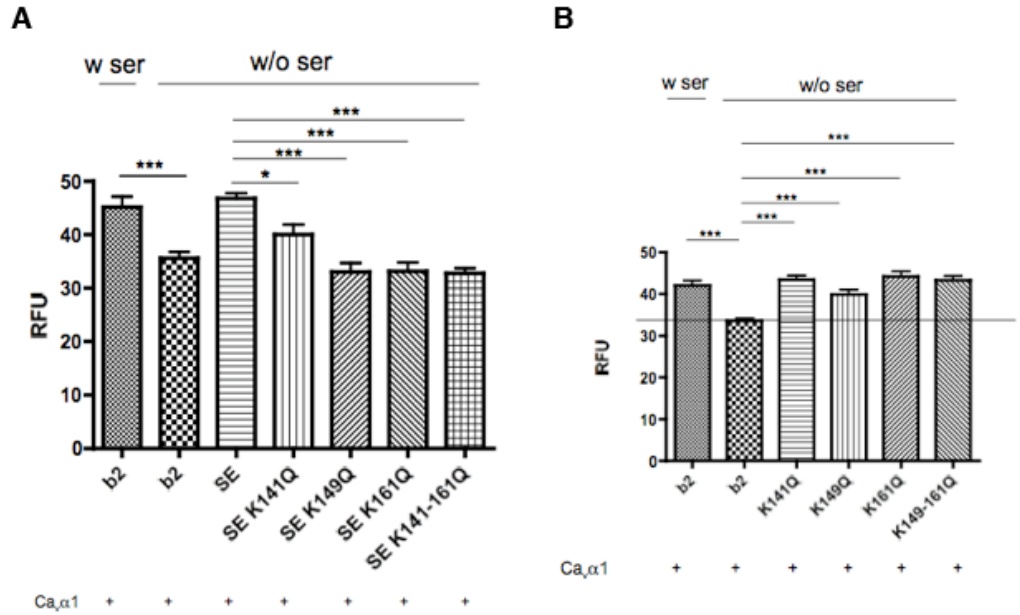

Figure 32. Fluorescent-based calcium assay for analyzing changes in intracellular calcium flux in cells cotransfected with A) each phosphomimetic mutant ($Ca_v\beta_2$-SE-K141Q, $Ca_v\beta_2$-SE-K149Q, $Ca_v\beta_2$-SE-K161Q, $Ca_v\beta_2$-SE-K149-161Q) and each (B) $Ca_v\beta_2$-WT control ($Ca_v\beta_2$-K141Q, $Ca_v\beta_2$-K149Q, $Ca_v\beta_2$-K161Q, $Ca_v\beta_2$-K149-161Q) together with plasmids encoding $Ca_v\alpha_1$ + $Ca_v\beta_2$ cultivated for 48 h in presence or absence of 10% FBS. (***, $p< 0.001$ compared with $Ca_v\beta_2$ w/o serum condition; ANOVA). Error bars show SEM. BayK8644 (1 µM) was used for LTCC activation. Here a representative experiment is shown (n=4). Error bars show SEM.

These data confirm the western blot analysis and reveal the importance of these Lysines for the interaction with the Akt-phosphorylated C-terminal tail. In particular, these results show that neutralizing the charge of these Lysines is sufficient for abolishing the $Ca_v\beta_2$-SE protective phenotype.

To better understand the interaction among Akt-phosphorylated tail and site-specific mutagenesis of K161Q in the TID, data were confirmed with a Y2H assay. Indeed, no interaction was found when retransformation of yeast cells was performed with the $Ca_V\beta_2$-SE bait and Mouse $Ca_V\beta_2$-K161Q TID. On the other hand, a strong binding was obtained when the same prey was cotransformed with $Ca_V\beta_2$-WT bait (Figure 33). This evidence corroborated the presence of a mechanism of action that rely on Akt-dependent phosphorylation.

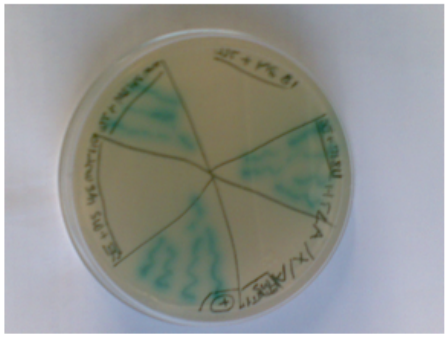

Sample	Colonies	Interaction
$Ca_v\beta_2$-WT bait + MOUSE $Ca_v\beta_2$-K161Q TID prey	+	yes
$Ca_v\beta_2$-SE bait + MOUSE TID prey	+	yes
Positive control (p53+large T-antigen)	+	yes
Empty + MOUSE TID prey	-	no
$Ca_v\beta_2$-WT bait + MOUSE TID prey	-	no
$Ca_v\beta_2$-SE bait + MOUSE $Ca_v\beta_2$-K161Q prey	-	no

Figure 33. Confirmation of a mechanism of action that rely on Akt-dependent phosphorylation. The interaction of the mouse prey $Ca_V\beta_2$-K161Q with $Ca_V\beta_2$-WT bait after cotransformation is shown. No colonies were obtained when the same prey were cotransformed with $Ca_V\beta_2$-SE bait.

In conclusion, the K161Q mutation might modify the structure of the $Ca_V\beta_2$ subunit and/or abolish the interaction with the Akt-dependent phosphorylated $Ca_V\beta_2$ C-terminal tail. This might contribute to loss of the protective effect of the $Ca_V\beta_2$-SE mutant in supporting $Ca_v\alpha_1$ stability in serum-free conditions.

4. DISCUSSION

This study reveals a mechanism through which the insulin IGF1/PI3K/PDK1/Akt pathway can sustain Ca^{2+} entry in cardiac cells via the LTCC and eventually modulate cardiac contractility. In particular, we demonstrated that the protein stability of the LTCC pore subunit ($Ca_v\alpha_1$) can be modulated by the Akt kinase. Phosphorylation of the C-terminal coiled coil of the $Ca_v\beta_2$ chaperone subunit enhances LTCC protein stability by prevention of PEST-mediated $Ca_v\alpha_1$ degradation. This Akt-dependent protective effect on $Ca_v\alpha_1$ stability relays on $Ca_v\beta_2$ structural rearrangements led by an intra-molecular fold-back of the phosphorylated C-terminal coiled coil on its globular domain. Therefore, it is tempting to speculate that the Akt-mediated phosphorylation of $Ca_v\beta_2$ and the consequent direct association of the $Ca_v\beta_2$ C-terminal tail with the globular domain of the $Ca_v\beta_2$ at a region we named "Tail Interacting Domain" (TID) may induce LTCC conformational changes that prevent PEST sequences from being recognized by the cell degradation system (Figure 34). Nevertheless, one cannot exclude the possibility that phosphorylated $Ca_v\beta_2$ might also act indirectly through other, as of yet unknown, LTCC protein partners.

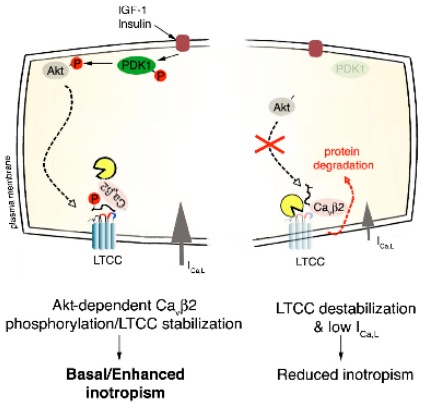

Figure 34. Proposed mechanism. Akt., followed by PDK1 activation, phosphorylates $Ca_v\beta_2$ at the C-terminal coiled-coil domain. The phosphorylation allows association of the C-terminal portion of $Ca_v\beta_2$ with the globular domain of the $Ca_v\beta_2$ at a region we named "Tail Interacting Domain" (TID) (Left). In turn, a conformational shift prevents PEST sequence recognition, stabilizing $Ca_v\alpha_1$ protein levels. The blue and red ribbons in $Ca_v\alpha_1$ represent AID and PEST sequences, respectively.

Several findings have shown the importance of the insulin IGF1/PI3K/Akt pathway in heart function. It has been previously demonstrated that overexpression of an active form of Akt1 results in improved cardiac inotropism both *in vivo* [15] and *in vitro* [47], augmenting $I_{Ca,L}$. Similar results were obtained in a mouse model with cardiac specific Akt1 nuclear-overexpression [48] and in mice deficient for PTEN, an antagonizer of PI3K activity [49]. In addition, short-term administration of IGF1 in animal studies has also been reported to increase cardiac contractility [25]. However, the mechanism through which the insulin IGF1/PI3K/Akt pathway affects Ca^{2+} current has remained elusive. In an elegant *in vitro* study, Viard and coworkers [105] demonstrated that a region of the $Ca_v\beta_{2a}$ subunit is involved in the PI3K-induced chaperoning of $Ca_v2.2a$ in neurons. This PI3K-induced regulation was shown to be mediated by Akt phosphorylation of the $Ca_v\beta_{2a}$ subunit, which in turn regulates $Ca_v2.2a$ trafficking from the ER to the plasma membrane. Notably, the C-terminal region containing the putative Akt-phosphorylation consensus site is conserved in all variants of the $Ca_v\beta_2$ subunit

both in neurons and heart [105], thus illustrating the importance of this site. In addition, strong conservation was found also among the TID region of all $Ca_v\beta$ isoforms including also the Lysines (underlined in the Figure 35) determinant for the binding with the Akt-phosphorylated C-terminal region (Figure 35):

```
Cavβ1119 VPVQGVAITFEPKDFLHIKEKYNNDWWIGRLVKEGCEVGFIPSPVKLDSLRLLQEQKL
Cavβ2129 VPVPGMAISFEAKDFLHVKEKFNNDWWIGRLVKEGCEIGFIPSPVKLENMRLQHEQRA
Cavβ378  CPVQGSGVNFEAKDFLHIKEKYSNDWWIGRLVKEGGDIAFIPSPQRLESIRLKQEQKA
Cavβ4109 VPVPSTAISFDAKDFLHIKEKYNNDWWIGRLVKEGCEIGFIPSPLRLENIRIQQEQ--
           **      *  ***** ***  ************    *****  *   * * **
```

Figure 35. Homology alignement of $Ca_v\beta_2$-TID with mouse $Ca_v\beta$ subunits. Conserved residues are shown in grey boxes. Blast analysis revealed that $Ca_v\beta_1$ shows 83.9%, $Ca_v\beta_3$ 77.4%, $Ca_v\beta_4$ 90.3% of identity in the 31 residues overlap with $Ca_v\beta_2$-TID (yellow box), respectively.

Interestingly, two very short human cardiac splice isoforms, $Ca_v\beta_{2f}$ and $Ca_v\beta_{2g}$ with preserved Akt-site have been shown to be essential for modulating Ca^{2+} channel function and $Ca_v\alpha_1$ channel density [74, 114]. Strikingly, the same two $Ca_v\beta_2$ variants do not contain the protein kinase PKA phosphorylation site [115], consistent with our data suggesting no PKA involvement in the modulation of LTCC density (data not shown). In line with our hypothesis, also the TID-site has been found conserved in the short $Ca_v\beta_{2f}$ isoform. As corollary, the presence of conserved C-terminal region and TID in all $Ca_v\beta_2$ splice isoforms corroborates the relevance of identifying new functional motifs that may give important insights into LTCC modulation. All together, these evidences support the notion that the C-terminal region of $Ca_v\beta_2$ might be a potential pharmacological target. In line with this, we showed that Akt-phosphomimetic sequences belonging to the C-terminal region of $Ca_v\beta_2$ are determinant for a positive effect in the control of LTCC density by maintaining $Ca_v\alpha_1$ protein stability and function. However, we couldn't exclude the possibility that Akt-dependent phosphorylation of $Ca_V\beta_2$ might also act indirectly through other LTCC protein partners, being a trigger for

the recruitment of other proteins involved in $Ca_v\alpha_1$ protein stability modification. Nevertheless, using a yeast two-hybrid system approach, we showed that only the Akt-phosphorylated $Ca_v\beta_2$ and not the $Ca_v\beta_2$-WT C-terminal interacts with the globular domain of the $Ca_v\beta_2$ at the "tail interaction domain" (TID), thus providing the proof of concept for a mechanism of action that relies on Akt-dependent phosphorylation. This corroborates the idea that the protective action of Akt-phosphomimetic sequences on $Ca_v\beta_2$ might occur through the direct interaction to the $Ca_v\beta_2$ TID. Notably, K161 was identified as the relevant aminoacid responsible for this interaction. Indeed, our data suggest that mutation of K161 is sufficient to abolish the interaction of the Akt-dependent phosphorylated $Ca_V\beta_2$ C-terminal tail (Figure 33-36) with the TID.

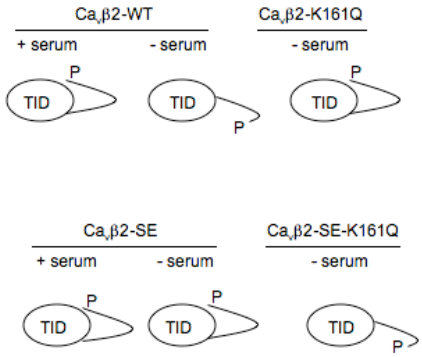

Figure 36. Proposed mechanism. K161 was identified as the relevant aminoacid responsible for this interaction.

Therefore, it is tempting to speculate that, when Akt is not phosphorylated, the alternate conformational status of the globular $Ca_V\beta_2$ determines a different interaction between $Ca_v\alpha_1$ and $Ca_v\beta_2$ subunits, that results with $Ca_v\alpha_1$ PEST sequences recognition by the cell degradation machinery.

In conclusion, results from this doctoral thesis led to further insights into the role of the insulin IGF1/Akt signaling pathway and its role in the modulation of myocardial physiology and HF. In fact, the re-establisment of cardiac function in HF could be obtained by finding a new equilibrium of this signaling pathway that favor physiological rather than pathological cardiac hypertrophy. This can be reached by acting on downstream targets modulated by the Akt kinase, in particular by positively affecting cardiac function through the modulation of myocardial Ca^{2+} handling. Notably, it has been demonstrated that diabetes and DCM are associated with impaired activation of the Akt signaling pathway [116, 117], while its reactivation has been shown to promote CMC survival, improving Ca^{2+} handling and contractile function [15]. Also alterations in the density or function of L-type calcium channels (LTCCs) have been related to a variety of cardiovascular diseases, including atrial fibrillation, heart failure, and DCM [58, 88, 89]. Therefore, unraveling the functional role of potential Akt-phosphomimetics $Ca_v\beta_2$ sequences might be of relevance for the development of therapeutic tools for the treatment of HF that could increase or reestablish a "correct" cardiac inotropism by increasing the number of functional LTCC in diseased CMCs. In addition, the high level of conservation of PEST sequences in the $Ca_v\alpha_1$ subunit throughout evolution (Table 5), the high homology of TID in all mouse $Ca_v\beta$ subunits and the Akt-consensus site conserved in all variants of $Ca_v\beta_2$ subunit indicate that our proposed mechanism may play a universal role in regulating cell Ca^{2+} handling and survival.

5. ACKNOWLEDGMENTS

The present PhD work was carried out during 2007-2010 in the Laboratory of Molecular Cardiology at IRCSS Multimedica, Milan (Italy) and at ITB/CNR, Segrate (Italy).

First, I want to thank my supervisor Dr.Daniele Catalucci for introducing me to the field of Akt pathway and Calcium Channels and sharing his knowledge, scientific work and enthusiasm. It was a challenge to start in the new lab...but we made it!

The present work wouldn't have been possible without the help and the scientific advice of Professor Gianluigi Condorelli.

A special thanks goes to Dr.Frank Aimond and Prof.Sylvain Richard from INSERM U637, Universités de Montpellier (France) for performing $I_{Ca,L}$ experiments on murine cardiomyocytes; to Dr.Magali Cazade and Dr.Jean Chemin from Institut de Génomique Fonctionnelle, INSERM U661, Universités de Montpellier (France) for performing $I_{Ca,L}$ experiments on recombinant $Ca_v\alpha_1$ currents; to Dr.Nancy Dalton from Division of Cardiology, Department of Medicine, University of California, La Jolla, CA (USA) for echo analysis; to Dr. Eckard Picht and Donald M. Bers from Department of Physiology and Cardiovascular Institute, Loyola University Chicago, Maywood, IL (USA) for calcium transients experiments; to Dr. Jeffrey D. Molkentin for MerCreMer α-MHC mice; to Dr.Dario Alessi for $PDK1^{floxed/floxed}$ mice; to Dr. Hannelore Haase for $Ca_v\alpha_1$ and $Ca_v\beta_2$ antibody and Dr. Nikolai Soldatov for YFP-$Ca_v\alpha_1$ cDNA.

6. REFERENCES

1. Mosterd A, Hoes AW: **Clinical epidemiology of heart failure.** *Heart* 2007, **93:**1137-1146.
2. Juenger J, Schellberg D, Kraemer S, Haunstetter A, Zugck C, Herzog W, Haass M: **Health related quality of life in patients with congestive heart failure: comparison with other chronic diseases and relation to functional variables.** *Heart* 2002, **87:**235-241.
3. Stewart S, MacIntyre K, Hole DJ, Capewell S, McMurray JJ: **More 'malignant' than cancer? Five-year survival following a first admission for heart failure.** *Eur J Heart Fail* 2001, **3:**315-322.
4. Latronico MV, Catalucci D, Condorelli G: **MicroRNA and cardiac pathologies.** *Physiol Genomics* 2008, **34:**239-242.
5. Meijs MF, de Windt LJ, de Jonge N, Cramer MJ, Bots ML, Mali WP, Doevendans PA: **Left ventricular hypertrophy: a shift in paradigm.** *Curr Med Chem* 2007, **14:**157-171.
6. Richey PA, Brown SP: **Pathological versus physiological left ventricular hypertrophy: a review.** *J Sports Sci* 1998, **16:**129-141.
7. Schaible TF, Malhotra A, Ciambrone GJ, Scheuer J: **Chronic swimming reverses cardiac dysfunction and myosin abnormalities in hypertensive rats.** *J Appl Physiol* 1986, **60:**1435-1441.
8. Wisloff U, Loennechen JP, Currie S, Smith GL, Ellingsen O: **Aerobic exercise reduces cardiomyocyte hypertrophy and increases contractility, Ca2+ sensitivity and SERCA-2 in rat after myocardial infarction.** *Cardiovasc Res* 2002, **54:**162-174.
9. Molkentin JD, Dorn GW, 2nd: **Cytoplasmic signaling pathways that regulate cardiac hypertrophy.** *Annu Rev Physiol* 2001, **63:**391-426.
10. Frey N, Olson EN: **Cardiac hypertrophy: the good, the bad, and the ugly.** *Annu Rev Physiol* 2003, **65:**45-79.
11. McKee PA, Castelli WP, McNamara PM, Kannel WB: **The natural history of congestive heart failure: the Framingham study.** *N Engl J Med* 1971, **285:**1441-1446.
12. Frey N, Katus HA, Olson EN, Hill JA: **Hypertrophy of the heart: a new therapeutic target?** *Circulation* 2004, **109:**1580-1589.
13. Mann DL, Deswal A, Bozkurt B, Torre-Amione G: **New therapeutics for chronic heart failure.** *Annu Rev Med* 2002, **53:**59-74.

14. Walsh K: **Akt signaling and growth of the heart.** *Circulation* 2006, **113:**2032-2034.
15. Condorelli G, Drusco A, Stassi G, Bellacosa A, Roncarati R, Iaccarino G, Russo MA, Gu Y, Dalton N, Chung C, et al: **Akt induces enhanced myocardial contractility and cell size in vivo in transgenic mice.** *Proc Natl Acad Sci U S A* 2002, **99:**12333-12338.
16. Catalucci D, Latronico MV, Ellingsen O, Condorelli G: **Physiological myocardial hypertrophy: how and why?** *Front Biosci* 2008, **13:**312-324.
17. Shiojima I, Yefremashvili M, Luo Z, Kureishi Y, Takahashi A, Tao J, Rosenzweig A, Kahn CR, Abel ED, Walsh K: **Akt signaling mediates postnatal heart growth in response to insulin and nutritional status.** *J Biol Chem* 2002, **277:**37670-37677.
18. Neri Serneri GG, Boddi M, Modesti PA, Cecioni I, Coppo M, Padeletti L, Michelucci A, Colella A, Galanti G: **Increased cardiac sympathetic activity and insulin-like growth factor-I formation are associated with physiological hypertrophy in athletes.** *Circ Res* 2001, **89:**977-982.
19. McMullen JR, Amirahmadi F, Woodcock EA, Schinke-Braun M, Bouwman RD, Hewitt KA, Mollica JP, Zhang L, Zhang Y, Shioi T, et al: **Protective effects of exercise and phosphoinositide 3-kinase(p110alpha) signaling in dilated and hypertrophic cardiomyopathy.** *Proc Natl Acad Sci U S A* 2007, **104:**612-617.
20. McMullen JR, Shioi T, Zhang L, Tarnavski O, Sherwood MC, Kang PM, Izumo S: **Phosphoinositide 3-kinase(p110alpha) plays a critical role for the induction of physiological, but not pathological, cardiac hypertrophy.** *Proc Natl Acad Sci U S A* 2003, **100:**12355-12360.
21. Belke DD, Betuing S, Tuttle MJ, Graveleau C, Young ME, Pham M, Zhang D, Cooksey RC, McClain DA, Litwin SE, et al: **Insulin signaling coordinately regulates cardiac size, metabolism, and contractile protein isoform expression.** *J Clin Invest* 2002, **109:**629-639.
22. Hu P, Zhang D, Swenson L, Chakrabarti G, Abel ED, Litwin SE: **Minimally invasive aortic banding in mice: effects of altered cardiomyocyte insulin signaling during pressure overload.** *Am J Physiol Heart Circ Physiol* 2003, **285:**H1261-1269.
23. Li B, Setoguchi M, Wang X, Andreoli AM, Leri A, Malhotra A, Kajstura J, Anversa P: **Insulin-like growth factor-1 attenuates the detrimental impact of nonocclusive coronary artery constriction on the heart.** *Circ Res* 1999, **84:**1007-1019.
24. Yamashita K, Kajstura J, Discher DJ, Wasserlauf BJ, Bishopric NH, Anversa P, Webster KA: **Reperfusion-activated Akt kinase prevents**

apoptosis in transgenic mouse hearts overexpressing insulin-like growth factor-1. *Circ Res* 2001, **88:**609-614.

25. Duerr RL, Huang S, Miraliakbar HR, Clark R, Chien KR, Ross J, Jr.: **Insulin-like growth factor-1 enhances ventricular hypertrophy and function during the onset of experimental cardiac failure.** *J Clin Invest* 1995, **95:**619-627.
26. Welch S, Plank D, Witt S, Glascock B, Schaefer E, Chimenti S, Andreoli AM, Limana F, Leri A, Kajstura J, et al: **Cardiac-specific IGF-1 expression attenuates dilated cardiomyopathy in tropomodulin-overexpressing transgenic mice.** *Circ Res* 2002, **90:**641-648.
27. Ren J, Samson WK, Sowers JR: **Insulin-like growth factor I as a cardiac hormone: physiological and pathophysiological implications in heart disease.** *J Mol Cell Cardiol* 1999, **31:**2049-2061.
28. Vanhaesebroeck B, Leevers SJ, Panayotou G, Waterfield MD: **Phosphoinositide 3-kinases: a conserved family of signal transducers.** *Trends Biochem Sci* 1997, **22:**267-272.
29. Paez J, Sellers WR: **PI3K/PTEN/AKT pathway. A critical mediator of oncogenic signaling.** *Cancer Treat Res* 2003, **115:**145-167.
30. Shioi T, Kang PM, Douglas PS, Hampe J, Yballe CM, Lawitts J, Cantley LC, Izumo S: **The conserved phosphoinositide 3-kinase pathway determines heart size in mice.** *EMBO J* 2000, **19:**2537-2548.
31. Crackower MA, Oudit GY, Kozieradzki I, Sarao R, Sun H, Sasaki T, Hirsch E, Suzuki A, Shioi T, Irie-Sasaki J, et al: **Regulation of myocardial contractility and cell size by distinct PI3K-PTEN signaling pathways.** *Cell* 2002, **110:**737-749.
32. Catalucci D, Condorelli G: **Effects of Akt on cardiac myocytes: location counts.** *Circ Res* 2006, **99:**339-341.
33. Alessi DR, Cohen P: **Mechanism of activation and function of protein kinase B.** *Curr Opin Genet Dev* 1998, **8:**55-62.
34. Konishi H, Kuroda S, Tanaka M, Matsuzaki H, Ono Y, Kameyama K, Haga T, Kikkawa U: **Molecular cloning and characterization of a new member of the RAC protein kinase family: association of the pleckstrin homology domain of three types of RAC protein kinase with protein kinase C subspecies and beta gamma subunits of G proteins.** *Biochem Biophys Res Commun* 1995, **216:**526-534.
35. Okano J, Gaslightwala I, Birnbaum MJ, Rustgi AK, Nakagawa H: **Akt/protein kinase B isoforms are differentially regulated by epidermal growth factor stimulation.** *J Biol Chem* 2000, **275:**30934-30942.

36. Sarbassov DD, Guertin DA, Ali SM, Sabatini DM: **Phosphorylation and regulation of Akt/PKB by the rictor-mTOR complex.** *Science* 2005, **307:**1098-1101.
37. Andjelkovic N, Zolnierowicz S, Van Hoof C, Goris J, Hemmings BA: **The catalytic subunit of protein phosphatase 2A associates with the translation termination factor eRF1.** *EMBO J* 1996, **15:**7156-7167.
38. Gao T, Furnari F, Newton AC: **PHLPP: a phosphatase that directly dephosphorylates Akt, promotes apoptosis, and suppresses tumor growth.** *Mol Cell* 2005, **18:**13-24.
39. Shioi T, McMullen JR, Kang PM, Douglas PS, Obata T, Franke TF, Cantley LC, Izumo S: **Akt/protein kinase B promotes organ growth in transgenic mice.** *Mol Cell Biol* 2002, **22:**2799-2809.
40. Matsui T, Li L, Wu JC, Cook SA, Nagoshi T, Picard MH, Liao R, Rosenzweig A: **Phenotypic spectrum caused by transgenic overexpression of activated Akt in the heart.** *J Biol Chem* 2002, **277:**22896-22901.
41. Shiojima I, Sato K, Izumiya Y, Schiekofer S, Ito M, Liao R, Colucci WS, Walsh K: **Disruption of coordinated cardiac hypertrophy and angiogenesis contributes to the transition to heart failure.** *J Clin Invest* 2005, **115:**2108-2118.
42. Chen WS, Xu PZ, Gottlob K, Chen ML, Sokol K, Shiyanova T, Roninson I, Weng W, Suzuki R, Tobe K, et al: **Growth retardation and increased apoptosis in mice with homozygous disruption of the Akt1 gene.** *Genes Dev* 2001, **15:**2203-2208.
43. Cho H, Thorvaldsen JL, Chu Q, Feng F, Birnbaum MJ: **Akt1/PKBalpha is required for normal growth but dispensable for maintenance of glucose homeostasis in mice.** *J Biol Chem* 2001, **276:**38349-38352.
44. Easton RM, Cho H, Roovers K, Shineman DW, Mizrahi M, Forman MS, Lee VM, Szabolcs M, de Jong R, Oltersdorf T, et al: **Role for Akt3/protein kinase Bgamma in attainment of normal brain size.** *Mol Cell Biol* 2005, **25:**1869-1878.
45. Kemi OJ, Haram PM, Wisloff U, Ellingsen O: **Aerobic fitness is associated with cardiomyocyte contractile capacity and endothelial function in exercise training and detraining.** *Circulation* 2004, **109:**2897-2904.
46. Donath MY, Jenni R, Brunner HP, Anrig M, Kohli S, Glatz Y, Froesch ER: **Cardiovascular and metabolic effects of insulin-like growth factor I at rest and during exercise in humans.** *J Clin Endocrinol Metab* 1996, **81:**4089-4094.

47. Kim YK, Kim SJ, Yatani A, Huang Y, Castelli G, Vatner DE, Liu J, Zhang Q, Diaz G, Zieba R, et al: **Mechanism of enhanced cardiac function in mice with hypertrophy induced by overexpressed Akt.** *J Biol Chem* 2003, **278:**47622-47628.
48. Rota M, Boni A, Urbanek K, Padin-Iruegas ME, Kajstura TJ, Fiore G, Kubo H, Sonnenblick EH, Musso E, Houser SR, et al: **Nuclear targeting of Akt enhances ventricular function and myocyte contractility.** *Circ Res* 2005, **97:**1332-1341.
49. Sun H, Kerfant BG, Zhao D, Trivieri MG, Oudit GY, Penninger JM, Backx PH: **Insulin-like growth factor-1 and PTEN deletion enhance cardiac L-type Ca2+ currents via increased PI3Kalpha/PKB signaling.** *Circ Res* 2006, **98:**1390-1397.
50. Kamp TJ, Chiamvimonvat N: **Mission impossible: IGF-1 and PTEN specifically "Akt"ing on cardiac L-type Ca2+ channels.** *Circ Res* 2006, **98:**1349-1351.
51. Bers DM, Perez-Reyes E: **Ca channels in cardiac myocytes: structure and function in Ca influx and intracellular Ca release.** *Cardiovasc Res* 1999, **42:**339-360.
52. Richard S, Perrier E, Fauconnier J, Perrier R, Pereira L, Gomez AM, Benitah JP: **'Ca(2+)-induced Ca(2+) entry' or how the L-type Ca(2+) channel remodels its own signalling pathway in cardiac cells.** *Prog Biophys Mol Biol* 2006, **90:**118-135.
53. Bers DM: **Cardiac excitation-contraction coupling.** *Nature* 2002, **415:**198-205.
54. Karunasekara Y, Dulhunty AF, Casarotto MG: **The voltage-gated calcium-channel beta subunit: more than just an accessory.** *Eur Biophys J* 2009, **39:**75-81.
55. De Waard M, Gurnett CA, Campbell KP: **Structural and functional diversity of voltage-activated calcium channels.** *Ion Channels* 1996, **4:**41-87.
56. Yamakage M, Namiki A: **Calcium channels--basic aspects of their structure, function and gene encoding; anesthetic action on the channels--a review.** *Can J Anaesth* 2002, **49:**151-164.
57. Wang MC, Dolphin A, Kitmitto A: **L-type voltage-gated calcium channels: understanding function through structure.** *FEBS Lett* 2004, **564:**245-250.
58. Bodi I, Mikala G, Koch SE, Akhter SA, Schwartz A: **The L-type calcium channel in the heart: the beat goes on.** *J Clin Invest* 2005, **115:**3306-3317.

59. Yang SN, Berggren PO: **The role of voltage-gated calcium channels in pancreatic beta-cell physiology and pathophysiology.** *Endocr Rev* 2006, **27:**621-676.
60. Carafoli E, Santella L, Branca D, Brini M: **Generation, control, and processing of cellular calcium signals.** *Crit Rev Biochem Mol Biol* 2001, **36:**107-260.
61. Catterall WA: **Structure and regulation of voltage-gated Ca2+ channels.** *Annu Rev Cell Dev Biol* 2000, **16:**521-555.
62. Takahashi M, Catterall WA: **Dihydropyridine-sensitive calcium channels in cardiac and skeletal muscle membranes: studies with antibodies against the alpha subunits.** *Biochemistry* 1987, **26:**5518-5526.
63. Cataldi M, Perez-Reyes E, Tsien RW: **Differences in apparent pore sizes of low and high voltage-activated Ca2+ channels.** *J Biol Chem* 2002, **277:**45969-45976.
64. Moosmang S, Lenhardt P, Haider N, Hofmann F, Wegener JW: **Mouse models to study L-type calcium channel function.** *Pharmacol Ther* 2005, **106:**347-355.
65. De Jongh KS, Warner C, Catterall WA: **Subunits of purified calcium channels. Alpha 2 and delta are encoded by the same gene.** *J Biol Chem* 1990, **265:**14738-14741.
66. Qin N, Yagel S, Momplaisir ML, Codd EE, D'Andrea MR: **Molecular cloning and characterization of the human voltage-gated calcium channel alpha(2)delta-4 subunit.** *Mol Pharmacol* 2002, **62:**485-496.
67. Muth JN, Varadi G, Schwartz A: **Use of transgenic mice to study voltage-dependent Ca2+ channels.** *Trends Pharmacol Sci* 2001, **22:**526-532.
68. Mori Y, Mikala G, Varadi G, Kobayashi T, Koch S, Wakamori M, Schwartz A: **Molecular pharmacology of voltage-dependent calcium channels.** *Jpn J Pharmacol* 1996, **72:**83-109.
69. Hofmann F, Biel M, Flockerzi V: **Molecular basis for Ca2+ channel diversity.** *Annu Rev Neurosci* 1994, **17:**399-418.
70. Felix R, Gurnett CA, De Waard M, Campbell KP: **Dissection of functional domains of the voltage-dependent Ca2+ channel alpha2delta subunit.** *J Neurosci* 1997, **17:**6884-6891.
71. Helton TD, Kojetin DJ, Cavanagh J, Horne WA: **Alternative splicing of a beta4 subunit proline-rich motif regulates voltage-dependent gating and toxin block of Cav2.1 Ca2+ channels.** *J Neurosci* 2002, **22:**9331-9339.

72. Hanlon MR, Berrow NS, Dolphin AC, Wallace BA: **Modelling of a voltage-dependent Ca2+ channel beta subunit as a basis for understanding its functional properties.** *FEBS Lett* 1999, **445:**366-370.
73. Pragnell M, De Waard M, Mori Y, Tanabe T, Snutch TP, Campbell KP: **Calcium channel beta-subunit binds to a conserved motif in the I-II cytoplasmic linker of the alpha 1-subunit.** *Nature* 1994, **368:**67-70.
74. De Waard M, Pragnell M, Campbell KP: **Ca2+ channel regulation by a conserved beta subunit domain.** *Neuron* 1994, **13:**495-503.
75. Richards MW, Butcher AJ, Dolphin AC: **Ca2+ channel beta-subunits: structural insights AID our understanding.** *Trends Pharmacol Sci* 2004, **25:**626-632.
76. Dolphin AC: **Beta subunits of voltage-gated calcium channels.** *J Bioenerg Biomembr* 2003, **35:**599-620.
77. Colecraft HM, Alseikhan B, Takahashi SX, Chaudhuri D, Mittman S, Yegnasubramanian V, Alvania RS, Johns DC, Marban E, Yue DT: **Novel functional properties of Ca(2+) channel beta subunits revealed by their expression in adult rat heart cells.** *J Physiol* 2002, **541:**435-452.
78. Neuhuber B, Gerster U, Mitterdorfer J, Glossmann H, Flucher BE: **Differential effects of Ca2+ channel beta1a and beta2a subunits on complex formation with alpha1S and on current expression in tsA201 cells.** *J Biol Chem* 1998, **273:**9110-9118.
79. Bichet D, Cornet V, Geib S, Carlier E, Volsen S, Hoshi T, Mori Y, De Waard M: **The I-II loop of the Ca2+ channel alpha1 subunit contains an endoplasmic reticulum retention signal antagonized by the beta subunit.** *Neuron* 2000, **25:**177-190.
80. Gerster U, Neuhuber B, Groschner K, Striessnig J, Flucher BE: **Current modulation and membrane targeting of the calcium channel alpha1C subunit are independent functions of the beta subunit.** *J Physiol* 1999, **517 (Pt 2):**353-368.
81. Van Petegem F, Clark KA, Chatelain FC, Minor DL, Jr.: **Structure of a complex between a voltage-gated calcium channel beta-subunit and an alpha-subunit domain.** *Nature* 2004, **429:**671-675.
82. He LL, Zhang Y, Chen YH, Yamada Y, Yang J: **Functional modularity of the beta-subunit of voltage-gated Ca2+ channels.** *Biophys J* 2007, **93:**834-845.
83. De Jongh KS, Murphy BJ, Colvin AA, Hell JW, Takahashi M, Catterall WA: **Specific phosphorylation of a site in the full-length form of the alpha 1 subunit of the cardiac L-type calcium channel by adenosine**

3',5'-cyclic monophosphate-dependent protein kinase. *Biochemistry* 1996, **35:**10392-10402.

84. Fitzgerald EM: **The presence of Ca2+ channel beta subunit is required for mitogen-activated protein kinase (MAPK)-dependent modulation of alpha1B Ca2+ channels in COS-7 cells.** *J Physiol* 2002, **543:**425-437.
85. Strube C, Beurg M, Powers PA, Gregg RG, Coronado R: **Reduced Ca2+ current, charge movement, and absence of Ca2+ transients in skeletal muscle deficient in dihydropyridine receptor beta 1 subunit.** *Biophys J* 1996, **71:**2531-2543.
86. Murakami M, Yamamura H, Murakami A, Okamura T, Nunoki K, Mitui-Saito M, Muraki K, Hano T, Imaizumi Y, Flockerzi T, Yanagisawa T: **Conserved smooth muscle contractility and blood pressure increase in response to high-salt diet in mice lacking the beta3 subunit of the voltage-dependent calcium channel.** *J Cardiovasc Pharmacol* 2000, **36 Suppl 2:**S69-73.
87. Arikkath J, Campbell KP: **Auxiliary subunits: essential components of the voltage-gated calcium channel complex.** *Curr Opin Neurobiol* 2003, **13:**298-307.
88. Pereira L, Matthes J, Schuster I, Valdivia HH, Herzig S, Richard S, Gomez AM: **Mechanisms of [Ca2+]i transient decrease in cardiomyopathy of db/db type 2 diabetic mice.** *Diabetes* 2006, **55:**608-615.
89. Mukherjee R, Spinale FG: **L-type calcium channel abundance and function with cardiac hypertrophy and failure: a review.** *J Mol Cell Cardiol* 1998, **30:**1899-1916.
90. Quignard JF, Mironneau J, Carricaburu V, Fournier B, Babich A, Nurnberg B, Mironneau C, Macrez N: **Phosphoinositide 3-kinase gamma mediates angiotensin II-induced stimulation of L-type calcium channels in vascular myocytes.** *J Biol Chem* 2001, **276:**32545-32551.
91. Benitah JP, Gomez AM, Fauconnier J, Kerfant BG, Perrier E, Vassort G, Richard S: **Voltage-gated Ca2+ currents in the human pathophysiologic heart: a review.** *Basic Res Cardiol* 2002, **97 Suppl 1:**I11-18.
92. Haase H, Kresse A, Hohaus A, Schulte HD, Maier M, Osterziel KJ, Lange PE, Morano I: **Expression of calcium channel subunits in the normal and diseased human myocardium.** *J Mol Med* 1996, **74:**99-104.
93. Bosch RF, Zeng X, Grammer JB, Popovic K, Mewis C, Kuhlkamp V: **Ionic mechanisms of electrical remodeling in human atrial fibrillation.** *Cardiovasc Res* 1999, **44:**121-131.

94. Splawski I, Timothy KW, Sharpe LM, Decher N, Kumar P, Bloise R, Napolitano C, Schwartz PJ, Joseph RM, Condouris K, et al: **Ca(V)1.2 calcium channel dysfunction causes a multisystem disorder including arrhythmia and autism.** *Cell* 2004, **119:**19-31.
95. Hart G: **Cellular electrophysiology in cardiac hypertrophy and failure.** *Cardiovasc Res* 1994, **28:**933-946.
96. Williams MR, Arthur JS, Balendran A, van der Kaay J, Poli V, Cohen P, Alessi DR: **The role of 3-phosphoinositide-dependent protein kinase 1 in activating AGC kinases defined in embryonic stem cells.** *Curr Biol* 2000, **10:**439-448.
97. Sohal DS, Nghiem M, Crackower MA, Witt SA, Kimball TR, Tymitz KM, Penninger JM, Molkentin JD: **Temporally regulated and tissue-specific gene manipulations in the adult and embryonic heart using a tamoxifen-inducible Cre protein.** *Circ Res* 2001, **89:**20-25.
98. Care A, Catalucci D, Felicetti F, Bonci D, Addario A, Gallo P, Bang ML, Segnalini P, Gu Y, Dalton ND, et al: **MicroRNA-133 controls cardiac hypertrophy.** *Nat Med* 2007, **13:**613-618.
99. Fields S, Song O: **A novel genetic system to detect protein-protein interactions.** *Nature* 1989, **340:**245-246.
100. Lawlor MA, Mora A, Ashby PR, Williams MR, Murray-Tait V, Malone L, Prescott AR, Lucocq JM, Alessi DR: **Essential role of PDK1 in regulating cell size and development in mice.** *EMBO J* 2002, **21:**3728-3738.
101. Catalucci D, Zhang DH, DeSantiago J, Aimond F, Barbara G, Chemin J, Bonci D, Picht E, Rusconi F, Dalton ND, et al: **Akt regulates L-type Ca2+ channel activity by modulating Cavalpha1 protein stability.** *J Cell Biol* 2009, **184:**923-933.
102. Mora A, Komander D, van Aalten DM, Alessi DR: **PDK1, the master regulator of AGC kinase signal transduction.** *Semin Cell Dev Biol* 2004, **15:**161-170.
103. Blair LA, Bence-Hanulec KK, Mehta S, Franke T, Kaplan D, Marshall J: **Akt-dependent potentiation of L channels by insulin-like growth factor-1 is required for neuronal survival.** *J Neurosci* 1999, **19:**1940-1951.
104. Bourinet E, Mangoni ME, Nargeot J: **Dissecting the functional role of different isoforms of the L-type Ca2+ channel.** *J Clin Invest* 2004, **113:**1382-1384.

105. Viard P, Butcher AJ, Halet G, Davies A, Nurnberg B, Heblich F, Dolphin AC: **PI3K promotes voltage-dependent calcium channel trafficking to the plasma membrane.** *Nat Neurosci* 2004, **7:**939-946.
106. Yamaguchi H, Hara M, Strobeck M, Fukasawa K, Schwartz A, Varadi G: **Multiple modulation pathways of calcium channel activity by a beta subunit. Direct evidence of beta subunit participation in membrane trafficking of the alpha1C subunit.** *J Biol Chem* 1998, **273:**19348-19356.
107. Bayascas JR, Wullschleger S, Sakamoto K, Garcia-Martinez JM, Clacher C, Komander D, van Aalten DM, Boini KM, Lang F, Lipina C, et al: **Mutation of the PDK1 PH domain inhibits protein kinase B/Akt, leading to small size and insulin resistance.** *Mol Cell Biol* 2008, **28:**3258-3272.
108. Smith LK, Bradshaw M, Croall DE, Garner CW: **The insulin receptor substrate (IRS-1) is a PEST protein that is susceptible to calpain degradation in vitro.** *Biochem Biophys Res Commun* 1993, **196:**767-772.
109. Rechsteiner M: **PEST sequences are signals for rapid intracellular proteolysis.** *Semin Cell Biol* 1990, **1:**433-440.
110. Krappmann D, Wulczyn FG, Scheidereit C: **Different mechanisms control signal-induced degradation and basal turnover of the NF-kappaB inhibitor IkappaB alpha in vivo.** *EMBO J* 1996, **15:**6716-6726.
111. Sandoval A, Oviedo N, Tadmouri A, Avila T, De Waard M, Felix R: **Two PEST-like motifs regulate Ca2+/calpain-mediated cleavage of the CaVbeta3 subunit and provide important determinants for neuronal Ca2+ channel activity.** *Eur J Neurosci* 2006, **23:**2311-2320.
112. Dice JF: **Molecular determinants of protein half-lives in eukaryotic cells.** *FASEB J* 1987, **1:**349-357.
113. Lao QZ, Kobrinsky E, Liu Z, Soldatov NM: **Oligomerization of Cav{beta} subunits is an essential correlate of Ca2+ channel activity.** *FASEB J.*
114. Kobrinsky E, Tiwari S, Maltsev VA, Harry JB, Lakatta E, Abernethy DR, Soldatov NM: **Differential role of the alpha1C subunit tails in regulation of the Cav1.2 channel by membrane potential, beta subunits, and Ca2+ ions.** *J Biol Chem* 2005, **280:**12474-12485.
115. Kamp TJ, Hell JW: **Regulation of cardiac L-type calcium channels by protein kinase A and protein kinase C.** *Circ Res* 2000, **87:**1095-1102.
116. Hu J, Klein JD, Du J, Wang XH: **Cardiac muscle protein catabolism in diabetes mellitus: activation of the ubiquitin-proteasome system by insulin deficiency.** *Endocrinology* 2008, **149:**5384-5390.

117. Bilim O, Takeishi Y, Kitahara T, Arimoto T, Niizeki T, Sasaki T, Goto K, Kubota I: **Diacylglycerol kinase zeta inhibits myocardial atrophy and restores cardiac dysfunction in streptozotocin-induced diabetes mellitus.** *Cardiovasc Diabetol* 2008, **7:**2.